A DEVELOPMENT OF THE MOTILE SPERM SORTING MICROFLUIDIC DEVICES

A Dissertation
Presented to
the Faculty of the Graduate School
University of Missouri-Columbia

In Partial Fulfillment
of the Requirements for the Degree
Doctor of Philosophy

By

DUCKBONG SEO

Dr. Frank Z. Feng, Dissertation Supervisor

AUGUST 2007

The undersigned, appointed by the Dean of the Graduate School, have examined the dissertation entitled

A DEVELOPMENT OF THE MOTILE SPERM SORTING MICROFLUIDIC DEVICES

presented by DUCKBONG SEO

a candidate for the degree of Doctor of Philosophy

and hereby certify that in their opinion it is worthy of acceptance

_____

Professor Frank Feng, Dissertation Supervisor

_____

Professor John Critser

_____

Professor Yuyi Lin

_____

Professor Kevin Gillis

_____

Professor Yuksel Agca

ACKNOWLEDGEMENTS

First of all, I would like to specially thank my thesis advisor Dr. Frank Feng for his guidance, assistance, encouragement, and support during my Ph. D. study.

I also thank Dr. Yuksel Agca, Dr. John Critser, Dr. Kevin Gillis, and Dr, Yuyi Lin for their time and efforts in reading this dissertation, serving on my thesis committee, and examining my dissertation in spite of their busy schedules. Their constructive suggestions and comments have been very useful.

I am grateful to Dr. John Critser and National Institutes of Health (NIH) for supporting me to complete Ph. D. study. I also thank to Dr. Kevin Gillis and National Science Foundation (NSF) for financial support during my master degree study. Their supports really help me to complete these courses.

Moreover, I would like to express special thanks to Yong-Sik Lee, Mingxuan Fan, Jung-Woo Yun, and David Shim for their friendship and encouragement.

Finally, I would like to give appreciation to my wife, Hye-Shin for her patience and support, my parents for their prayers, and my lovely kid, David for his love.

This work was funded by grant from the NIH (RR1482) to JCK.

Above of all, I specially thank to God.

A DEVELOPMENT OF THE MOTILE SPERM SORTING MICROFLUIDIC DEVICES

DUCKBONG SEO

Dr. Frank Z. Feng, Dissertation Supervisor

ABSTRACT

The objectives of this research are developing and improving an inexpensive and convenient microfluidic device to apply to sperm cell sorting. Based on well known soft-lithography fabrication method which contains rapid prototyping and wet-etching, the polymeric microfluidic devices, mainly microchannels, are fabricated. The fabrication processes of microfluidic devices are completed without an expensive cleanroom facility.

To successfully design the microfluidic devices, we built mathematical flow models for single and multiple microchannels using fluid flow equations that govern the motion of the Newtonian liquid. These mathematical models are used to optimize the design of the microfluidic devices. The flows in the completed microfluidic system are observed using an inverted microscope and recorded by a digital camera. Experiments on fluid flow and on the movement of small particles including cells are conducted. These experiments lead to the development of a Motile sperm Sorting Microfludic System (MSMS).

TABLE OF CONTENTS

LIST OF FIGURES

LIST OF TABLES

Table **Page**

Chapter 1

INTRODUCTION

1.1. Micro-Electro-Mechanical Systems (MEMS)

The idea of Micro-Electro-Mechanical Systems (MEMS) was first introduced by Richard P. Feynmam when he presented the observation: "There is Plenty of Room at the Bottom", at the American Physical Society Meeting in 1959 [1]. His approach was based on scaling down the size of devices. He suggested that reducing power consumption and increasing performance can be achieved by reducing the size. His idea was too far to be practical at that time. However, in the 1960s, the advent of microfabrication technologies in the integrated circuit (IC) and semiconductor industries had shown the possibility of his presentation. These technologies also affect the development of manufacturing methods for microsized structures conducting mechanical and electrical functions. In results, MEMS have attracted many engineers and scientists since the 1980s. Furthermore, MEMS have rapidly become one of popular research areas lately.

Recent MEMS devices enable new functions and improve their performance. Because MEMS are miniaturized systems, that are comprised of sensors, actuators and electronic devices typically smaller than 100 μm, integrating multi-functions and reducing size can be achieved. MEMS devices are typically manufactured on silicon wafers; therefore, micro devices and microelectronics can be integrated to the same chip. MEMS also have several advantages such as improving capabilities and reducing manufacturing costs. A comparison between ENIAC, the world's first electric computer

in 1946, and the present day compact laptop is a good example. The size of ENIAC was huge because it had 19,000 vacuum tubes. It weighed over 30 tons and occupied over 1800 square feet. Although its cost was almost $500,000, it was only used for numerical calculations [2]. In contrast, the compact laptop computer not only can perform numerical calculations but also can even play music. However, it weighs less than 10 pounds and costs around $1,000. The advent of micro fabrication technology has allowed these developments possible.

MEMS are finding many applications in a variety of industrial fields with great potential market. The market of MEMS technology is rapidly growing since 1990s. The MEMS markets were almost $0.9 billion in 1994, however, the market grown to $7 billion in 2005 (an annual growth rate close to 15%) [3-5]. Many micromachining technologies to fabricate MEMS devices have been developed and documented recently along with growing MEMS market. As a result, several MEMS devices have been completed and are shown in many areas. Microaccelerometers [6-8], micropumps [8-12], and micro pressure sensors [13, 14] are good examples. Those devices can be commercially applied to automobile airbag systems, dense arrays of micromirrors for high definition optical displays, micro-heat exchangers, ink-jet printers, and drug delivery systems etc. In addition, many MEMS researches have being performed in potential and practical applications such as medical, chemical, and biological areas to integrate more functions and to reduce consuming resources.

1.2. Microfluidics and sperm sorting

Miniaturization and MEMS gave birth to microfluidics, the manipulation of liquids and gases in microchannels typically having less than 100 μm sizes, during the 1990s. Recently, the development of microfabrication technologies applying MEMS has made the microfluidics systems as the main technology in chemical, biological, and medical applications. Microfluidic systems also have many advantages including reduced consumption of reagents and reduced analysis time; increased separation efficiency; and decreased cost in fabrication. Therefore, microfluidic systems have been applied to wide potential areas as shown in Table 1.1 reproduced from [15]. In addition, the market for microfluidic technologies is rapidly growing and is also worth an estimated $2.9 billion in 2005 [5].

Many microfluidics researchers have focused their studies on integrating many functions on one chip, the so-called labs-on-chip (LOC) or micro total analysis systems (μTAS), to achieve two main goals; (1) to simplify working mechanism and (2) to reduce time consumption and cost. Manipulating the flow in the microchannels with small size samples, such as cells and sperm, is important to develop such LOC microfluidic devices. The development of fabrication technologies based on polymer, such as soft-lithography, easily enable fabrication of microchannels [15]. Therefore, the polymeric microchannels have been used in many microfluidic applications like cell sorting [16], drug delivery systems [17], and sperm sorting [18-21].

Table1. 1. Potential applications and areas of microfluidic devices [15]

AREA	APPLICATION
• **Miniaturized analytical systems** • **Genomics and proteomics**	Rapid, high density sequencing, DNA fingerprinting, combinatorial analysis, forensics, gene expression assays, integration of fluidics with DNA arrays.
• **Chemical/biological warfare defenses**	Early detection and identification of pathogens and toxins; early diagnosis; triage.
• **Clinical analysis**	Rapid analysis of blood and bodily fluids, point of care diagnostics; based on immunological or enzymatic assays, electrochemical detection, and cell counting.
• **High throughput screening**	Combinatorial synthesis and assaying for drugs. Toxicological assays.
• **Environmental testing**	In situ analysis of environmental contamination.
• **Biomedical devices** • **Implantable devices**	Devices for in vivo drug delivery, in vivo monitoring for disease and conditions.
• **Tools for chemistry and biochemistry** • **Small-scale organic synthesis** • **Sample preparation** • **Amplification of nucleic acids/sequences**	Combinatorial synthesis. Purification of biological samples for further analysis.
• **Systems for fundamental research** • **Systems with which to study the flow of fluids** • **Studies of chemical reactions** • **Systems to study small amounts of sample**	Studies on EOF and laminar flow in small channels, studies of diffusion. Enzyme-substrate. Development of machines that mimic biological functions. Detection of single molecules.

Microfluidic devices are widely studied to apply to biomedical research, agriculture application, and medical procedures related to human reproduction. In reproduction applications, separating motile sperm from non-motile sperm is critical for successful intracytoplasmic sperm injection (ICSI) and in vitro fertilization (IVF), which are the most commonly used in assisted reproductive technologies to overcome male infertility problems. In addition, orientation and separation of the head from the tail is another obstacle for ICSI.

The polymeric microfluidic devices assisting reproduction and sorting cells have recently been introduced [22-28]. The motile sperm sorting microfluidic devices [18-21] have also been reported. However, it is still a challenge to improve devices' performance and convenience of use. For example, in the system introduced by Cho et al. [18], the pressure has to be stable during sorting and flow velocity has to be large enough to prevent motile sperm from swimming against the direction of flow. In addition, they reported sorting results only for human sperm. In view of the limitations of the sorting devices reported in the literatures, we developed a novel motile sperm sorting device which can be used for multiple species. Additionally, the orientation and alignment of the sperm cell can be simultaneously controlled.

1.3. Literature reviews

Among many established micromachining technologies, the development of etching and sealing technologies helps to easily complete fabricating microchannels. Additionally, the micromachining ability to treat etching and sealing using silicon and polymers such as PDMS shows many results of complete microchannels.

Sobek, et al. [29] developed a microchannel using etching and sealing processes in fused silica substrate. They used buffered oxide etch with $2.5\mu m$ low pressure chemical vapor deposition (LPCVD) polysilicon masks and bonded two fused silica wafers at $1{,}000°C$.

Harrison, et al. [30], Jacobson, et al. [31], Manz, et al. [32], and Woolley and Mathies [33] have also completed similar microchannels in glass using fluoride-based aqueous etching.

Tjerkstra, et al. [34] demonstrated a variety of fluidic channel fabrication techniques based on combining wet and dry bulk etching with deposition of dielectric films to form the walls of the channels. They also presented the formation of channels that were “buried” in a silicon substrate and formed through a narrow slit, which can later be sealed through the deposition of a suitable thin-film material.

Lin, et al. [35] introduced an approach to surface micromachined flow channel fabrication. Their approach used only surface micromachining for channel formation, and can be generalized to other channel materials, with its primary limitation being the achievable channel height.

Man, et al. [36] developed a technique for forming surface micro-machined organic fluidic channels at low temperatures. They deposited several layers using poly-p-xylylene (Parylene ^{TM} C), AZ4620 photoresist, and polyimide.

Many engineers have used polymers to complete fabrication of microfluidic devices, because they can be used to fabricate such devices inexpensively and fast without much experience and expensive facilities. Polymers often possess the properties needed for various microfluidic uses. The use of polymers in the production of micro-fluidic devices has been well documented. For example, Duffy et al. at [37] introduced Rapid Prototyping by using polymers, such as SU-8 and PDMS to produce microfluidic devices. Their procedure makes it possible to design and fabricate (including sealing) microfluidic systems in an elastomeric material (PDMS) in less than 24 *hours*.

Chan et al. [38] reported how to construct and use PDMS microfabricated soft polymer devices with mass spectrometry for protein analysis. Their paper particularly detailed the kind of instruments and chemicals needed to fabricate a microfluidic device.

Sperm sorting systems using microfludic devices have also been recently reported [18-21]. Among the sperm sorting microfluidc systems, Cho et al. [18] introduced a motile human sperm sorting device. This system uses the self-movement of motile sperm to escape from the initial inlet streamline, which is generated by passive pumping systems using hydrostatic pressure, and then collects motile sperm in one of two outlet reservoirs.

1.4. Objectives

For last two decades, engineers and researchers have developed and demonstrated many micromachining technologies including the microfabrication methods for microchannel-based microfluidic devices. Fabrication time and cost are also much decreased because of development of techniques. However, fabrication cost is still relatively expensive because special facility, such as cleanroom, is still required to fabricate MEMS and microfluidic devices. In addition, skilled dexterity is also necessary to complete polymeric microchannels without defects. However, the polymeric microchannels fabrication methods which can be completed without cleanroom facility and without defects are not well reported. Therefore, we have focused our research on completing inexpensive and convenient microfluidics devices consisting of polymeric microchannels. Applying the completed device to one of biological areas, specifically motile sperm sorting, is another objective of this research.

Using demonstrated fabrication methods, such as rapid prototyping and etching, and materials, such as polymer and photoresist, the microfluidic devices are fabricated in a regular laboratory. After completing simple microfluidic devices consisting of single microchannel, the complex microfluidic devices consisting of multi-microchannels are also completed. Then, we build single and multi microchannels mathematical model to regulate the flow in the channel using fluid flow equation that governs the motion of Newtonian liquid. Based on fluid flow equations, the flow velocities equations in microchannels are derived. These equations are used to optimize the design of microfluidic devices. The flow velocities in the microchannels are predicted from

mathematical equations. Analyzing and optimizing processes are conducted for single and multi microchannels to develop proper devices performing multi-functions, such as sorting and aligning cell or sperm. The flows in the microchannel are observed using an inverted microscope and a digital camera. Microbeads are injected with solution to analyze and to observe the fluid flow in the microchannels. The movement of sperm in the microchannels depending on fluid flow is also observed. Based on observed results, finally, the motile sperm sorting device is developed to assist reproduction such as ICSI and IVF.

1.5. Overview

This dissertation starts from the fabrication of polymeric microchannels. In Chapter 2, fabricating processes for polymeric microchannels which can be achieved inexpensively are introduced. More specifically, this chapter focuses on fabrication processes that can be used for polymeric materials and silicon wafers. Based on our fabrication experience, the defects-free fabrication methods including diluted hydrochloride (HCl) bonding are also mentioned.

In Chapter 3 to Chapter 5, we discuss the designs and the applications of microfluidic devices related to both theoretical and experimental points. Both Chapter 3 and Chapter 4 show the basic mathematical model and calculation results. The theoretical models are built using governing equation to regulate the flow in the microchannel and to manipulate movement of small particles. Several equations for the flow in the single and multi-microchannels are derived. The derived equations are numerically calculated using

MATLAB. Based on the calculating results, we optimize the design of the microfluidic device for sorting motile sperm.

In Chapter 5, the experimental results for both the fluid flow and motile sperm sorting are presented. This chapter also discusses how the mechanical forces (pressures) can transport microbeads and affect the movement of motile sperm in low Reynold's number flow. The movement of microbeads in the microchannels shows the fluid flow visually. Similarly, the movement of motile sperm in the microchannels is also presented.

Chapter 2

FABRICATION OF MICROCHANNELS

2.1. Introduction

The early stages of MEMS technologies were focused on developing fabrication methods and finding proper materials. Therefore, many advanced micromachining technologies which can fabricate micron-sized structures and parts have been introduced during the last two decades. Based on such advanced fabrication techniques and materials, many MEMS devices were completed like microbeams, micromirrors, polymeric microchannels, and micropumps. Such developments and results make MEMS technologies to be applied and to be expanded in many areas such as optical, biological, and medical fields. Especially, the developments of MEMS technologies have also attracted considerable applications in both biological and medical fields. Therefore, many micromachining studies to fabricate microfluidic devices which can be applied in these applications have also been developed. Most microfluidic devices are commonly consisting of the polymeric microchannels which can be completed using photo-lithography and chemical etching. In addition, these devices are researched and studied to develop the micro total analysis systems (μTAS) lately.

Polymers are used in the production of microfluidic devices for biological and medical applications because of their own properties, such as elasticity, optical properties, biocompatibility, and even inexpensive cost. Several trials to fabricate the microchannels using polymers have already been successful. However, the most fabricating methods

were still conducted with expensive facility like cleanroom to improve quality and to avoid defects.

In this chapter, we discuss the fabrication method of microfluidic devices, mainly polymeric microchannels. SU-8 and an elastometric material, polydimethylsiloxane (PDMS), are used to complete microchannels in less than 2 days without a cleanroom facility. The microfluidic devices are fabricated following the defects-free fabrication processes. If the microfluidic devices do not consist of complex shapes and do not occupy relatively wide area (less than 500 μm × 500 μm), the devices can be fabricated in a regular laboratory. The described method makes it possible to rapidly and inexpensively carry out a complete cycle of design, fabrication, and testing of microchannels. The design and fabrication procedures outlined should be useful in prototyping micro systems, and specialized systems that are being developed for biological applications. The method that described in this chapter could also reduce the manufacturing cost and be used in mass production.

2.2. Instruments and materials for fabrication

To complete the fabrication of microchannels, the following instruments and supplies are required. A Spin-coater (Model P6700, A Specialty Coating System. INC, Figure 2.1 (a)) is used to coat the silicon wafer with SU-8 photoresist. The spin speeds, time, and acceleration are controllable by programming. Coating thickness can be defined by spin speeds, time and material properties, such as SU-8 viscosity.

Ultraviolet (UV) exposure unit (KVB – 30.KINSTEN, 55mW/cm^2, Figure 2.1 (b)) is used to expose a coated wafer. It includes a vacuum pump to mount the

transparent mask with a wafer. The exposing is completed using six 15-watt UV-light sources, which are located on both bottom and top sides (each side has three sources respectively). Exposing time is only controllable during process. Therefore, to properly define exposing time is most important.

Pre-baking and post-baking processes are completed using a digital heater (Model HP 30.TERREY PINES SCIENTIFIC, Figure 2.1 (c)). It consists of a heat plate and temperature controller. The heating time and temperature can be simultaneously controllable.

We used a 6-inch diameter silicon wafer (Figure 2.1 (d)) which has a polish side and an oxide side to complete the mold. Wafers and SU-8 2000 series photoresist were used as the mold for subsequent molding. Propyleneglycol monomethylether acetate (PGMEA) solvent, called SU-8 developer, was used to develop the UV exposed wafer. PDMS was prepared by mixing SYLGARD 184 SILICONE ELASTOMER base and agent with 10:1 weight ratio. The compressed air is also important not only to remove dust on the silicon wafer and completed PDMS microchannels but also to run the spin-coater.

(a)

(b)

(c)

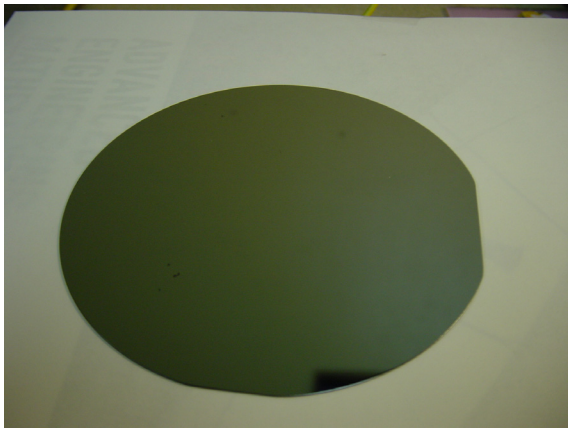

(d)

Figure 2.1. The instruments for fabricating microchannels: (a) Spincoater Model P6700 (A Specialty Coating System) (b) Exposure Unit KVB – 30 (KINSTEN) (c) Model Hp30(Torrey Pines Scientific) digital heater (d) 6" Silicon wafer

2.3. Fabrication of microchannels

The fabrication processes of microchannels start with designing pattern of a transparent mask for photolithograph using commercial design software. AUTOCAD 2002 was used to complete the transparency mask for the mold. The format of designing file was converted to EPS (for Adobe Illustrator) from DWG (for AUTOCAD) before printing. Finally, the design is printed on a transparency using 5080 dpi ($5\mu m$ diameter each point) high resolution printer obtained from a commercial printing shop (University of Illinois at Urbana-Champaign, Urbana, IL). After completing the transparency film called "mask", it was checked against the original design using a microscope. Using transparency created from a high resolution printer, we are able to rapidly and reliably produce channels using photoresist.

The silicon master construction is usually processed in a cleanroom to avoid many defects that could appear in regular rooms. Chan et al. [38], for example, conducted this procedure in a 10,000 class clean room. However in this Chapter, we will demonstrate how it is possible to complete the processes in a regular room while still reducing various defects. The complete processes for fabricating the microchannels consist of five steps: 1) coating, 2) exposing, 3) etching, 4) molding, and 5) bonding (Figure 2.2). Several obstacles must be overcome when coating and developing the wafer. Therefore, some conditions which are mentioned by Seo [39] and Collins [40] for avoiding defects must be considered. In addition, it is better to use the polish side of the wafer to easily bond PDMS and glass plate.

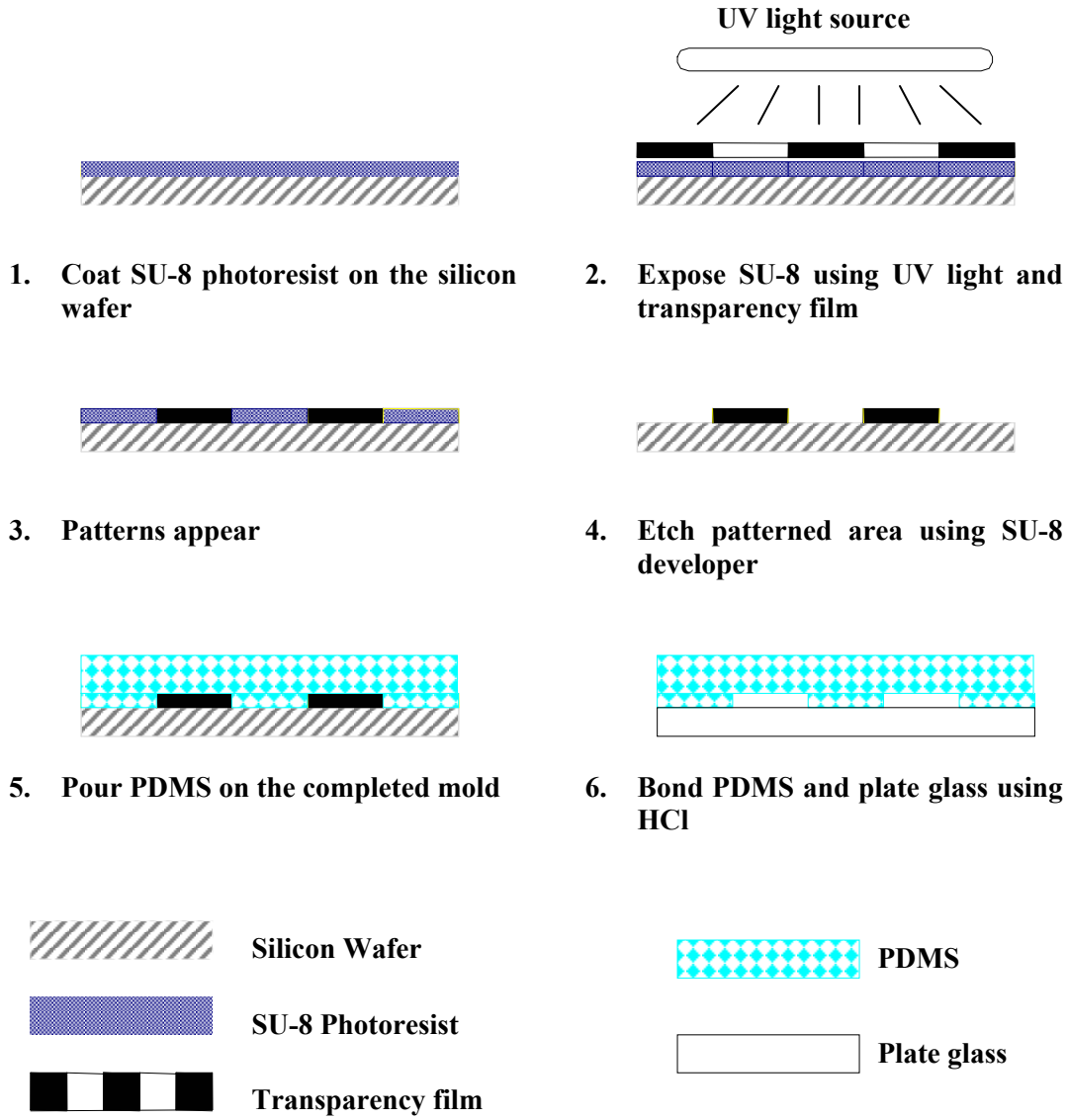

Figure 2.2. A schematic showing the steps involved in the fabrication procedures of the microchannel.

2.3.1. Coating and baking

Before starting the coating process, the silicon wafer must be cleaned using purified compressed air until the surface humidity and dust on the wafer are completely removed. If the cleaning process is skipped, many bubbles may develop after the spin-coating (Figure 2.3). Coating starts from placing the silicon wafer on the rotary plate located in the coater. The center of wafer is adjusted to the center of the rotary plate as close as possible. Adjusting is an important step to spread SU-8 well during coating. After pouring the proper amount of SU-8 negative photoresist on the wafer, the coater keeps less than 500 *rpm* speed for 10 seconds or until SU-8 covers whole wafer. The coater increases speed up to 4000 *rpm* for 30 seconds after the SU-8 covers whole wafer. However, the coating speed is various depending on types of SU-8.

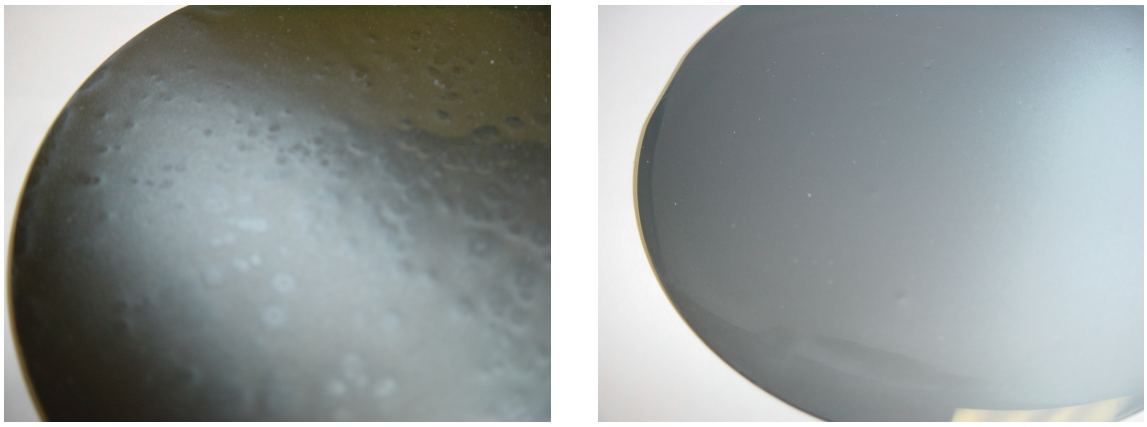

(a) (b)

Figure 2.3. Examples of coated wafers (a) irregular surface coated wafer with bubbles and (b) uniform surface coated wafer

The thickness of coated surface is defined by types of SU-8 and coating processes. Depending on the viscosity of SU-8 photoresist, the thickness can be limited. If we use SU-8 2025, for example, the limited thickness can not be less than 25 μm although we give enough spin time and speed.

Once spin-coating is completed, the pre-baking process follows. Pre-baking consists of heating the coated wafer to 45 ~ 55 ^{o}C for 1 *minute*. Then the wafer is heated to 85 ~ 95 ^{o}C until the total pre-bake time reaches 19 ~ 20 *minutes* using the Corning Model PC-220 Heater (Figure 2.1 (c)). To avoid generating new bubbles when pre-baking, the temperature is increased slowly (100 ^{o}C/*minute*) until it reaches around 50 ^{o}C. The pre-baking temperature should not exceed 95 ^{o}C at this time. If the pre-baking temperature exceeded 95 ^{o}C, some bubbles could be generated from the boiling that occurred on the SU-8 photoresist surface.

After completing the baking, the wafer is removed from the heater and returned to room temperature. Then it is allowed to dry overnight with a protective cover. The cover used as a screen to prevent sticking dust on the wafer and to isolate the coated SU-8 photoresist thin layer from any form of UV-light. To avoid over drying, caution is taken not to leave the coated wafer at room temperature for more than 36 hours, because over-drying makes the photoresist too strong to react to the SU-8 developer solution. Also, exposure to even weak forms of UV-light could make the surface too strong to respond to SU-8 developer.

2.3.2. UV exposure

The exposing process utilizes reciprocal action between photoresist and UV-light. After UV-light exposure to particular areas through the mask, exposed areas do not respond to chemicals, and therefore it can not be etched by a wet etching process. This process is very useful in particular MEMS fields, such as micro-fluidic and bio-MEMS, because it is a fast, easy, and inexpensive process.

To develop the coated wafer, it is aligned with a patterned mask through direct contact using vacuum compression and exposed to ultraviolet light ($0.0552 W/cm^2$) using Exposure Unit KVB – 30.KINSTEN (Figure 2.1 (b)). The length of exposure time should vary according to the strength of the ultraviolet light and the type of photoresist. Proper time is crucial for getting a precise pattern during the wet-etching process. Through trial and error, we found that 90 *seconds* exposure is appropriate when we used SU-8 2025. Over-exposure could change the channels' widths so that they become wider than the designed pattern. In addition, the printed surface of the transparent mask film has to contact directly to the coated wafer. Although the thickness of transparency is very small, it may affects the width of design pattern as shown in Figure 2.4.

Following the ultraviolet exposure, the wafer is placed on a heater again for post-baking. The post-baking process takes 4~5 *minutes* at temperature range 90~100 ^{o}C. Care must be taken not to exceed this temperature by checking that the heater has not reached 100 ^{o}C before the wafer is placed on it. During post-baking, the pattern slowly begins to appear, while it is possible that new bubbles are generated on unexposed surface.

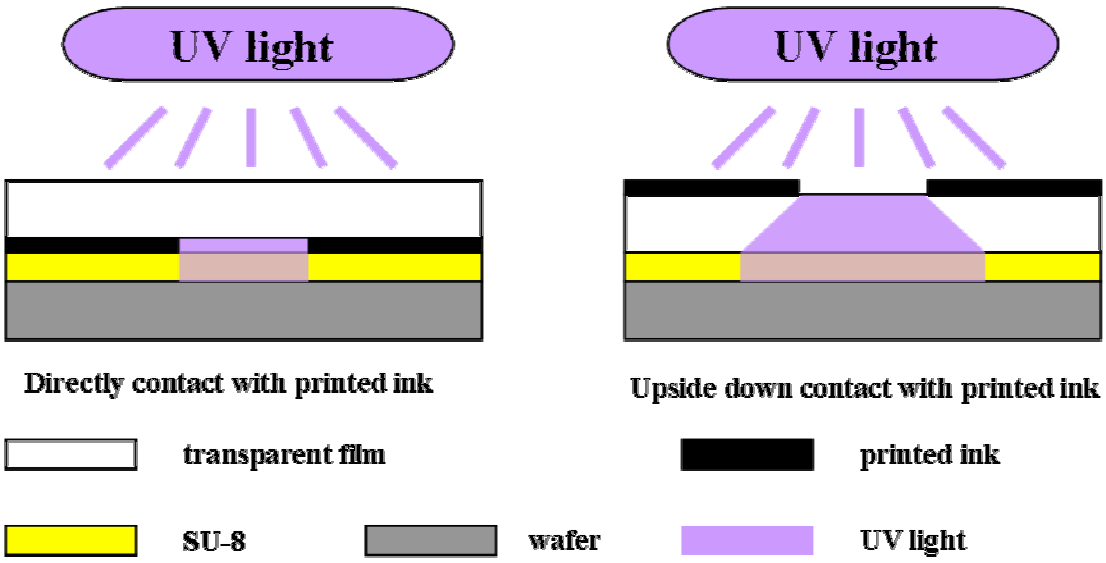

Figure 2.4. Schematic of placing patterned transparent mask to reduce errors between the design and silicon mold.

2.3.3. Etching

After the patterns have appeared, the wafer is immediately etched using SU-8 developer. During etching process, the whole wafer is usually immersed into SU-8 developer. However, we applied the SU-8 developer drops on the surface of coated wafer to avoid removing SU-8 mold on the wafer. When the whole wafer is immersed into SU-8 developer, about 100 *ml* of SU-8 developer was consumed. In contrast, applying drops can reduce the consumed amount of SU-8 developer to less than 30 *ml*.

After the wafer is slantingly placed, the developer slowly drops until the patterns are showing. Areas of photoresist chemically modified by the ultraviolet light are resistant to the SU-8 developer solution. Then the wafer is dried using compressed air. If the patterns on the wafer are not clear and SU-8 still remains, we can repeat above etching process to get precise patterns.

As shown in Figures 2.5 (a), SU-8 still remains on the wafer when the whole wafer is immersed into SU-8 developer. However, the patterns are clear when we use the SU-8 drops to etch SU-8 as shown in Figure 2.5 (b).

2.3.4. Molding

After completing all of the previous processes, the developed silicon wafer master is ready for use in the fabrication of PDMS devices. The monomer and curing agent components of the SYLGARD 184 SILICONE ELASTOMER KIT are mixed at 10:1 weight ratio. The mixture is degassed in a vacuum until no air bubbles remain. A PDMS device is cast against the patterned silicon master by pouring the mixture over the master. Then it cures at 65 ~ 70 ^{o}C in a vacuum oven for 2 *hours*. After curing, the polymer device is peeled off the silicon master as shown in Figure 2.6. Figure 2.7 shows the cross sectional shape of the molded PDMS obtained by cutting.

Before completing the PDMS microchannels, the reservoirs were joined with the molded PDMS. The molded PDMS is placed on the plate glass then the PDMS is smeared under the reservoirs to use as glue (Figure 2.8). The molded PDMS joining reservoirs cures again in a vacuum oven for 1 hour to harden the PDMS between reservoirs and the molded PDMS.

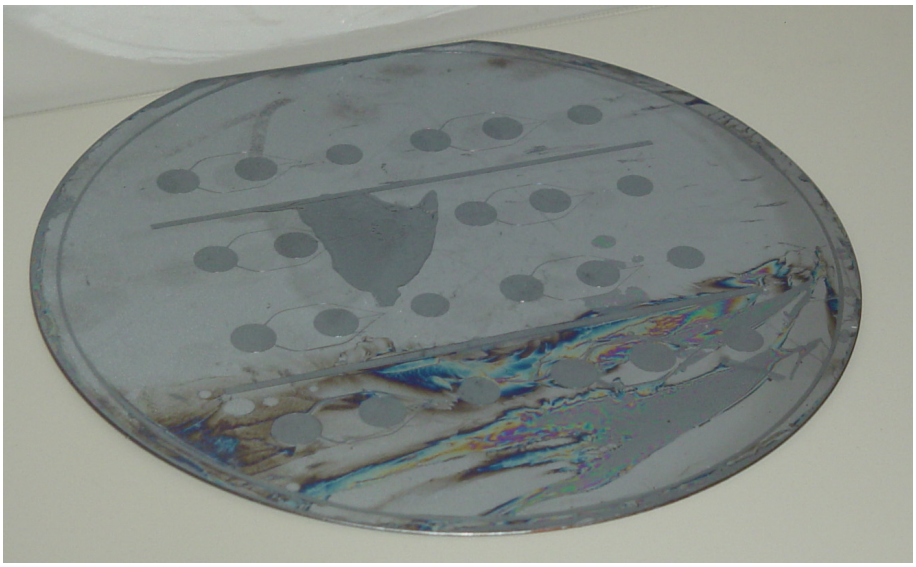

(a)

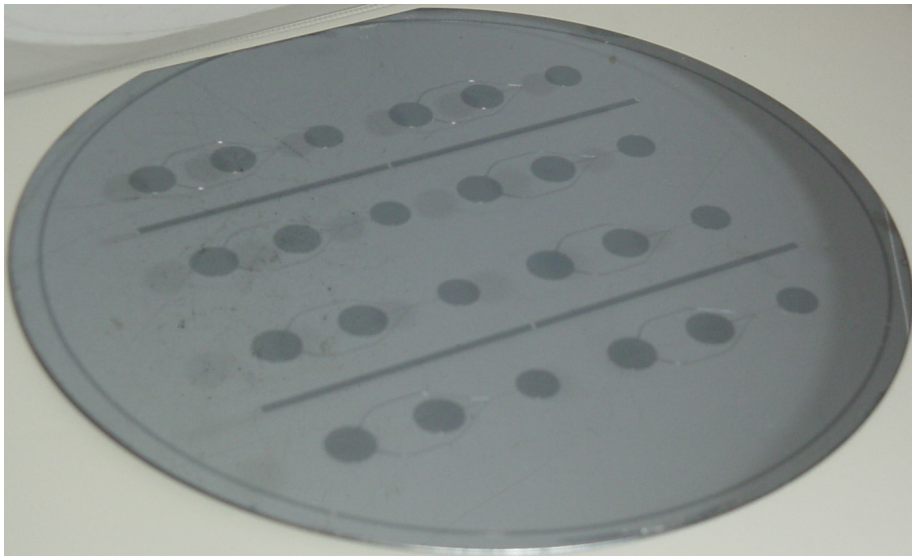

(b)

Figure 2.5. Comparisons of developed silicon masters depending on etching methods: (a) the patterns are developed by immersing whole wafer into the SU-8 developer, (b) the patterns are developed by applying SU-8 drops.

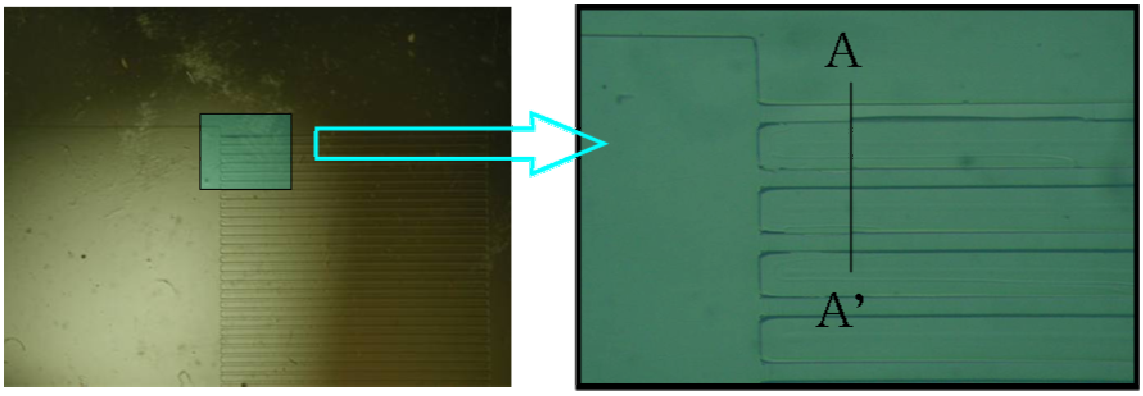

(a)

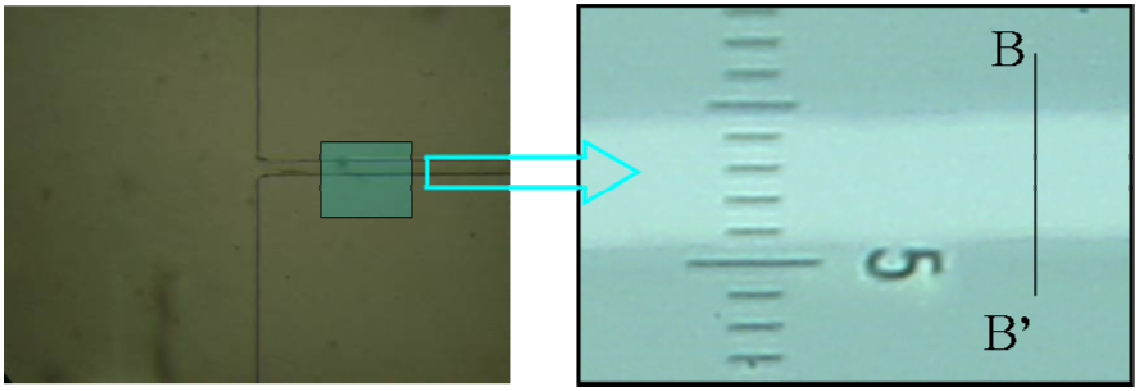

(b)

Figure 2.6. The magnified pictures of PDMS microchannel devices (a) multi channels and (b) single channel

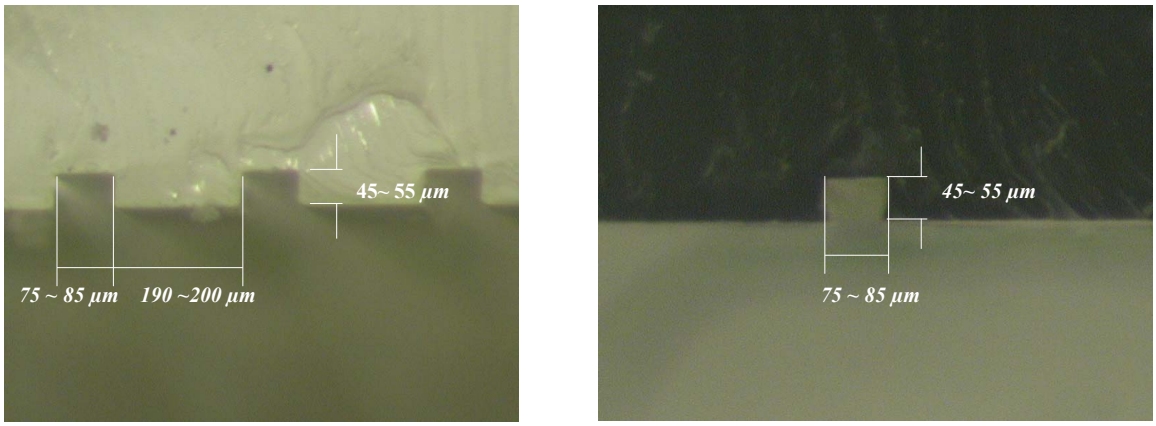

(a) (b)

Figure 2.7. Cross sectional pictures of PDMS microchannels (a) multi channels and (b) single channel

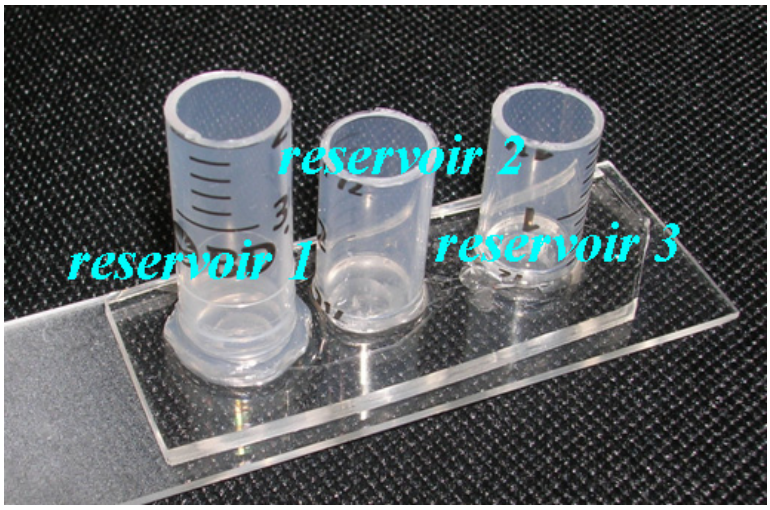

Figure 2.8. Joining the molded PDMS and reservoirs. PDMS is used as glue.

2.3.5. Bonding

Among the several bonding methods, the adhesive bonding is commonly used. However, the disadvantage of using adhesive bonding method is that adhesives such as epoxy could possibly block the flow of the liquid in the channels. For example, resin-gas injection assisted bonding leaves a little resin in the corner of the channels and reservoir [34]. Additionally, to generate liquid flow in the microchannel, surface properties have to be considered because surface tension becomes a dominant force in micro scale flow. Therefore, it is hard to drive flow in the channels without any surface modification. To solve these problems at the bonding stage, diluted hydrochloride (HCl) bonding has been introduced in recent years. This bonding technique is very simple and can be completed is an hour. Because HCl bonding can be reversible, PDMS device may be reused for more bonding. Another advantage is that it can modify surface properties in the channel from hydrophobic to hydrophilic to facilitate the liquid flow easily (Figure 2.9).

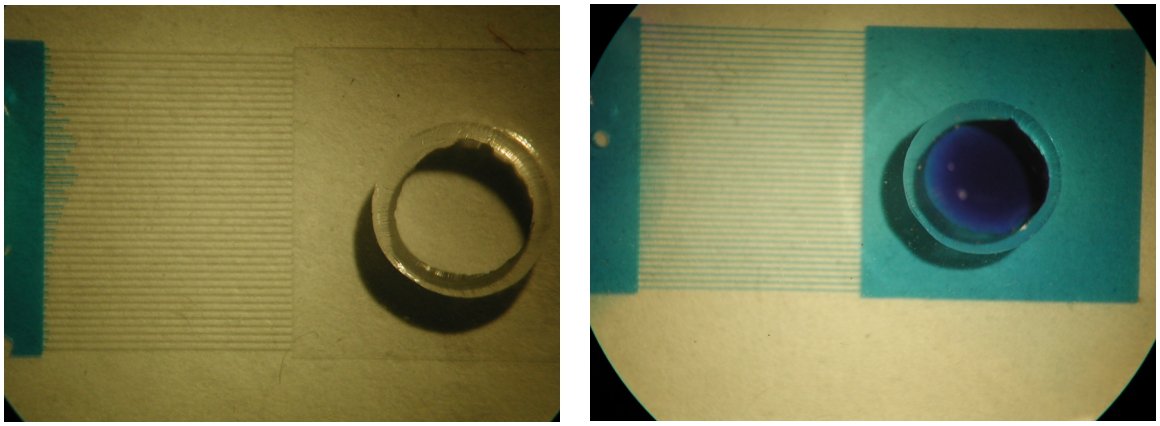

(a) (b)

Figure 2.9. Surface tension effect in the microchannels. (a) The dye hardly flow without surface modification. (b) After HCl bonding, the dye easily fills in the microchannels

To complete the HCl bonding process, we first took one of the patterns, single or multiple channels that is cut from cured PDMS. After cleaning the devices, including a plate glass and PDMS microchannels, using clean compressed air, they are then put into the diluted HCl solution (0.1% concentration). The diluted solution is placed on the heater and boiled for 5 *minutes*. After completing boiling, the PDMS device and a plate glass are cleaned with compressed air again. The device and the plate glass are then bonded with forces by our fingers. Following this bonding process, containers are carefully set at the punched holes to form reservoirs. Finally, the bonded device is left at room temperature for 10 *minutes* after 10 *minutes* degassing process in a vacuum oven.

2.4. Defects-free fabrication

Several obstacles must be confronted during the fabrication processes. Such obstacles have to be diminished and avoided to produce good quality PDMS microfluidic devices. Defects-free fabrication starts at design process. The collapse, for example, easily appears when the channel's height is too smaller than its width as shown in Figure 2.10. Therefore, the dimensions of channel are first consideration before starting fabrication. The other example of obstacles is reducing the number of bubbles on the wafer during spin-coating and baking. Therefore, we found several defect-free conditions through trial and error. By following defect-free fabrication processes listed in Table 2.1, the PDMS microfluidic devices can be completed without cleanroom facility.

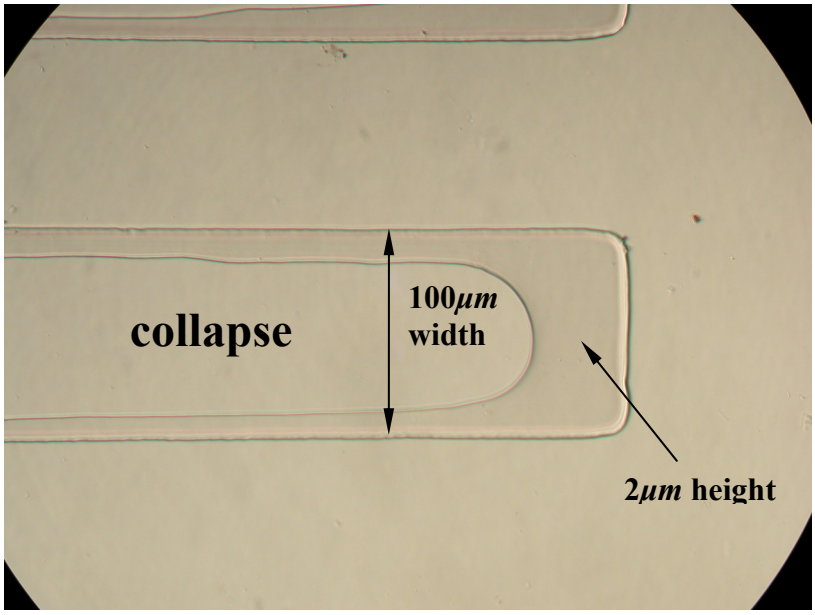

Figure 2.10. An example of the collapse which occurs when the height of PDMS channel is relatively smaller than width.

Table 2.1. Considerations for defect-free fabrication

Process	Considerations
Designing	▪ The ratio between height and width must be considered to avoid collapse after completing the PDMS microfluidic device
Coating	▪ Wafer must be cleaned by compressed air before coating ▪ Dust must be removed as much as possible ▪ An ample amount of photoresist is required to cover whole wafer ▪ Appropriate angular acceleration, spin speed, and time are necessary ▪ Spin-coating must start immediately after photoresist is poured on the wafer
UV exposing	▪ The printed side of the transparency is in direct contact with the silicon wafer before starting UV exposing ▪ Over exposure causes wider dimensions and etching problems. ▪ Under exposure causes detaching patterns from the wafer
Etching	▪ Etch the exposed wafer as soon as possible ▪ Etch the wafer by applying SU-8 developer drops ▪ Dry etched wafer using purified compressed air ▪ Repeat etching process until the patterns appear clearly
Molding	▪ Degas the PDMS mixture ▪ Use ample amount of PDMS ▪ Make PDMS devices with proper thickness to avoid the collapse ▪ Perform degas process with room temperature in the vacuum oven ▪ Cure with 65 ~ 70 ℃ at least 2 hours after degassing
Bonding	▪ Apply moderate pressure to bond plate glass and the PDMS device ▪ To fill devices with solution easily, inject solution within 2 hours after bonding.

2.5. Results and discussion

To detect any leakage, blue dye is filled in one side. The dye goes through the inlet reservoir and the microchannels. Then it finally reaches at the other side as shown in Figure 2.11 (a). After dye is filled in the whole microchannel, no leakage or blockage in the bonded PDMS microchannel is detected. Figure 2.11 shows the bonded microchannels filled with dye and magnified portion of one part of multiple microchannels. According to Figure 2.11, we could conclude that diluted HCl bonding method is very useful for micro-fluidic PDMS devices.

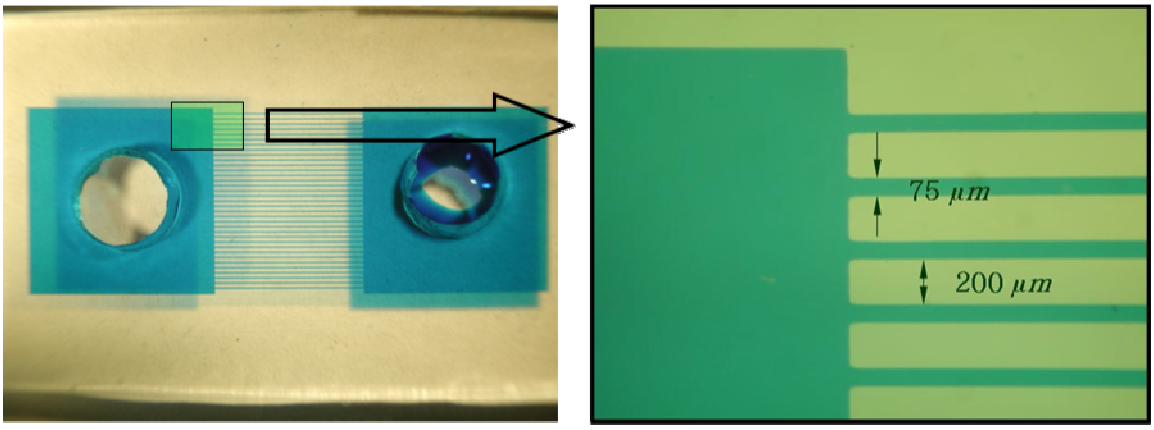

(a) (b)

Figure 2.11. Top view of a bonded micro-fluidic PDMS device filled with dye

After completing the fabrication of microchannels, we can reach at several conclusions. First, the PDMS microchannel can be fabricated without cleanroom facilities. However, whether the fabricated micro-channels can achieve small feature size is yet to be determined. We have developed protocol to make the process repeatable and the

fabricated device defects-free. Additionally, micro-channels can be sealed without any blockage and leakage using diluted HCl.

Chapter 3

MATHEMATICAL ANALYSIS FOR LOW REYNOLD'S NUMBERS FLUID FLOW IN THE MICROCHANNELS

3.1. Introduction

The rapidly growing field of research on microelectromechanical systems (MEMS) has affected the development of small biological systems and devices such as micro-total analysis systems (μTAS) and Lab-on-the-chip (LOC) in recent years [42-47]. One main advantage of applications of microchannels-based microfluidic devices is that laboratory examinations of samples can be completed in much less time, with less wasted material and pollution. Therefore, microfluidic devices are becoming more prevalent both in commercial and scientific fields [3, 4, 42-45].

The transportation of fluid in the microchannels is an important topic of interest in engineering and medical science to develop micro sized mixers, pumps, and sorters. Analyzing the fluid flow in microchannels is also important because the liquids are the most important media in biomedical analysis and diagnostics. Therefore, one key to a well-functioning LOC is the quantitatively controlled flow and mass in the microchannels. Even though the flow velocities and directions can be observed and measured using microscopes or other instruments, it is also important to predict and to control flow in the complex microchannels before designing and constructing them. Therefore, many microchannels' flow analysis researches are documented [48-52] and many studies have been conducted to develop microfluidic devices in recent years [53-58].

Precise control of flow directions and velocities is not easy in short microchannels using hydrostatic pressures because the maximum velocity is in inverse proportion to length. Additionally, the flow velocity is dictated by the pressure differences and the channel geometry. Therefore, the length of channel has to be long or the pressure differences have to be small to generate slow flow.

In this chapter, we introduce a three reservoir design which can generate slow flow in short main channels. We will also discuss the mathematical models of the three reservoirs microfluidic systems (TRMS) to control the flow. TRMS are mainly consisting of three reservoirs, two driven channels (channel A), main channels (channel B), and outlet channels (channel C). Depending on numbers of main channels, TRMS may have junctions and junction channels (JC). In TRMS, if three channels intersect at one point, we call this point ‘junction’. In addition, if a channel begins and ends at junctions, we call these channels ‘junction channels (JC)’. The channel connecting reservoir 2 to a junction is called the main channel and the channel connecting reservoir 1 to a junction is called the driven channel. If the channel connects between a junction and reservoir 3 we call this channel ‘outlet channel’. Figure 3.1 clarifies TRMS components.

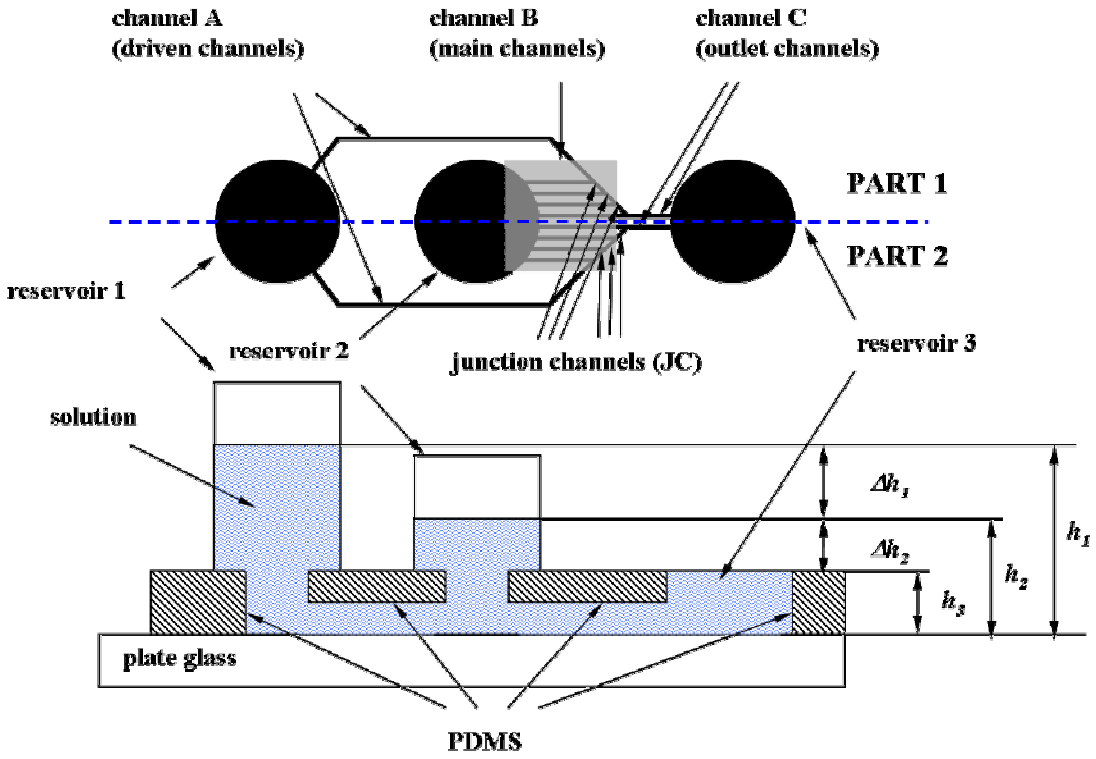

Figure 3.1. The microfluidic system (Three Reservoirs Microfluidic System : TRMS) which consists of three reservoirs generating hydrostatic pressures, two driven channels (PART 1 and PART 2 have a channel respectively), 2*M* main channels (PART 1 and PART 2 have *M* channels respectively), 2(*M*-1) junction channels (PART 1 and PART 2 have *M*-1 channels respectively), and one or two outlet channels.

The mathematical models start from the single rectangular channel. Using Navier-Stokes equation, the flow rate (Q) and the flow velocity (u) for a single channel model can be expressed in terms of pressures and geometries, such as lengths and widths. Both the flow rate and the flow velocity are applied to several TRMS models to find out unknown pressure at the junctions. The unknown pressures and given pressures are applied to formulate the maximum flow velocities in each main channel. In addition, the maximum flow velocities in single channel and in a TRMS with a single main channel will also be compared.

3.2. Single rectangular microchannel

The mathematical analysis for low Reynold's number flow (associated with fluid flow) in the multi main microchannels can be calculated using a single channel model. The single rectangular channel model consists of *2b* height along the z-direction, *2a* width and *l* length as shown in Figure 3.2. Since the flow velocity is determined by the pressures in the reservoirs and the flow resistance, we calculated the relationship between the flow rate and the channel geometry in the following. In addition, the fluid velocity and flow rate in a channel with a rectangular cross section are well described by Seo [32] and Pozrikidis [59].

The equation that governs the motion of the Newtonian liquid is the Navier-Stokes equation described by:

$$\rho\left[\frac{\partial \vec{u}}{\partial t} + \vec{u}\cdot\nabla\vec{u}\right] = -\nabla P + \mu\nabla^2\vec{u} + \vec{g} \tag{3.1}$$

where $\vec{u}$ is the velocity, P is pressure, $\vec{g}$ is gravitation acceleration, ρ is liquid density, and μ is liquid viscosity.

Viscous effect dominates for flow in the microchannels; the inertia force and gravity can be ignored. Therefore, the equation can be written as:

$$-\nabla P + \mu\nabla^2\vec{u} = 0. \tag{3.2}$$

For flow in a long channel as shown in Figure 3.2, if the length of the channel is much greater than the cross section dimensions, the flow can be considered unidirectional.

Therefore, the velocity only has one component in the streamwise direction.

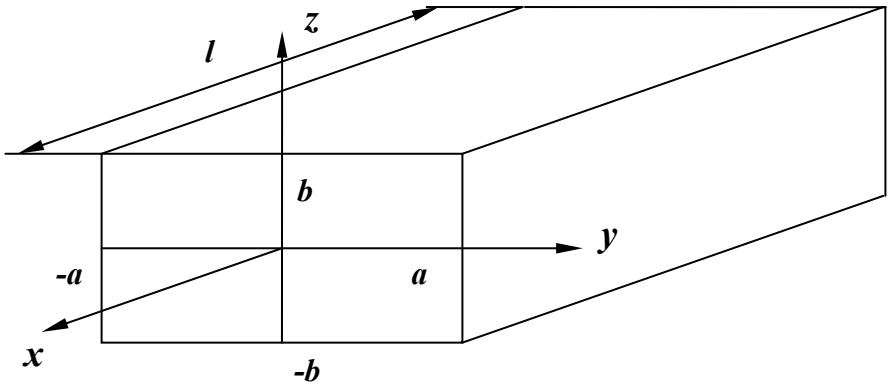

Figure 3.2. Geometry of a microchannel with rectangular crosssection.

The equation of motion can be written as:

$$\frac{\partial^2 u}{\partial y^2} + \frac{\partial^2 u}{\partial z^2} = -\frac{G}{\mu} \tag{3.3}$$

where $-G$ is the pressure gradient in the streamwise direction (i.e. $G = -\partial P/\partial x$). Corresponding to the rectangular channel in Figure 3.2, the no-slip boundary conditions are:

$$u\,(y = \pm a) = u\,(z = \pm b) = 0\,. \tag{3.4}$$

The partial differential equation (3.3) is known as Poisson's equation. We solve Poisson's equation by first converting it into Laplace's equation. Let $u = G/2\mu(b^2 - z^2) + \tilde{u}$ and substitute it into equation (3.3). We obtain the following

Laplace's equation:

$$\frac{\partial^2 \tilde{u}}{\partial y^2} + \frac{\partial^2 \tilde{u}}{\partial z^2} = 0 . \tag{3.5}$$

The boundary conditions are

$$\tilde{u}(z = \pm b) = 0$$

and

$$\tilde{u}\ (y = \pm a\ )\ = -\frac{G}{2\mu}\ (\ b^2\ -\ z^2\ ) . \tag{3.6}$$

Laplace's equation over a rectangular domain can be solved by separating the variables. Let $\tilde{u} = Y(y)Z(z)$ and substitute it into Laplace's equation. Then we have

$$\frac{Y''}{Y} = -\frac{Z''}{Z} . \tag{3.7}$$

The boundary condition for *Z* is

$$Z(-b) = Z(b) = 0 . \tag{3.8}$$

Since the two sides of equation (3.7) are functions of *y* and *z* respectively, we set these equal to a constant. Only positive constants are allowed by the boundary condition of *Z(z)*.

$$\frac{Y''}{Y} = -\frac{Z''}{Z} = \alpha^2 \tag{3.9}$$

Solving for Z, we get

$$Z = A\cos(\alpha z) + B\sin(\alpha z). \tag{3.10}$$

Boundary conditions require

$$B = 0$$

and

$$\alpha = \frac{(2n-1)\pi}{2b}. \tag{3.11}$$

Similarly, we solve for $\boldsymbol{Y}$ to get

$$Y = C\cosh\frac{(2n-1)\pi}{2b}y. \tag{3.12}$$

In the above expressions, n = 1, 2, 3,…

The complete solution of Laplace's equation can be written as superposition of the solution obtained above

$$\tilde{u} = \sum_{n=1}^{\infty} C_n \cosh\left[\frac{(2n-1)\pi}{2b}y\right]\cos\left[\frac{(2n-1)\pi}{2b}z\right] \tag{3.13}$$

where the coefficients C_n are determined by the boundary condition (3.6) i.e.

$$\tilde{u}(y = \pm a, z) = \sum_{n=1}^{\infty} C_n \cosh\left[\frac{(2n-1)\pi}{2b}a\right]\cos\left[\frac{(2n-1)\pi}{2b}z\right]$$

$$= -\frac{G}{2\mu}(b^2 - z^2)\,. \tag{3.14}$$

The coefficients are obtained by expanding $-\frac{G}{2\mu}(b^2 - z^2)$ as Fourier series i.e.

$$-\frac{G}{2\mu}(b^2 - z^2) = \sum_{n=1}^{\infty} d_n \cos\frac{(2n-1)\pi}{2b} z \tag{3.15}$$

where, according to Fourier series expansion

$$d_n = \frac{2}{b}\int_0^b -\frac{G}{2\mu}(b^2 - z^2)\cos\left[\frac{(2n-1)\pi}{2b} z\right] dz\,. \tag{3.16}$$

The above integral can be evaluated easily using Mathematica® or Matlab®. Then we get

$$d_n = \frac{Gb^2}{\mu\alpha_n^3}(-1)^n \tag{3.17}$$

where $\alpha_n = (2n-1)\pi/2$.

Since $C_n \cosh\left[\frac{(2n-1)\pi}{2b} a\right] = d_n$, we have

$$C_n = \frac{2G}{\mu} b^2 \frac{(-1)^n}{\alpha_n^3 \cosh(\alpha_n a/b)}\,. \tag{3.18}$$

Then, we get the fluid velocity in the channels with rectangular cross section as shown in Figure 3.3 and can express it as:

$$u(y,z)=\frac{G}{2\mu}\left[b^2-z^2+4b^2\sum_{n=1}^{\infty}\frac{(-1)^n}{\alpha_n^3}\frac{\cosh(\alpha_n y/b)}{\cosh(\alpha_n a/b)}\cos(\alpha_n\frac{z}{b})\right]. \tag{3.19}$$

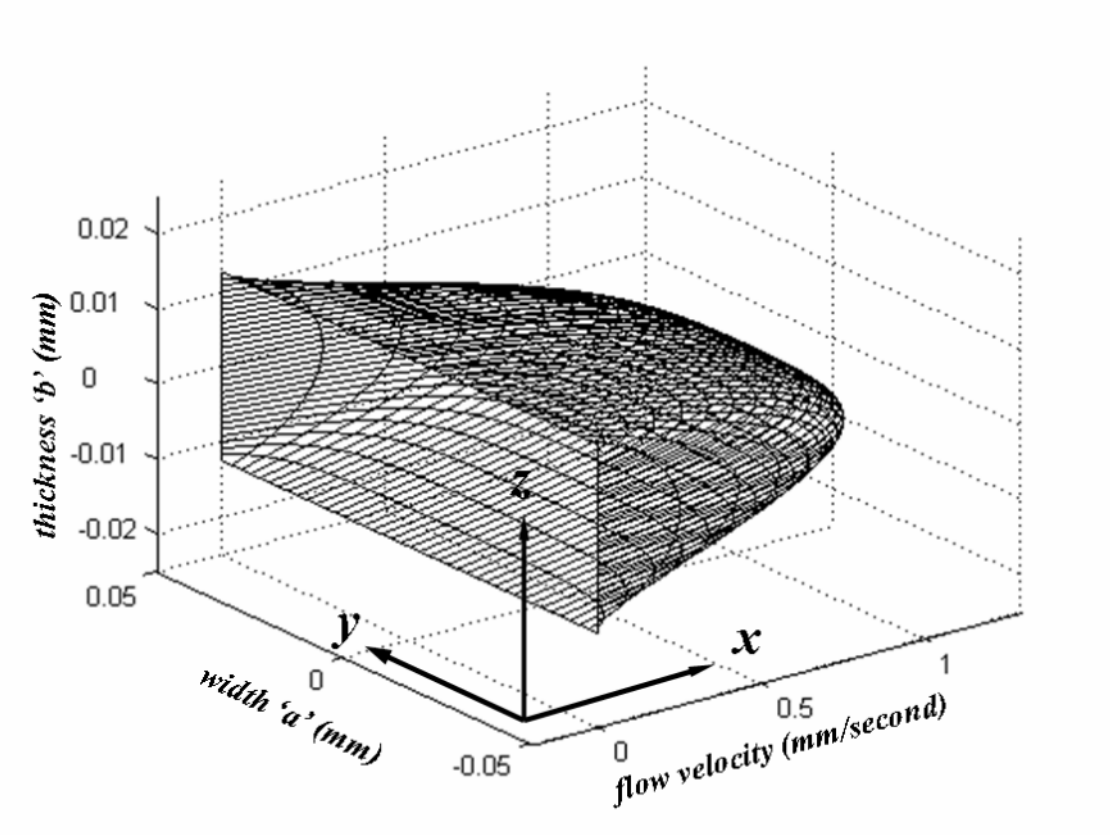

Figure 3.3. The profile of the flow in the single rectangular cross-section microchannel consisting of 4*mm* length, 100μm width, and 25 μm height when 48.9 N/m^2 pressure is applied.

Furthermore, integrating over the cross-section, we can also find the volumetric flow rate Q as;

$$Q=4\int_0^a\int_0^b u(y,z)dzdy\,. \tag{3.20}$$

The above integral can be evaluated easily using Mathematica®. Finally, we get

$$Q = \frac{4Gab^3}{3\mu}\left[1 - \frac{6b}{a}S_Q(a/b)\right]. \tag{3.21}$$

where

$$S_Q(a/b) = \sum_{n=1}^{\infty} \frac{\tanh(\alpha_n a/b)}{\alpha_n^5} \ .$$

We can assume that the center of the channel (y = 0 and z = 0) is the point of the maximum flow velocity (u_{max}). By substituting y = 0, and z = 0 into equation (3.19), the velocity at the center of the channel can be expressed as:

$$u_{max} = u(0,\ 0) = \frac{G}{2\mu}\left[b^2 + 4b^2 S_{u\_max}(a/b)\right] \tag{3.22}$$

where

$$S_{u\_max}(a/b) = \sum_{n=1}^{\infty} \frac{(-1)^n}{\alpha_n^3 \cosh(\alpha_n a/b)}.$$

In the above equations, both functions, $S_Q(a/b)$ and $S_{u\_max}(a/b)$, are the functions of the ratio a/b where $2a$ is the width and $2b$ is the thickness of the channel. In particular, $S_Q(a/b)$ and $S_{u\_max}(a/b)$ converge to 0.10504 and 0 respectively when $a/b = \infty$ (Figure 3.4). Although the convergence points for $S_Q(a/b)$ and $S_{u\_max}(a/b)$ exist if $a/b = \infty$, we can assume $S_Q(a/b \geq 4) \fallingdotseq 0.10504$ and $S_{u\_max}(a/b \geq 4) \fallingdotseq 0$. Therefore, if $a/b \geq 4$, the equations (3.21) and (3.22) can be simply expressed as:

$$Q = \frac{4Gab^3}{3\mu}\left[1 - 0.10504\,\frac{6b}{a}\right] \tag{3.23}$$

and

$$u_{max} = u(0,\,0) = \frac{G}{2\mu}\,b^2 . \tag{3.24}$$

In addition to velocity and volumetric flow rate, Reynold's number (R_e) can be expressed as:

$$R_e = \frac{\rho u D_h}{\mu} \tag{3.25}$$

where ρ is the density of the liquid, u is the velocity, μ is the viscosity of the liquid and $D_h\,(=4ab/(a+b))$ is the hydraulic diameter.

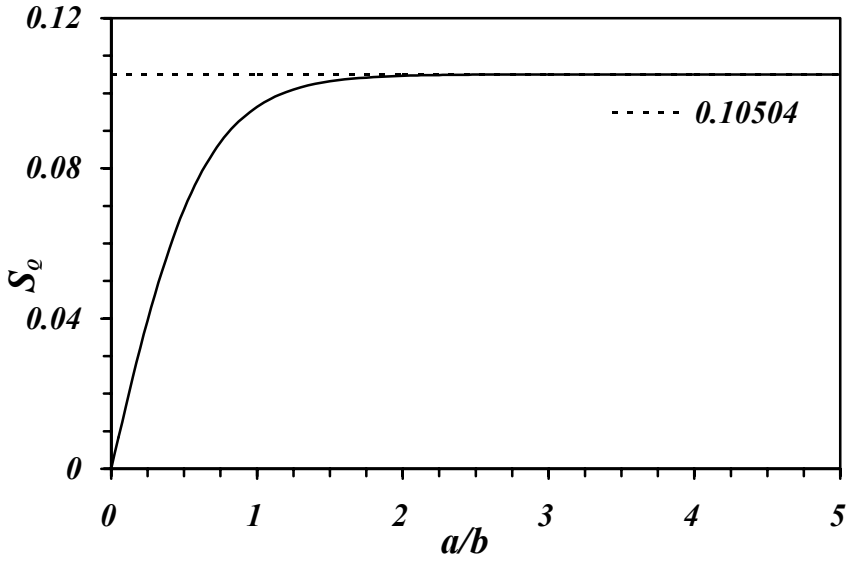

(a)

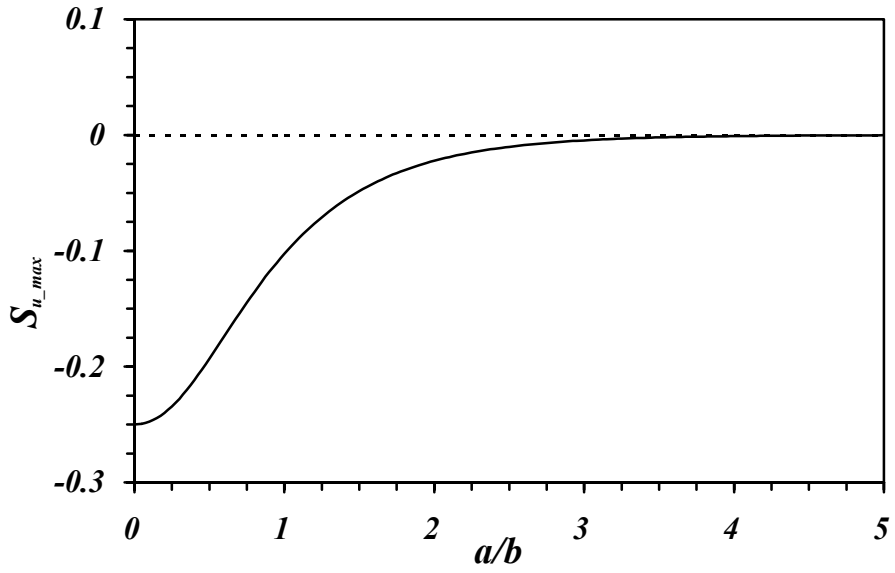

(b)

Figure 3.4. Convergence of (a) S_Q and (b) S_{u_max} as functions of the ratio *a/b*

3.4. Flow in the TRMS

To precisely control the flow rates and velocities in the main channels, we only need three reservoirs to generate hydrostatic pressures. Even though it is easier to precisely control the flow in the channels when we have more than three reservoirs, the limitations of surface area on the silicon wafers and two-dimensional design patterns hardly allow more than three reservoirs in the one design pattern. Therefore, in this section, we would like to introduce several cases of the TRMS. The unknown junction pressures can be found using equation (3.23). Afterwards, the results are applied to find the maximum flow velocities in the main channels.

3.4.1. Single main channel (one junction)

The basic TRMS design is the single main channel model as shown in Figure 3.5. This model also has the single junction point. If channels A, B, and C are denoted n = 1, 2, and 3 respectively in the single main channel model, the flow rate in each channel can be expressed using equation (3. 23) as:

$$Q_n = \frac{4G_n a_n b^3}{3\mu}\left[1 - 0.10504\,\frac{6b}{a_n}\right]. \tag{3.26}$$

where a_n denote the widths of the each channel which have same height b and we assume that the cross sectional dimensions of channel are such that $a_n/b \geq 4$. The flow velocities can also be generalized using equation (3.19) as:

$$u_n(y,z) = \frac{G_n}{2\mu} A_n(y,z) \tag{3.27}$$

where

$$A_n(y,z) = [b^2 - z^2 + 4b^2 \sum_{N=1}^{\infty} \frac{(-1)^N \cosh(\alpha_N y/b)}{\alpha_N^3 \cosh(\alpha_N a_n/b)} \cos(\alpha_N \frac{z}{b})]. \tag{3.28}$$

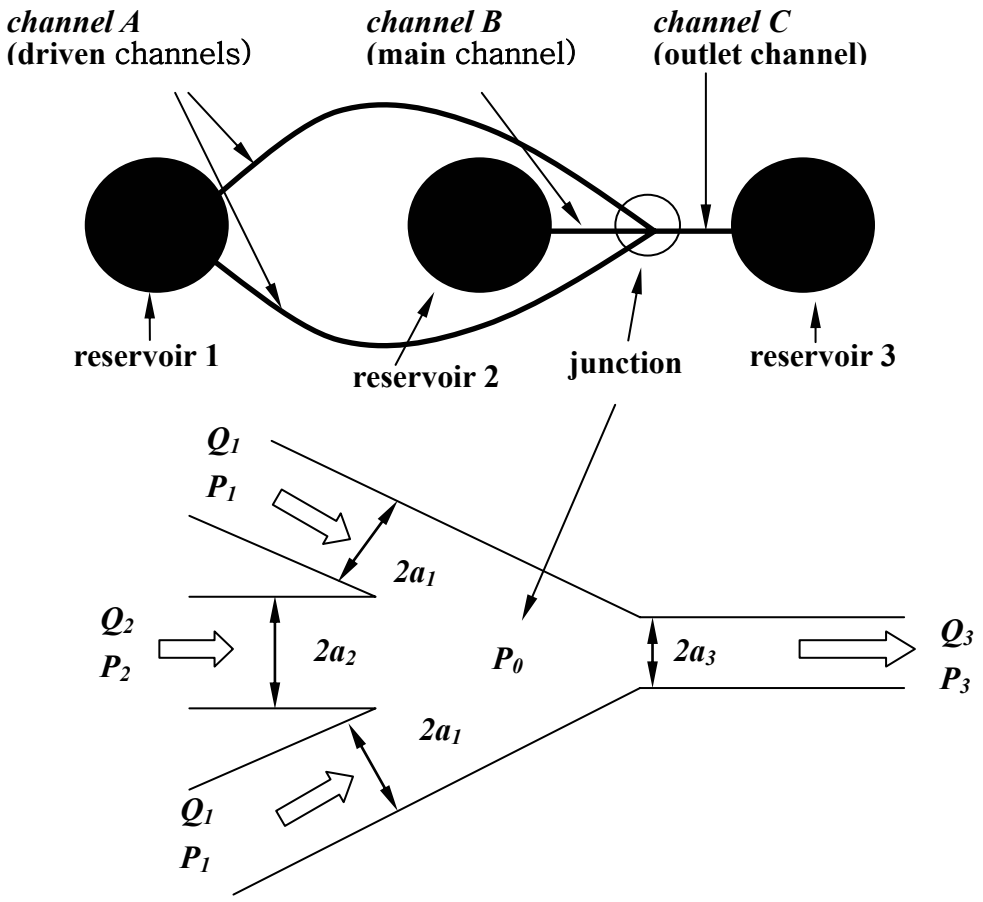

Figure 3.5. The basic TRMS design which consists of two driven channels (channel A), one main channel (channel B), and one outlet channel (channel C).

Let P_1, P_2, and P_3 be the pressure at each reservoir and P_0 be the pressure at the junction. The pressure differences can be expressed as:

$$\begin{aligned} \Delta P_1 &= P_1 - P_0 \\ \Delta P_2 &= P_2 - P_0 \\ \Delta P_3 &= P_0 - P_3 \end{aligned} . \tag{3.29}$$

The pressure gradient can be expressed in terms of the pressure at the reservoir if the unknown pressures at the junction can be found:

$$G_n = \Delta P_n / l_n \tag{3.30}$$

where l_n is the length of channel.

The equation (3.26) is simplified in terms of pressure difference as:

$$Q_n = B_n \Delta P_n \tag{3.31}$$

where:

$$B_n = \frac{4 a_n b^3}{3 \mu l_n} \left[1 - 0.10504 \frac{6b}{a_n} \right]. \tag{3.32}$$

To calculate the flow rates and flow velocities in the main channel using equation (3.31), the unknown pressure, P_0, at the junction must be found. To determine the unknown junction pressure P_0, referring to Figure 3.5, we obtain the continuity equation as follows:

$$2Q_1 + Q_2 = Q_3 . \tag{3.33}$$

Substituting equations (3.30) and (3.32) into the above equation, we can obtain the junction pressure P_0 as:

$$P_0 = \frac{2B_1P_1 + B_2P_2 + B_3P_3}{2B_1 + B_2 + B_3}. \tag{3.34}$$

Once the junction pressure is obtained, the pressure gradients are known and the flow velocities can be determined using equation (3.27). The pressure gradient for main channel, G_2, can be expressed in terms of three known pressures P_1, P_2, and P_3 as:

$$G_2 = \frac{B_3(P_2 - P_3) - 2B_1(P_1 - P_2)}{l_2(2B_1 + B_2 + B_3)}. \tag{3.35}$$

Note also that the pressure at each reservoir is due to the hydrostatic pressure of the liquid columns at each reservoir, i.e.

$$P_n = \rho g h_n \tag{3.36}$$

(n =1, 2, and 3 denote channel A, B, and C respectively)

where h_1, h_2, and h_3 represent the height of the liquid columns at reservoirs 1, 2, and 3 respectively. Therefore, the pressures can be obtained by measuring the height of the liquid columns at the reservoirs. The flow velocity in the main channel is thus expressed as:

$$u_2(y,z) = \frac{\rho g}{2l_2\mu(2B_1 + B_2 + B_3)}(B_3\Delta h_2 - 2B_1\Delta h_1)A_2(y,z) \tag{3.37}$$

where Δh_1 is the height difference of the liquid column between reservoir 1 and reservoir 2, and Δh_2 the difference between reservoir 2 and reservoir 3.

The lengths of main channels are one of the important considerations for developing the motile sperm sorting microfluidic devices. If the motile sperm swims a relatively long distance, it can exhaust itself. Therefore, it is better to have shorter channels for motile sperm to swim against the flow. Figure 3.6 shows the comparison of the flow velocities between the TRMS having a single main channel and the single channel having two reservoirs. The additional reservoir allows us to achieve slow flow velocity when Δh is the same without increasing the length of channel.

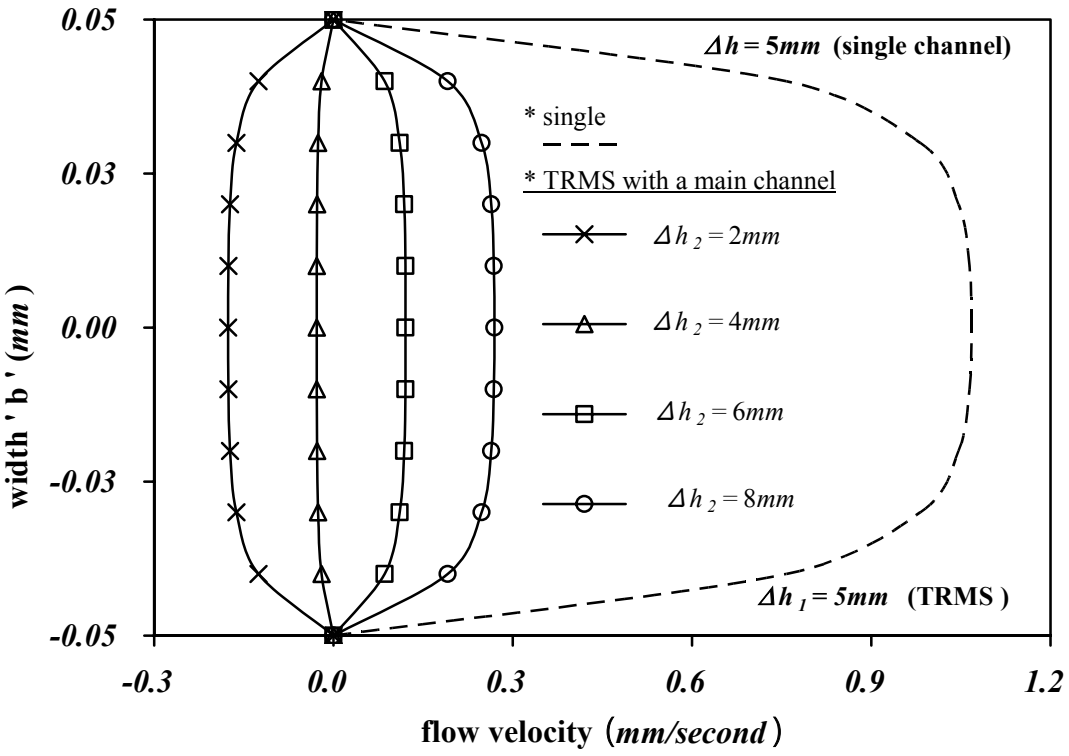

Figure 3.6. Comparison of the maximum flow velocities (when z = 0, middle of channel) between the single channel having two reservoirs (dash line) and the single main channel TRMS model (solid line) having three reservoirs. The 48.9 N/m^2 pressure ($\Delta h = \Delta h_1 = 5mm$) is applied to both models with 4mm length channels.

3.4.2. Double main channels (two junctions)

As shown in Figure 3.7, two main channels model does not have junction channels. However, it contains two junctions. Assume that the inlet flow rate and outlet flow rate are conserved in the channels. We can get a continuity equation as:

$$2Q_1 + 2Q_2 = 2Q_3 . \tag{3.38}$$

Substituting equations (3.29) and (3.31) into the above equation, we obtain the unknown junction pressures P_0 as:

$$P_0 = \frac{B_1P_1 + B_2P_2 + B_3P_3}{B_1 + B_2 + B_3} . \tag{3.39}$$

In addition, the pressure gradient for main channel, G_2, can be express in terms of three know pressures P_1, P_2, and P_3 as:

$$G_2 = \frac{B_3(P_2 - P_3) - B_1(P_1 - P_2)}{l_2(B_1 + B_2 + B_3)} . \tag{3.40}$$

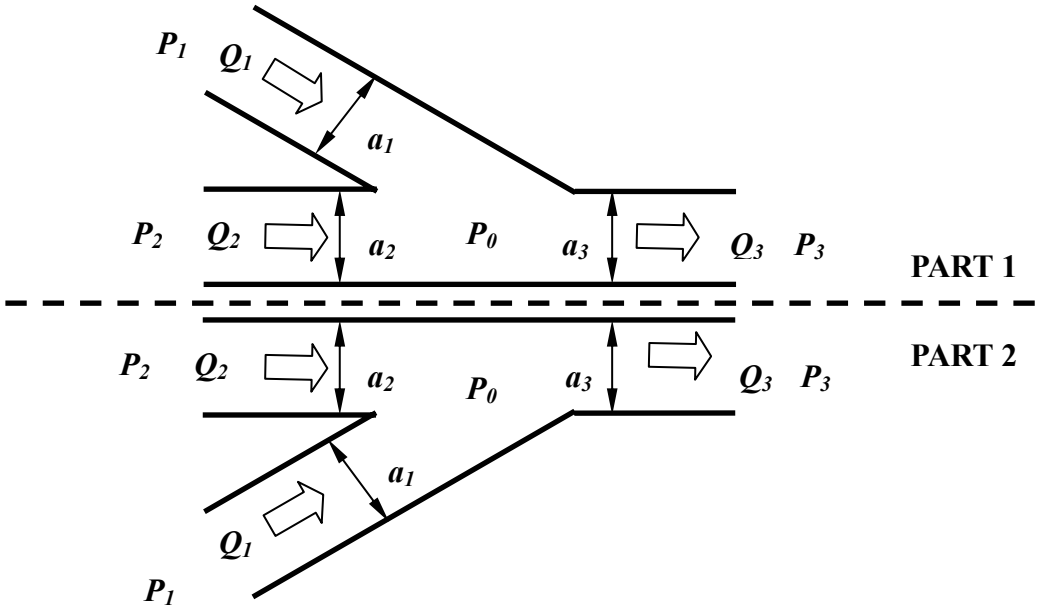

(a)

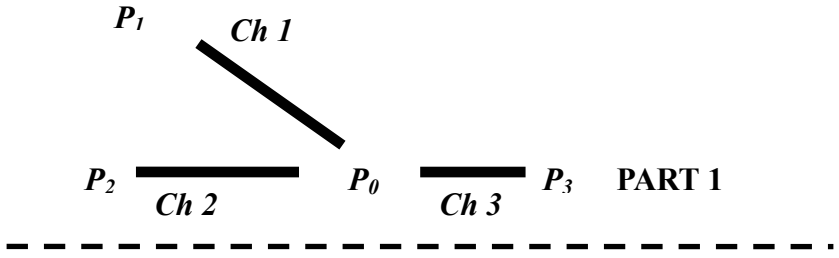

(b)

Figure 3.7. The schematic of two main channels model with (a) specifications and parameters. The simplified schematic with (b) channel numbers in PART. The PART 1 and the PART 2 each have one main channel respectively and are symmetrical.

3.4.3. Multiple main channels connected with junction channels (*M* junctions)

Similar to the single main channel model and double main channels model, the unknown pressures at the junctions must be found to calculate the flow rates and the flow velocities for a multi main channels design with junction channels. The unknown pressures at the junctions, P_0^m, can be calculated by applying the simplified flow rate equation (3.30) and the continuity equations. The continuity equations can be obtained using the flow rate relationships between channels. The flow rate relationships are determined by the number of channels and channels' geometry. If the TRMS has *M* numbers of main channels at the PART 1 and the PART 2 respectively and these main channels are connected with *M-1* junction channels as shown in Figure 3.8, the continuity equations can be generally expressed as:

$$Q_{2m-1} + Q_{2m} = Q_{2m+1}\,. \tag{3.41}$$

In the above expressions, m =1, 2, 3, …., M (M is the total number of main channels at PART 1 ; PART 1 and PART 2 are symmetrical).

To formulate calculations of the unknown pressures, let us begin with the simple design model which has two main channels in PART 1 and PART 2 respectively. PART 1 consists of two main channels, two junctions, and a junction channel in this TRMS model. Because PART 1 and PART 2 are symmetrical, we can obtain two continuity equations from equation (3.41) as:

$$\begin{aligned} Q_1 + Q_2 &= Q_3 \\ Q_3 + Q_4 &= Q_5 \end{aligned}. \tag{3.42}$$

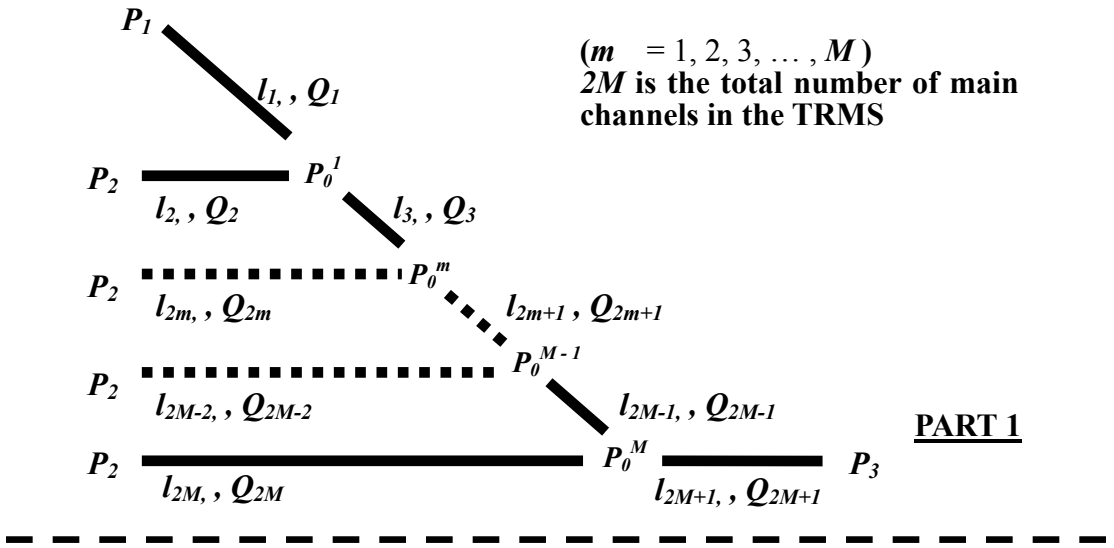

(a)

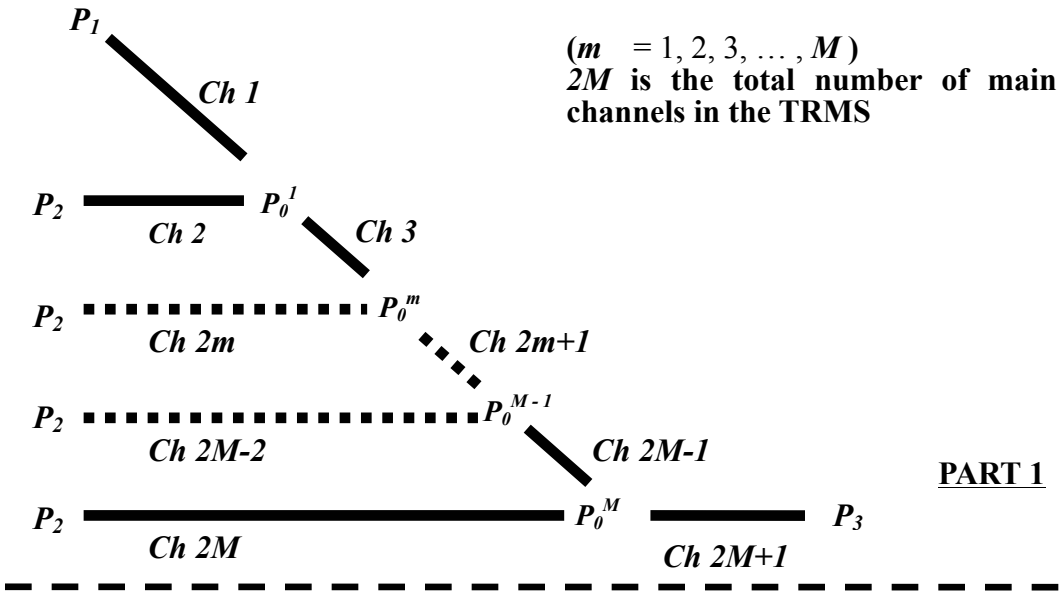

(b)

Figure 3.8. The generalized schematic of TRMS design at PART 1; (a) numbering flow rates and channels' lengths, (b) channel numbering. The design has *M* main channels and *M-1* junction channels in the PART 1. PART 1 and PART 2 are symmetrical.

The pressure difference for two main channels can be expressed as;

$$\begin{aligned}
\Delta P_1 &= P_1 - P_0^1 \\
\Delta P_2 &= P_2 - P_0^1 \\
\Delta P_3 &= P_0^1 - P_0^2 \\
\Delta P_4 &= P_2 - P_0^2 \\
\Delta P_5 &= P_0^2 - P_3
\end{aligned} \quad . \tag{3.43}$$

By applying equations (3.30), (3.42), and (3.43), we can get the two equations:

$$(B_1 + B_2 + B_3)P_0^1 - B_3 P_0^2 = B_1 P_1 + B_2 P_2 \tag{3.44}$$

and

$$-B_3 P_0^1 + (B_3 + B_4 + B_5)P_0^2 = B_4 P_2 + B_5 P_3 \,. \tag{3.45}$$

Equations (3.44) and (3.45) can be written in compact matrix form as:

$$[\hat{B}][\hat{P}_0] = [\hat{M}] \tag{3.46}$$

where

$$[\hat{B}] = \begin{bmatrix} B_1 + B_2 + B_3 & -B_3 \\ -B_3 & B_3 + B_4 + B_5 \end{bmatrix},$$

$$[\hat{P}_0] = \begin{bmatrix} P_0^1 \\ P_0^2 \end{bmatrix},$$

and

$$[\hat{M}]=\begin{bmatrix} B_1P_1 + B_2P_2 \\ B_4P_2 + B_5P_3 \end{bmatrix}.$$

The compact matrix form, equation (3. 46) consists of a 2×2 matrix $[\hat{B}]$, the 2×1 matrix $[\hat{P}_0]$, and 2×1 matrix $[\hat{M}]$. The unknown pressures at junctions, P_0^1 and P_0^2, can be found using the inverse matrix $[\hat{B}]^{-1}$ and can be expressed as:

$$[\hat{P}_0] = [\hat{B}]^{-1}\,[\hat{M}]. \tag{3.47}$$

Using the same method, we can also find the unknown pressures at the junction points if PART 1 has three main channels. Three continuity equations can be obtained from equation (3.41) because PART 1 and PART 2 are symmetrical. The continuity equations can be written as:

$$\begin{aligned} Q_1 + Q_2 &= Q_3 \\ Q_3 + Q_4 &= Q_5 \\ Q_5 + Q_6 &= Q_7 \end{aligned}. \tag{3.48}$$

There are seven pressure differences, ΔP_m (where m = 1, 2, …, 2M+1), which are related with the unknown junction pressures P_0^m. These seven pressure differences can be expressed as:

$$
\begin{aligned}
\Delta P_1 &= P_1 - P_0^1 \\
\Delta P_2 &= P_2 - P_0^1 \\
\Delta P_3 &= P_0^1 - P_0^2 \\
\Delta P_4 &= P_2 - P_0^2 \\
\Delta P_5 &= P_0^2 - P_0^3 \\
\Delta P_6 &= P_2 - P_0^3 \\
\Delta P_7 &= P_0^3 - P_3
\end{aligned}
\qquad (3.49)
$$

By applying equations (3.30), (3.48), and (3.49), we can get a matrix equation, similar to equation (3.46) as:

$$[\hat{B}][\hat{P}_0]=[\hat{M}], \qquad (3.50)$$

where

$$[\hat{B}] = \begin{bmatrix} B_1 + B_2 + B_3 & -B_3 & 0 \\ -B_3 & B_3 + B_4 + B_5 & -B_5 \\ 0 & -B_5 & B_5 + B_6 + B_7 \end{bmatrix},$$

$$[\hat{P}_0] = \begin{bmatrix} P_0^1 \\ P_0^2 \\ P_0^3 \end{bmatrix},$$

and

$$[\hat{M}] = \begin{bmatrix} B_1 P_1 + B_2 P_2 \\ B_4 P_2 \\ B_6 P_2 + B_7 P_3 \end{bmatrix}.$$

Finally, the unknown pressures, P_0^m, can be calculated by multiplying the inverse matrix $[\hat{B}]^{-1}$ and the matrix $[\hat{M}]$.

According to the above two cases, the three matrices ($[\hat{B}]$, $[\hat{P}_0]$, and $[\hat{M}]$) can be generally expressed if the TRMS has $2M$ main channels. First, the $M \times M$ matrix $[\hat{B}]$ can be generally formulated as:

$$[\hat{B}] = \begin{bmatrix} \hat{B}_{11} & \hat{B}_{12} & \cdots & 0 & \cdots & 0 \\ \hat{B}_{21} & \hat{B}_{22} & \cdots & 0 & \cdots & 0 \\ \cdot & \cdot & \cdots & \cdot & \cdots & \cdot \\ 0 & 0 & \cdots & \hat{B}_{mm} & \cdots & 0 \\ \cdot & \cdot & \cdots & \cdot & \cdots & \cdot \\ 0 & 0 & \cdots & 0 & \cdots & \hat{B}_{MM} \end{bmatrix} \tag{3.51}$$

where

$$\hat{B}_{mm} = B_{2m-1} + B_{2m} + B_{2m+1} \tag{3.52}$$

and

$$\hat{B}_{m(m-1)} = \hat{B}_{(m-1)m} = -B_{2m-1}. \tag{3.53}$$

The $M \times 1$ matrix $[\hat{P}_0]$ and $[\hat{M}]$ can be also generally formulated as:

$$[\hat{P}_0] = \begin{bmatrix} P_0^1 \\ P_0^2 \\ \cdot \\ P_0^m \\ \cdot \\ P_0^M \end{bmatrix} \tag{3.54}$$

and

$$[\hat{M}] = \begin{bmatrix} B_1 P_1 + B_2 P \\ B_4 P_2 \\ . \\ B_{2m} P_2 \\ . \\ B_{2M} P_2 + B_{2M+1} P_3 \end{bmatrix}. \tag{3.55}$$

Additionally, the pressure differences which are related to the unknown pressures can be formulated as:

$$\begin{aligned} \Delta P_1 &= P_1 - P_0^1 \\ \Delta P_{2i} &= P_2 - P_0^i \\ \Delta P_{2j+1} &= P_0^j - P_0^{j+1} \\ \Delta P_{2M+1} &= P_0^M - P_3 \end{aligned}. \tag{3.56}$$

In the above expressions, i =1, 2, 3, …., M, and j = 1, 2, 3, …., M-1 (where M is the total number of main channels in the PART 1 and PART 2 respectively). Finally, the unknown pressure can be formulated in matrix form as:

$$[\hat{P}_0] = [\hat{B}]^{-1} [\hat{M}]. \tag{3.57}$$

3.5. Maximum flow velocity in the main channels

As shown in above sections, we could find the relationships between unknown pressures at junctions and given pressures at reservoirs. The unknown pressures for the designs of single and double main channels can be simply expressed as equations (3.34) and (3.49). In addition, the unknown pressures, P_0^m, at the junctions for the TRMS having

M main channels can be formulated using the matrix multiplication as equation (3. 57). In particular, once the unknown pressures are found, the maximum flow velocities in each channel, $u_{n\_\max}$, can also be calculated and can be expressed in terms of pressure differences from equation (3. 25) as:

$$u_{n\_\max} = \frac{b^2}{2\mu l_n} \Delta P_n . \tag{3.58}$$

If *n* is an even number, it denotes the main channels, and the maximum flow velocities in the main channels can be generally formulated as:

$$u_{2m\_\max} = \frac{b^2}{2\mu l_{2m}} \Delta P_{2m} \tag{3.59}$$

where *m* =1, 2, 3, …., *M* (*M* is total number of main channels at PART 1 and PART 2 respectively). Since $[\hat{P}_0] = [\hat{B}]^{-1} [\hat{M}]$, the matrix of pressure differences between reservoir 2 and the junction points, $[\Delta P_{2m}]$, can be written as:

$$[\Delta P_{2m}] = [\hat{P}_2] - [\hat{P}_0] = [\hat{P}_2] - ([\hat{B}]^{-1} [\hat{M}])$$

$$= \begin{bmatrix} P_2 \\ P_2 \\ \cdot \\ P_2 \\ \cdot \\ P_2 \end{bmatrix} - \begin{bmatrix} P_0^1 \\ P_0^2 \\ \cdot \\ P_0^m \\ \cdot \\ P_0^M \end{bmatrix}. \tag{3.60}$$

By substituting equation (3. 60) to equation (3. 58), finally, the maximum flow

velocities matrix, $[\hat{u}_{max}^{main}]$, for the main channels can be formulated as:

$$[\hat{u}_{max}^{main}] = \frac{b^2}{2\mu l_{2i}}[\Delta P_{2i}]. \tag{3.61}$$

3.6. Conclusions

Using the fluid flow equation, we can find the junction pressures in the TRMS. Even though the TRMS has many main channels, the maximum flow velocities can be estimated after getting unknown junction pressures using single channel flow calculations. Therefore, finding maximum flow velocities in main channels is useful to design any TRMS requiring specific flow velocity ranges.

Chapter 4

FLOW CONTROL IN THE MAIN CHANNELS AND OPTIMIZATION OF TRMS DESIGNS

4.1. Introduction

Understanding the dynamics of fluid flow in the microchannels is important in designing and developing the microfluidic devices since manipulations using them are closely related with the microflows. In the microflows, the pressure driven flow and the electrokinetic flow are commonly used methods to actuate fluid through microchannels [60-62]. Additionally, controlling the flow in the microchannels is also important in medical science and biological engineering.

Recent studies of flow in microchannels have been focused on developing functions and enhancing performance of the microfluidic devices [63-66]. Therefore, experimental and analytical studies for the microscale fluid flow phenomenon have been performed and are well documented [67-70]. In addition, the control of microflow has been studied and reported. Hahm et al. [71] present numerical simulation results for flow and species transport control in grooved microchannels using locally applied electric fields and zeta potential patterned groove surfaces. The resulting mixed electro-osmotic/pressure-driven flow enables entrapment and release of prescribed amounts of scalar species in the microchannels. Esashi [72] has reported an integrated micro flow control system consisting of a small thermal mass flow sensor and a normally closed

microvalve to precisely control gas**.** Chen et al. [73] have analyzed the mixing phenomena for two fluid streams in pressure-driven rectangular microchannel. They also directly compared with measurements of mixing intensity for a wide range of aspect ratio.

Controlling of fluid flow in the microfluidic devices is the main topic of this chapter. We will discuss two issues; 1) designing channel dimensions to control flows using hydrostatic pressures and; 2) optimizing TRMS design to obtain the same flow velocities in multiple main channels. We will show how the geometries and the pressures affect the flow in the main channels. We also explain how the maximum flow velocity is effectively controlled within desired ranges.

4.2. Controlling pressure driven flow in the TRMS main channels

In the pressure driven microflow, the pressure can be a main parameter to generate fluid transport in the microchannels. The flow velocities and directions can be controlled by applying pressure. Mechanical micropumps are possible ways to generate pressure and fluid flow. However, TRMS uses the height differences in liquid columns in the reservoirs to generate hydrostatic pressures. In addition to pressures, the dimensions of channels, such as lengths and widths, affect the fluid flow. By controlling these parameters, the flow velocities in TRMS main channels are theoretically adjusted in specific ranges. Therefore, it is important to define these parameters using theoretical results and it is also useful for designing TRMS properly.

As mentioned previous chapter, TRMS are mainly consisting of three reservoirs, two driven channels (channel A), main channels (channel B), and outlet channels (channel C). Depending on numbers of main channels, TRMS may have junctions and

junction channels (JC). We define a junction to be the point where three channels meet. In addition, a channel which begins and ends at junctions is called a junction channels (JC). The channel connecting reservoir 2 to a junction is called the main channel and the channel connecting reservoir 1 to a junction is called the driven channel. If the channel connects between a junction and reservoir 3 we call this channel 'outlet channel'.

4.2.1. TRMS with no junction channels (NJC-TRMS)

There are two No-Junction-Channel TRMS (NJC-TRMS) designs. Figure 4.1 (a) and (b) show two designs which have junctions but without junction channels. The first one is a single main channel TRMS (SMC-TRMS) which consists of two driven channels and an outlet channel as shown in Figure 4.1 (a). The double main channels TRMS (DMC-TRMS) is another possible design of NJC-TRMS. The DMC-TRMS consists of two main channels and two outlet channels as shown in Figure 4.1 (b). The maximum flow velocities in main channels are calculated for channel widths $a_1=100\ \mu m$ and $a_2=a_3=50\ \mu m$.

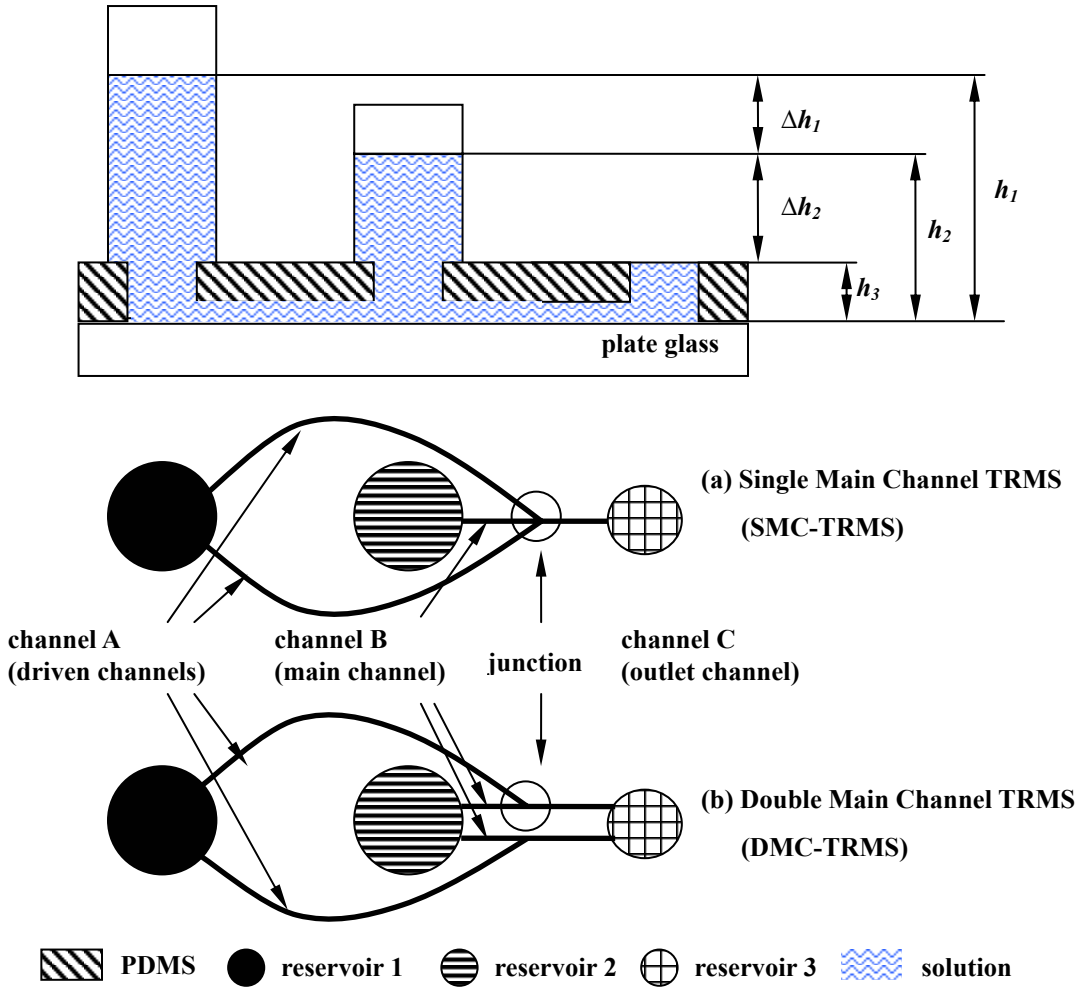

Figure 4.1. Schematic of NJC-TRMS with (a) single main channel and (b) double main channels

4.2.1.1. SMC-TRMS

The SMC-TRMS consists of two driven channels, a single main channel, and a single outlet channel as shown in Figure 4.1 (a) and Figure 4.2. Let l_1, l_2, and l_3 be the lengths of driven channels, the main channel, and the outlet channel respectively. The hydrostatic pressures are generated in three reservoirs by height of solution. The indexes, h_1, h_2, and h_3 as shown in Figure 4.1 (a), indicate the heights of solutions in reservoir 1,

reservoir 2, and reservoir 3 respectively. From equation (3.37), the flow direction in main channel points toward reservoir 2 from the junction, if $\Delta h_1 > \frac{B_3}{2B_1}\Delta h_2$. We call this flow 'reverse flow', as shown in Figure 4.2. Additionally, the thickness of the channel also affects the flow velocity contours as shown in Figure 4.3.

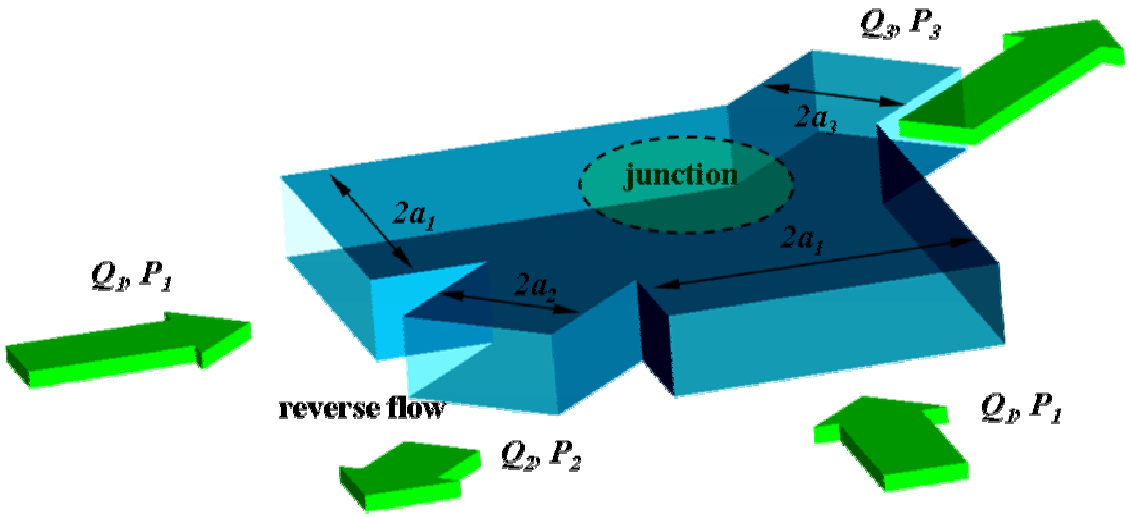

Figure 4.2. The schematic of flow directions at the junction if $\Delta h_1 > \frac{B_3}{2B_1}\Delta h_2$

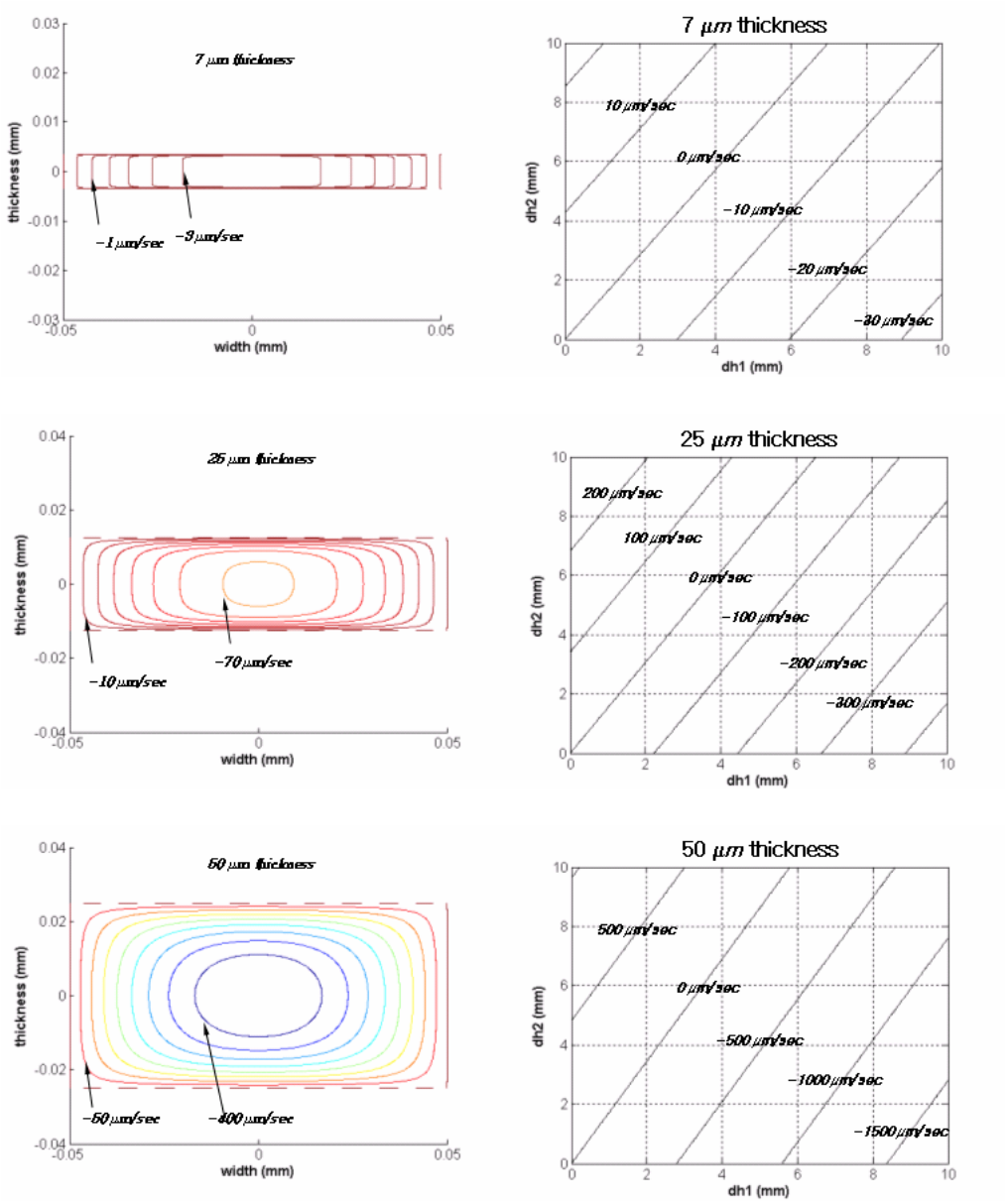

(a) (b)

Figure 4.3. Velocity contours for three different channel heights 7 μm, 25 μm, and 50 μm when the single main channel TRMS has dimensions a_1=100 μm, a_2=a_3=50 μm, l_1=23.5 mm, l_2=8 mm, and l_3=5.5 mm : (a) The contours correspond to pressure differences: Δh_1= 6.9 mm and Δh_2= 7.3 mm. (b) Dependence of maximum flow velocity on pressure differences Δh_1 and Δh_2 for channels of different heights: 7 μm, 25 μm, and 50 μm respectively.

The lengths of driven channels affect the maximum flow velocity in the main channel as well as the pressures (Figure 4. 4). The magnitude of maximum flow velocity is increased when the lengths of the driven channels are decreased. Additionally, the lengths of the main channel and the outlet channel also affect the maximum velocity as shown in Figure 4.5 (a). Figure 4.5 (b) shows that the maximum flow velocity in the main channel (u_{2_max}) is smaller than the maximum flow velocities in the driven channels and the outlet channel. The pressure differences between reservoirs are also important parameters to sensitively control the flow velocity and direction in the main channel. Figure 4.6 shows the sensitivity of the flow velocity in the main channel depending on ratio of height differences (pressures' ratio, $\Delta h_1/\Delta h_2$). Increasing the height differences causes increasing velocity gradient.

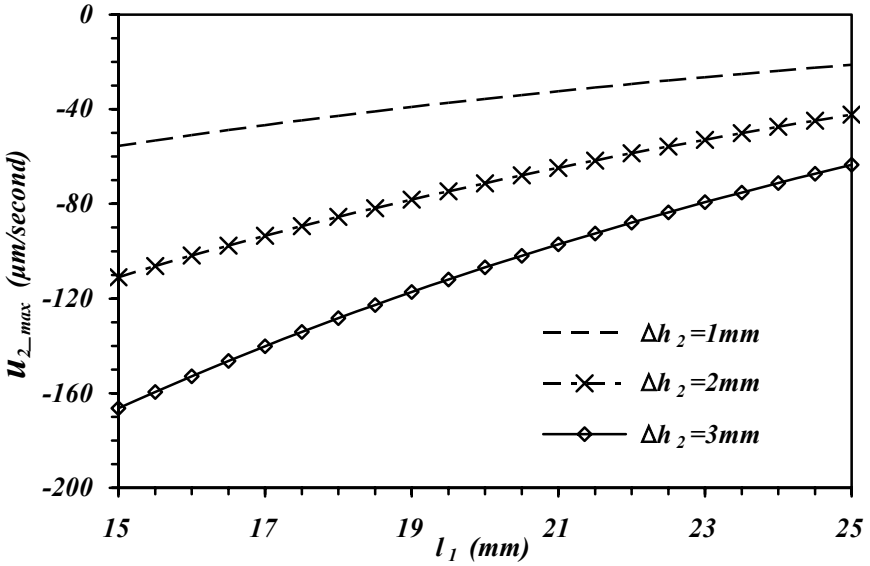

Figure 4.4. The maximum flow velocity in the main channel of SMC-TRMS depending on the length of driven channel, l_1. ($\Delta h_1/\Delta h_2$= 2, l_2=*8 mm*, and l_3=*4 mm*)

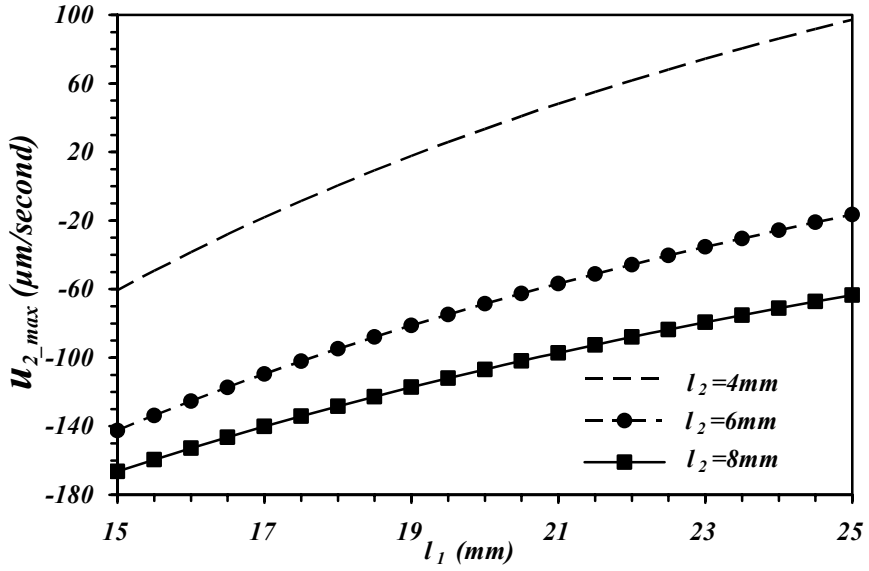

(a)

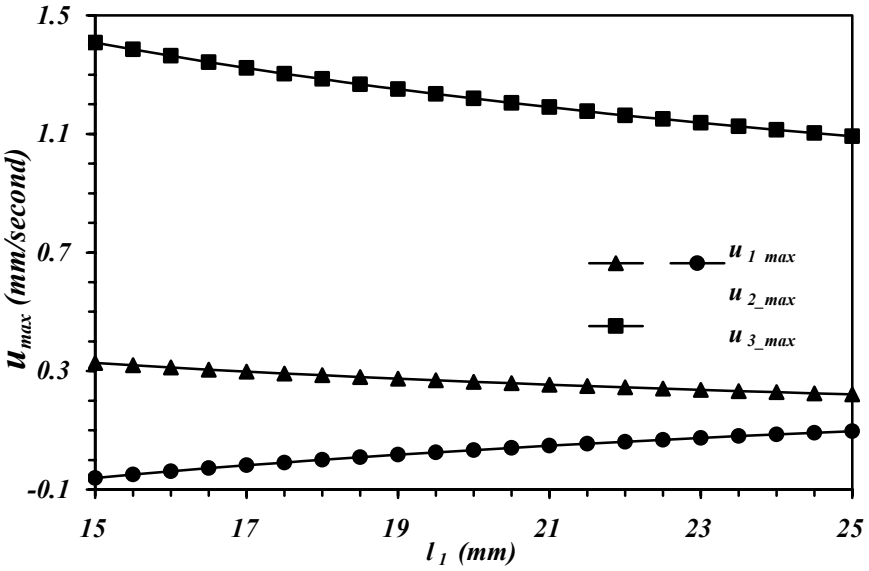

(b)

Figure 4.5. The maximum flow velocities in the channels with height differences Δh_1=6 *mm* and Δh_2=3 *mm*; (a) maximum velocities in the main channel depending on length of the driven channels (l_1) when l_2/l_3=2, (b) the comparison of maximum flow velocities in three channels when l_2=4 *mm* and l_3=2 *mm*

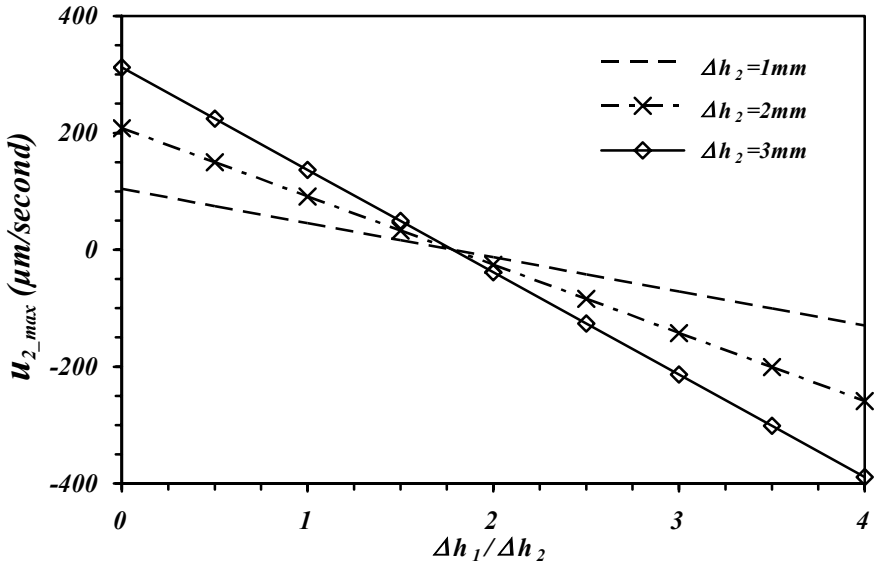

Figure 4.6. The dependence of the maximum flow velocities in the main channel on the ratio of the pressure differences ($\Delta h_1/\Delta h_2$) when l_1=16 mm, l_2=4 mm, and l_3=2 mm

4.2.1.2. DMC-TRMS

The flow velocity in the main channels of DMC-TRMS can be regulated by the dimensions of the design and the pressures in reservoirs like SMC-TRMS. Because PART 1 and PART 2 of DMC-TRMS are symmetrical (Figure 3.7), the flow velocities in PART 1 (Figure 4.7) can be analyzed in a way similar to SMC-TRMS presented above. However, the continuity equation at the junctions is different from the case for SMC-TRMS. As a result, the reverse flow hardly occurs when the ratio of height difference ($\Delta h_1/\Delta h_2$) is relatively small as shown in Figure 4.8. Therefore, the pressure in reservoir 1 must be big enough to reverse the flow in the main channels. The maximum flow velocities in three channels in DMC-TRMS show similar behaviors with SMC-TRMS when the lengths of the driven channels are changed (Figure 4.9).

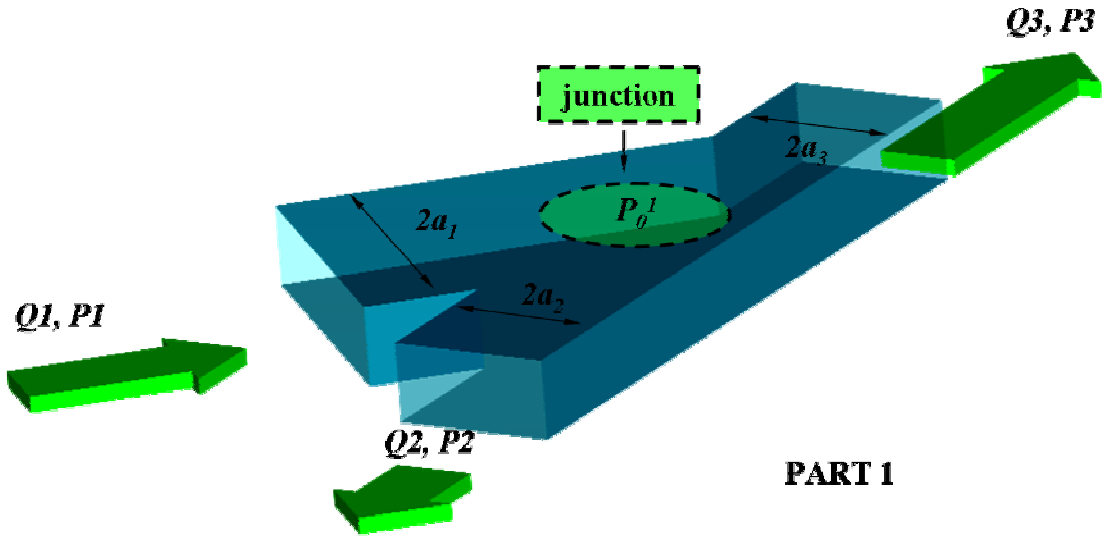

Figure 4.7. The flow schematic of double main channel TRMS (DMC-TRMS) at the PART 1 junction.

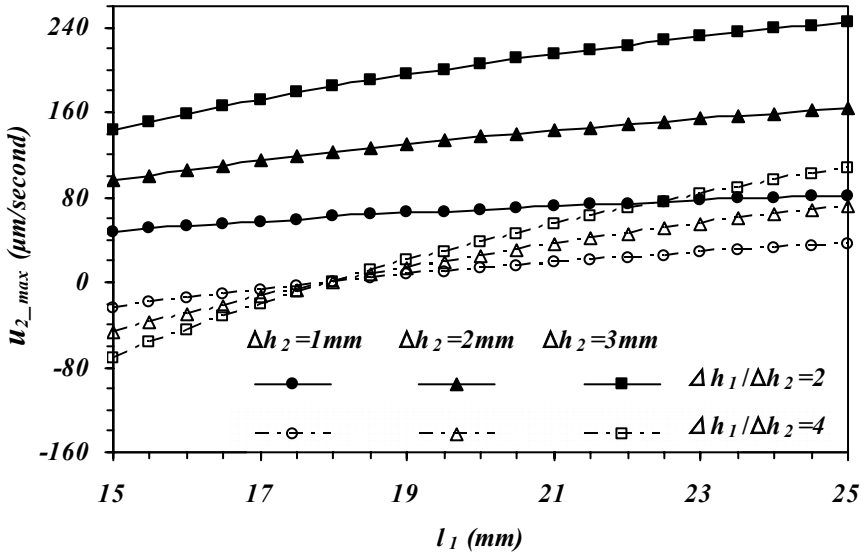

Figure 4.8. Comparisons of maximum flow velocities in main channels of DMC-TRMS design depending on the ratio of height differences and the length of driven channel (l_1) when l_2=4 *mm* and l_3=2 *mm*.

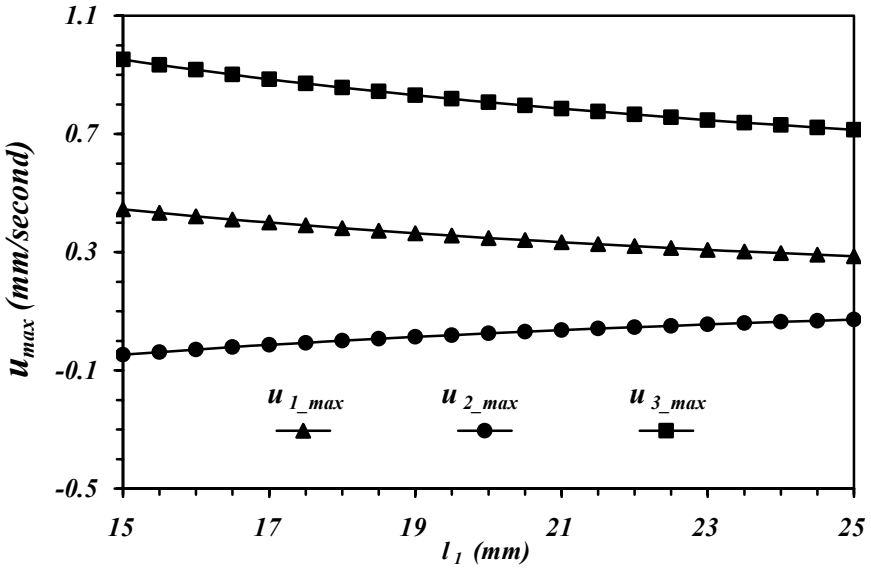

Figure 4.9. The comparison of maximum flow velocities in three channels when l_2=4 *mm*, l_3=2 *mm,* Δh_1=8 *mm*, and Δh_2=2 *mm.*

4.2.2. TRMS with junction channels (JC-TRMS)

So far, we have discussed two TRMS designs, SMC-TRMS and DMC-TRMS, which do not have junction channels (NJC-TRMS). In NJC-TRMS, only the maximum flow velocity of one main channel's flow is considered. If the TRMS has at least one junction channel in PART 1 and PART 2 as shown in Figure 3.8, the TRMS must have at least three main channels. However, if the TRMS has only one outlet channel to produce the relatively fast flow, regulating the flow directions and velocities in main channels is more difficult than in NJC-TRMS designs. Therefore, we are interested in TRMS designs which have at least two outlet channels. We will discuss junction channel TRMS (JCs-TRMS) designs which consist of an even number of main channels (four and eight main channels) and two outlet channels in this section.

4.2.2.1. Two junction channels TRMS (Two-JCs-TRMS)

Although there are two kinds of Two-JCs-TRMS models, consisting of three or four main channels, we will discuss the four main channels' model as shown in Figure 4.10. Similar to DMC-TRMS, the Two-JCs-TRMS is also symmetrical between PART 1 and PART 2. Therefore, we just need to consider PART 1 or PART 2. Let P_0^1 and P_0^2 be the pressures at the junctions. These two unknown pressures are important to determine the maximum flow velocities in the main channels, u_{2_max} and u_{4_max}. To generate the reverse flow in the main channels, the junction pressures must satisfy $P_2 < P_0^1$ and $P_2 < P_0^2$. Additionally, to produce JC flow toward the outlet channels, the junction pressures must be $P_0^1 > P_0^2$. To calculate the maximum flow velocities in the main channels, we have selected the channel widths a_1=*200 μm*, and a_2=a_3=*50 μm*. The lengths of junction channels (l_3) are also fixed at *0.5 mm*.

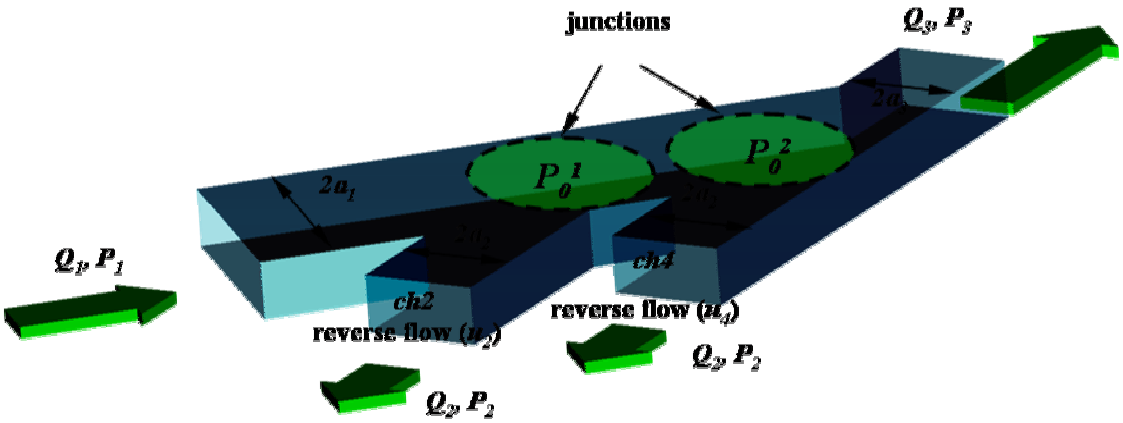

Figure 4.10. The flow schematic in Two-JCs-TRMS on the PART 1.

If the size and dimensions of two main channels are the same, the maximum flow velocities in two main channels are not close to each other (Figure 4.11). When the ratio of height differences ($\Delta h_1/\Delta h_2$) remains constant, the difference between u_{2_max} and u_{4_max} are decreased by decreasing Δh_2. In addition, the magnitudes of u_{2_max} and u_{4_max} are increased by decreasing lengths of the driven channels. Furthermore, u_{2_max} and u_{4_max} are significantly different for a wide range of the outlet channel length as shown in Figure 4.12. The other parameters which can affect the magnitude of the flow velocities in the main channels are the lengths of main channels and outlet channel. If the ratios of length between main channels and outlet channel, l_2/l_5 and l_4/l_5, are fixed, the maximum flow velocities and directions in the main channels are changed depending on lengths of the main channels as shown in Figure 4.13. Additionally, differences of the maximum flow velocities between two main channels are increased when the lengths of main channels are increased.

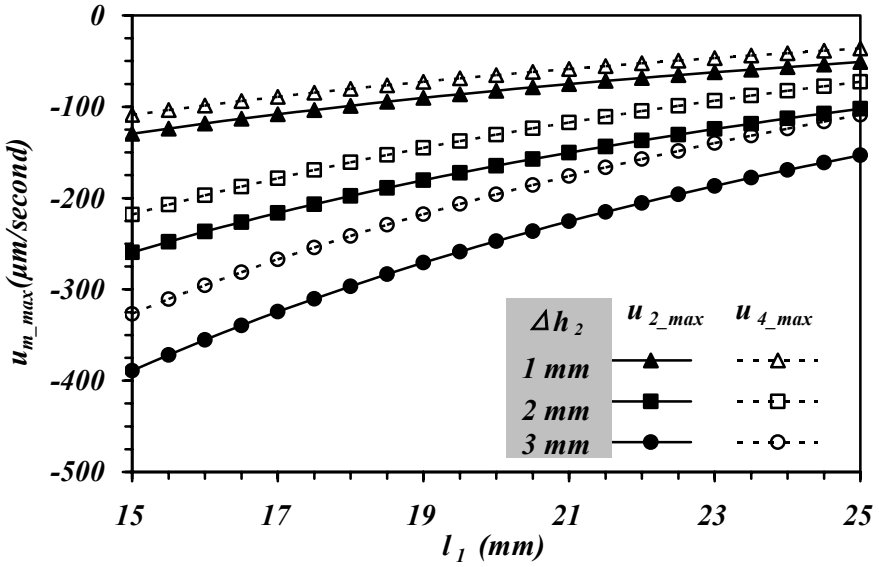

Figure 4.11. The maximum flow velocities in the main channels depending on driven channel length (l_1). ($l_2/l_5 = l_4/l_5 = 2$ with $l_5 = 2$ *mm* and $\Delta h_1/\Delta h_2 = 4$ regardless Δh_2)

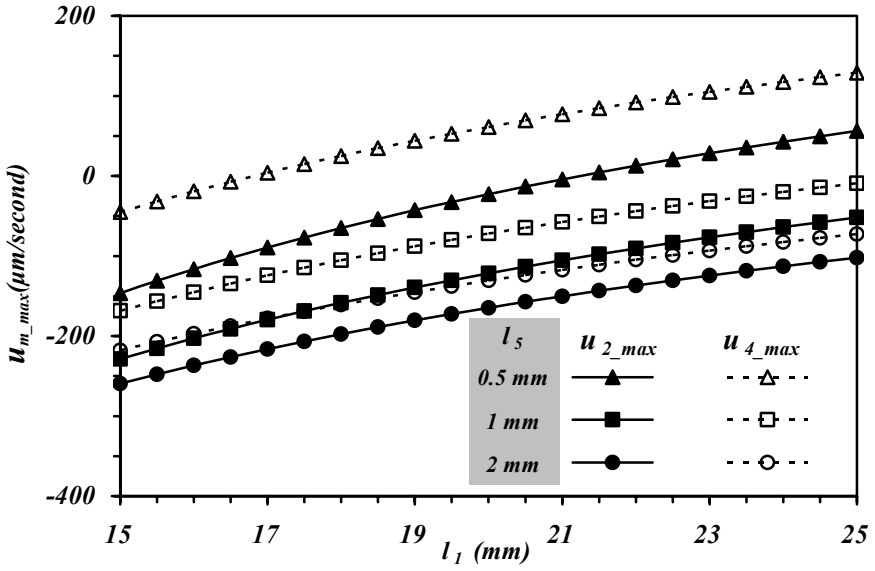

Figure 4.12. The maximum flow velocities in the main channels depending on the driven channel length (l_1). ($l_2/l_5 = l_4/l_5=2$ regardless l_5 and $\Delta h_1/\Delta h_2= 4$ when $\Delta h_2 =2$ *mm*)

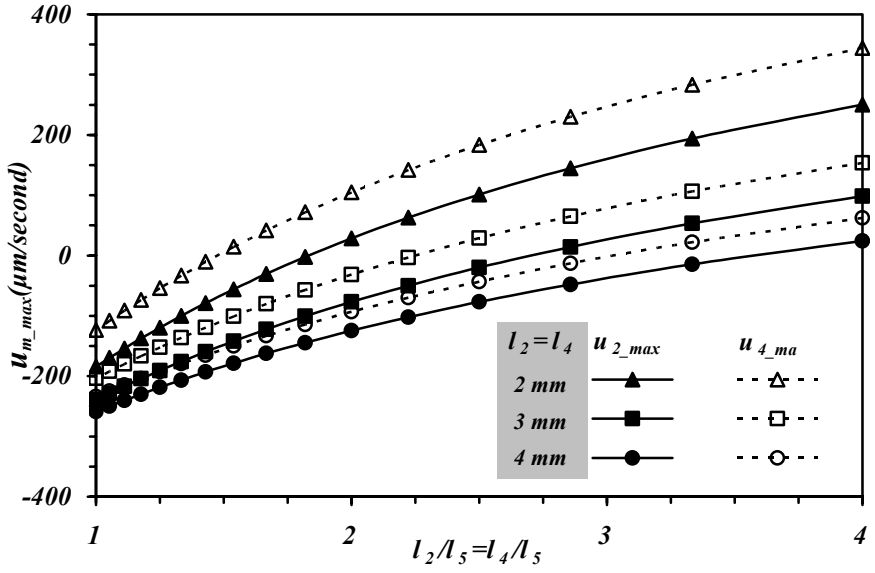

Figure 4.13. The variation of the maximum flow velocities in the main channels depending on the length ratio between the main channels and the outlet channel ($l_2/l_5 = l_4/l_5$) when $l_1 = 23$ *mm*, $\Delta h_1 = 8$ *mm*, and $\Delta h_2 = 2$ *mm*

According to above figures, the reverse flows in both main channels occur when several conditions are satisfied. However, the maximum flow velocities can not be made the same if the dimensions of both main channels are the same. In addition, the first junction pressure P_0^1 must be greater than the second junction pressure P_0^2 to make the flow in junction channels to the outlet channel. Therefore, the length of first main channel (***ch2***) must be greater than the length of second main channel (***ch4***) to achieve the equal reverse flow velocities in both main channels because the maximum flow velocity is inversely proportional to channel length as presented in equation (3.25). The equal maximum velocities in both main channels only occur when length of ***ch4*** (l_4) is less than length of ***ch2*** (l_2) as shown in Figure 4.14 (highlighted by the triangle and the ellipse respectively).

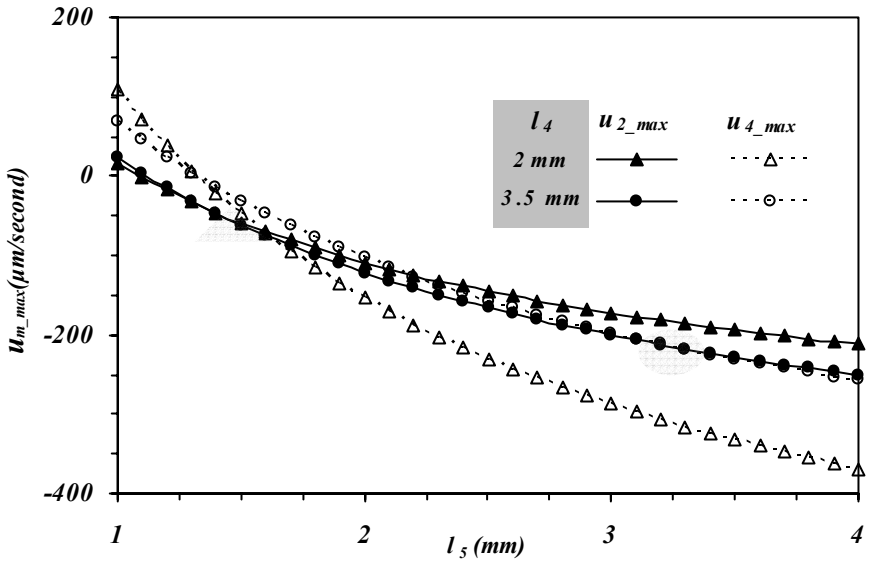

Figure 4.14. The maximum flow velocities in both main channels depending on length of outlet channel (l_5) when $l_1 = 23$ *mm,* $l_2 = 4$ *mm,* $\Delta h_1 = 8$ *mm,* $\Delta h_2 = 2$ *mm,* and $l_2 > l_4$

In addition, the length of the outlet channel (l_5) has to be limited depending on the length of ***ch4*** (l_4), especially, if both main channels must have the same maximum flow velocities and directions. Setting the two velocities in the main channels equal, we iterated calculations to obtain the corresponding length of the outlet channel as shown in Figure 4.15. When the value of l_4 is close to l_2, the length of the outlet channel (l_5) is rapidly increased. Similar to Figure 4.15, Figure 4.16 also shows relationship between the ratio of height differences and length of the outlet channel to have equal maximum flow velocities in both main channels. Finally, if specific hydrostatic pressures are applied in the reservoirs, the TRMS design has be defined to induce the equal maximum flow velocities as shown in Table 1.

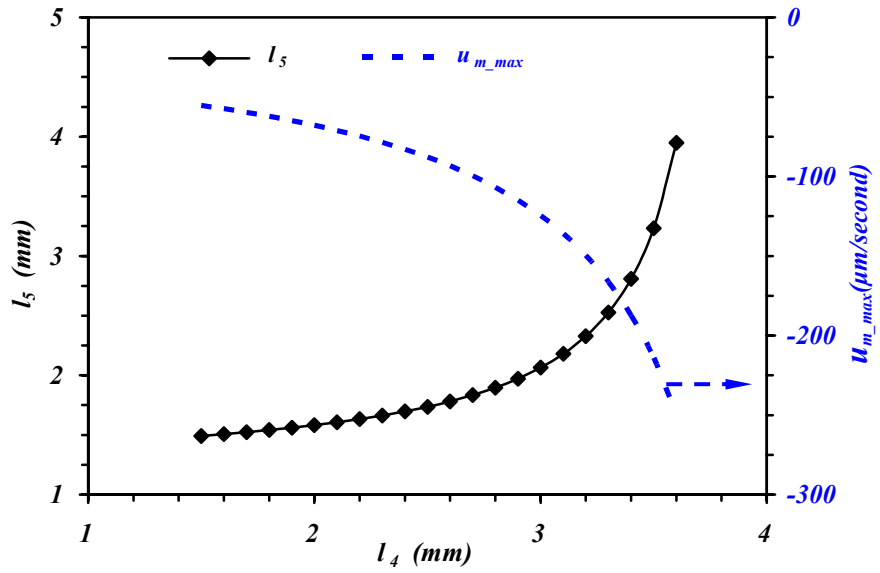

Figure 4.15. The relationship between l_4 and l_5 to have equal maximum main channels' velocities when (a) Δh_1=8mm (ΔP_1=78.23 N/m^2), Δh_2=2 mm (ΔP_2=19.56 N/m^2), l_1=23 mm, and l_2=4 mm.

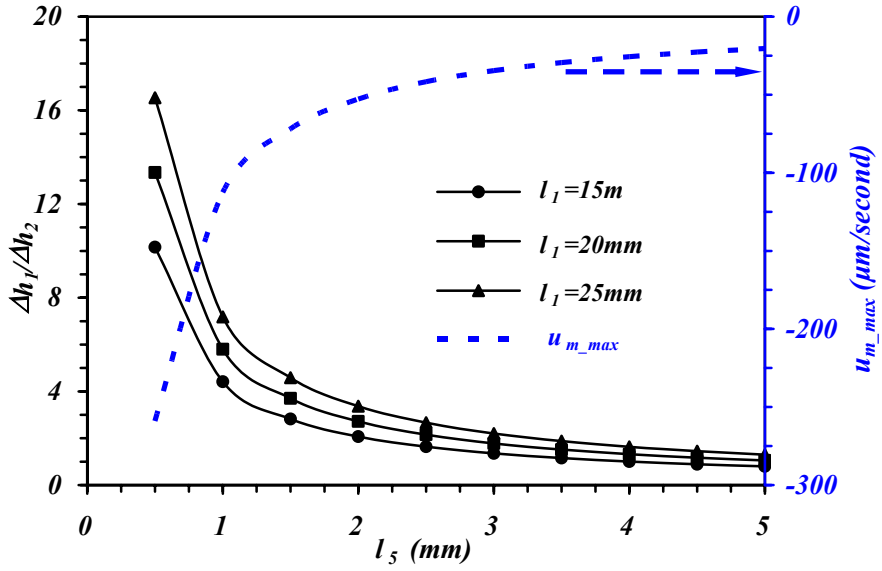

Figure 4.16. The relationship between l_5 and $\Delta h_1/\Delta h_2$ to have same maximum main channels' velocities when Δh_2=2 *mm*, l_2=4 *mm*, and l_4=2 *mm*. The dotted line indicates the value of the maximum flow velocities depending on l_5

Table 4. 1. An example of Two-JCs-TRMS design to have equal maximum flow velocities in both main channels when Δh_1=8 *mm* (ΔP_1=78.23N/m^2) and Δh_2=2 *mm* (ΔP_2=19.56N/m^2).

channel	***ch1*** **(driven)**	***ch2*** **(main)**	***ch4*** **(main)**	***ch5*** **(outlet)**
length	*23 mm*	*4 mm*	*2 mm*	*1.5227 mm*
max. velocity	*286.48 μm/sec*	*-67.97 μm/sec*	*-68.03 μm/sec*	*1170.7 μm/sec*

4.2.2.2. TRMS with six junction channels (Six-JCs-TRMS)

From above discussions, we have verified that the maximum flow velocities in the main channels can be the same in cases of Two-JCs-TRMS. However, if the TRMS has more than four main channels, it will be more complex to produce the same velocities in the main channels. In case of TRMS which has six junction channels (Six-JCs-TRMS), there are four main channels at PART 1 (Figure 4.17) and PART 2 respectively. To have the reverse flow with equal flow velocities in the Six-JCs-TRMS main channels, the junction pressures and lengths in the Six-JCs-TRMS must satisfy following conditions:

$$P_0^1 > P_0^2 > P_0^3 > P_0^4 \tag{4. 1}$$

and

$$l_2 > l_4 > l_6 > l_8 . \tag{4. 2}$$

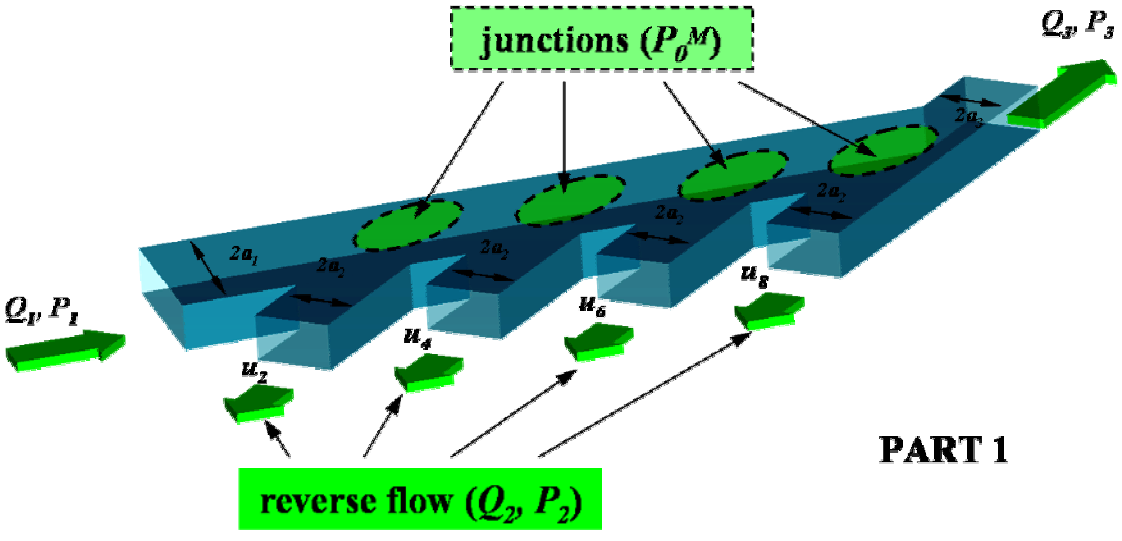

Figure 4.17. The flow schematic in Six-JCs-TRMS on the PART 1.

Eight main channels in the Six-JCs-TRMS induce larger flow rates than either four or two main channels TRMS if we suppose that the maximum flow velocities are equal in the main channels. Therefore, flow rates in the driven channels must be increased to limit the maximum flow velocities within specific ranges. In the Six-JCs-TRMS, we increase the width of driven channel to $a_1=150\mu m$ to increase flow rates. Although the flow rate can be drastically increased by increasing the thickness of channel (b) according to equations (3.21) and (3.23), it is hard to change the thicknesses of driven channels because the SU-8 photoresists is coated on the whole silicon wafer through the coating process. The other two channels' widths are fixed as previous models ($a_2= a_3=50\ \mu m$). In addition, we specify the lengths of four main channels as $l_2=4\ mm$, $l_4=3\ mm$, $l_6=2\ mm$, and $l_8=1\ mm$ to calculate maximum flow velocities. The junction channel lengths are also fixed to be $0.5\ mm$ similar to the case for Two-JCs-TRMS.

Figures 4.18 shows the variations of maximum flow velocities in the four main channels respectively. By increasing the length of the outlet channel (l_9) the maximum flow velocities in the main channels can be controlled and limited within specific ranges as shown in highlighted area in Figure 4.18 (b). The maximum flow velocities are relatively smaller than the maximum flow velocities in the driven channels and outlet channel as shown in Figure 4.19.

If the Six-JCs-TRMS dimensions are fixed, the pressure is the only parameter to control the flow. Therefore, we calculate the maximum flow velocities when the pressures are changed. Figure 4.20 shows the relationship between pressures and the maximum flow velocities for specific design of Six-JCs-TRMS. The design includes the lengths of the driven channel and four main channels as l_1=20 mm, l_2=4 mm, l_4=3 mm,

l_6=2*mm*, and l_8=1*mm,* respectively. In addition, the lengths of the outlet channel and the junction channels are l_9=3 *mm,* and l_3= l_5= l_7= l_8=0.5 *mm* respectively.

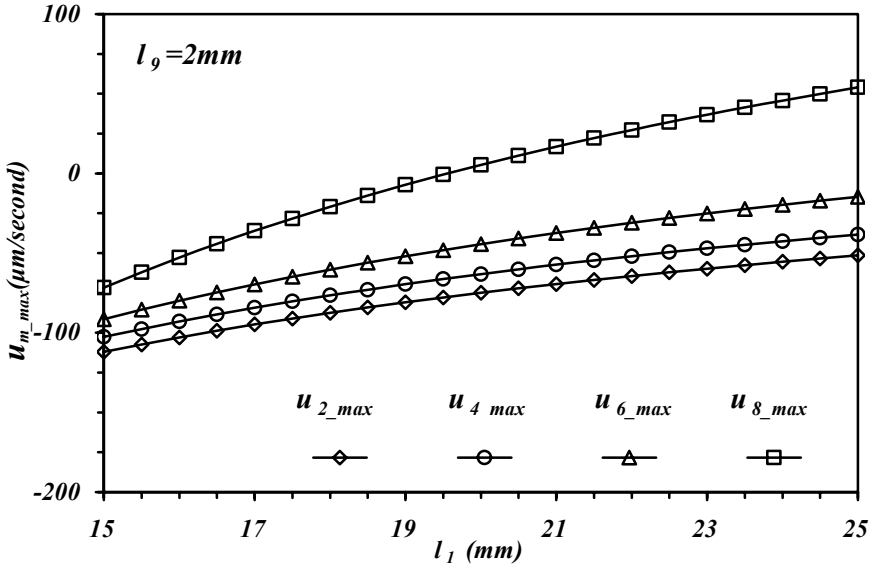

(a)

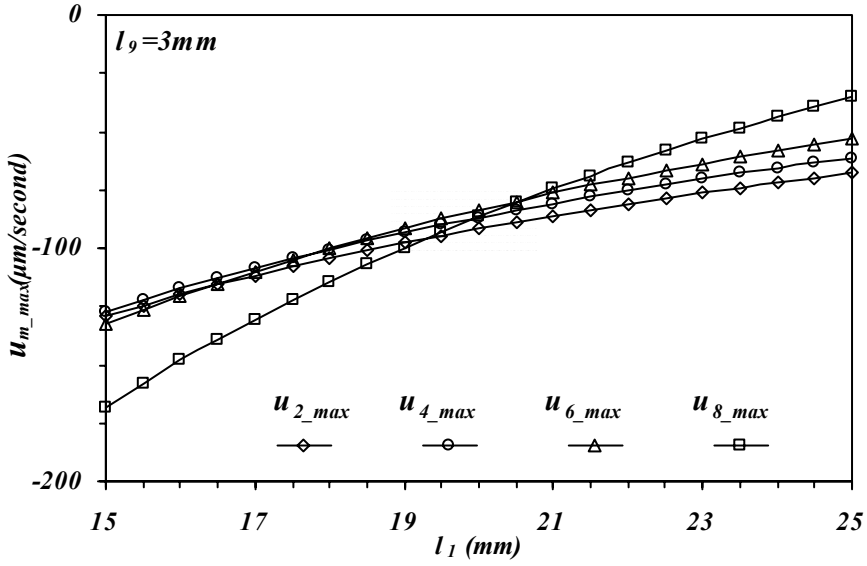

(b)

Figure 4.18. The maximum flow velocities in the Six-JCs'-TRMS main channels depending on driven channel length (l_1); (a) l_9=2 *mm*, (b) l_9 = 3 *mm*. The two pressure differences are Δh_1=7.5 *mm* and Δh_2=1.5 *mm*

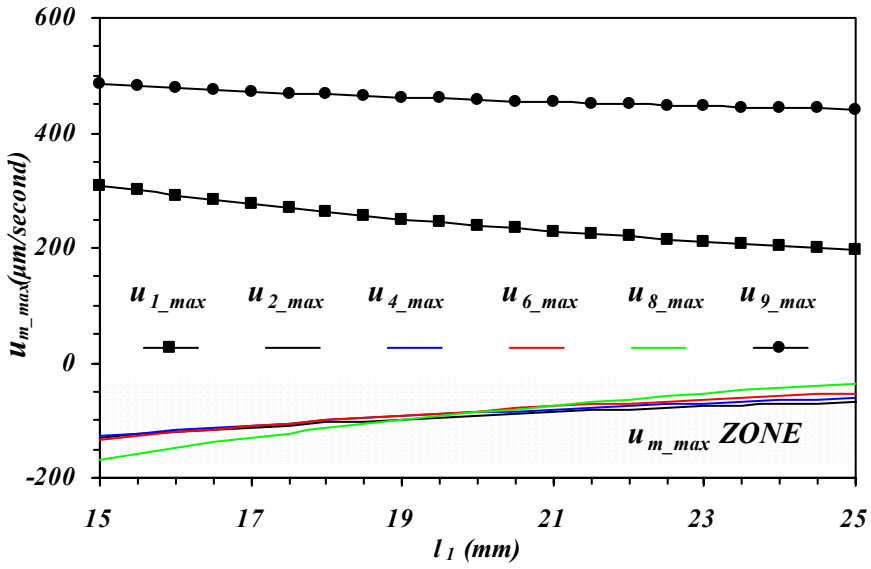

Figure 4.19. The comparison of maximum flow velocities in driven, main, and outlet channels of Six-JCs-TRMS when l_9=*3 mm*. The highlight indicates the ranges of maximum flow velocities in the main channels called $\boldsymbol{u_{m\_max}}$ ***ZONE***.

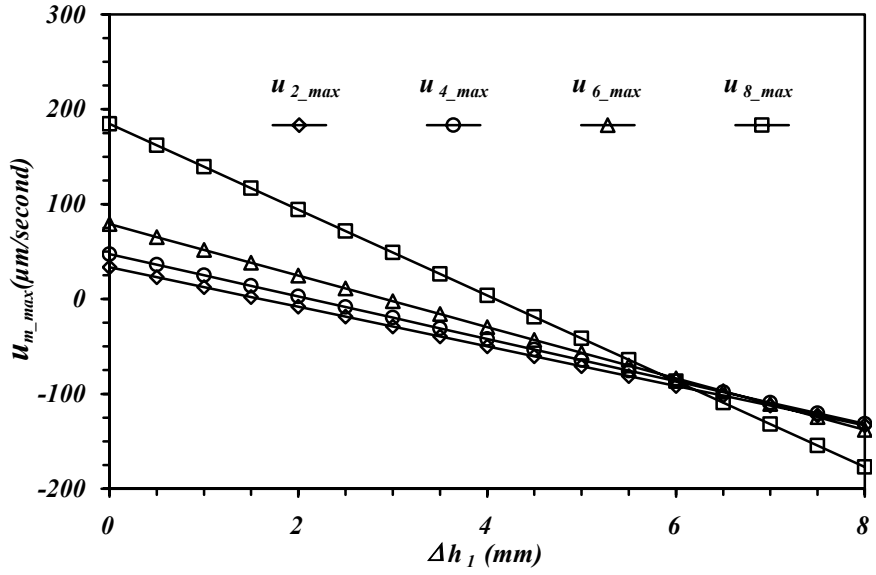

Figure 4.20. The variation of the maximum flow velocities in the main channels depending on Δh_1 when Δh_2=*1.5 mm*, l_1=*20 mm*, and l_9=*3 mm*.

4.3. Conclusions and discussion

The maximum flow velocities in the TRMS main channels can be regulated by changing both pressures and dimensions in TRMS. The flow velocities in the microchannels are proportional to applied pressures. However, the dimensions are not proportional to the maximum flow velocities. Therefore, the dimensions must be considered before designing TRMS to limited the maximum flow velocities to within specific ranges. In addition, the dimensions are important parameters to control flow velocities and direction in the main channels properly. These theoretical results are essential for designing and developing TRMS microfluidic devices.

Chapter 5

EXPERIMENTS OF FLUID FLOW IN THE MICROCHANNELS AND SEPARATING MOTILE SPERM USING HYDROSTATIC PRESSURE AND TRMS

5.1 Introduction

In previous chapters, we have discussed the theoretical calculations of the fluid flow in the TRMS main channels. These calculation results are applied to develop the motile sperm sorting devices and to optimize the design. Especially, we use the self-movement of motile sperm against a flow direction to develop the motile sperm sorting devices. Therefore, it is very important to visually observe the flow in the microchannels after completing the motile sperm sorting device. Microparticle image velocimetry (μPIV), which consists of a CCD camera, a microscope, and an in-line illumination source, is recently introduced and applied to visually observe the microflows [74-80].

The μPIV originates from the particle-based flow velocimetry technique introduced by Adrian [74] in the 1991. In this technique, the observed velocity of marker particles implied the motion of the bulk fluid in several centimeter scales. Afterward, Lanzilloto et al. [75] demonstrated the microflow measurement technique using X-ray micro-imaging technology to measure velocity fields in 500~1000 μm diameter microtubes. After Santiago et al. [80] applied the PIV to microscale flow in the 1998, the μPIV have become a popular method to measure the flow velocity and to observe the

flow in the microchannels. Although, the μPIV is commonly used in the microflow studies, the flow in the microchannels can be visually observed using an inverted microscope (ECLIPSE TE200, Nikon) and a digital camera (COOLPIX 5000, Nikon). After inserting microbeads with the solution, we recorded the microbeads' movement representing the flow in the microchannels using a digital camera. The recorded digital images and movies are edited and analyzed using Photo Shop 6.0.

In this chapter, we focus on discussing the experimental results using Motile sperm Sorting-Microfluidic-System (MSMS) based on TRMS. To develop MSMS, the maximum flow velocities in the main channels depending on applying hydrostatic pressures are first measured. The hydrostatic pressures are important parameters to control the flow in the main channels. We also discuss motile sperm sorting results. The experimental results are reported on the variability among different species' sperm: bull, mouse, and human. It is shown that the hydrostatic pressure and self-movement of motile sperm can be used to solve separating, aligning and orienting sperm in the microchannel.

5.2 Flow experiment

The fluid flow and flow velocities in the microchannels were observed using a microscope, a digital camera, and microbeads. The completed microfluidic devices are placed on the microscope (Figure 5.1), and then the hydrostatic pressures are applied to generate fluid flow in a desired direction. The movement of microbeads is observed along the fluid flow in the channels. Then the motion of microbeads is recorded as a digitalized movie file using a digital camera which captures at least 15 frames per second. The movie file was analyzed using Photo Shop 6.0 to track the flow behaviors in the channel.

After recording the movement of microbeads in the channels, each frame in the movie file is captured. The captured images are edited and overlapped using Photo Shop 6.0. Figure 5.2 shows an example of a profile of fluid flow, edited by Photo Shop, in the microfluidic system which consists of an inlet channel and a outlet channel connecting a circular reservoir in the middle.

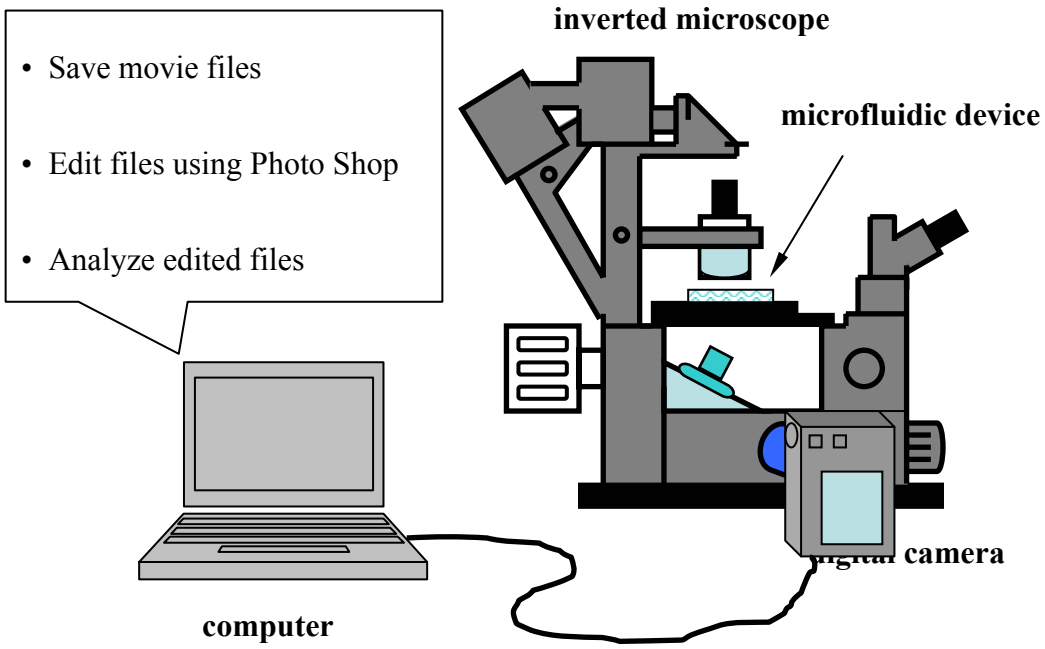

Figure 5.1. Experimental setup for observing flow using 1μm microbeads

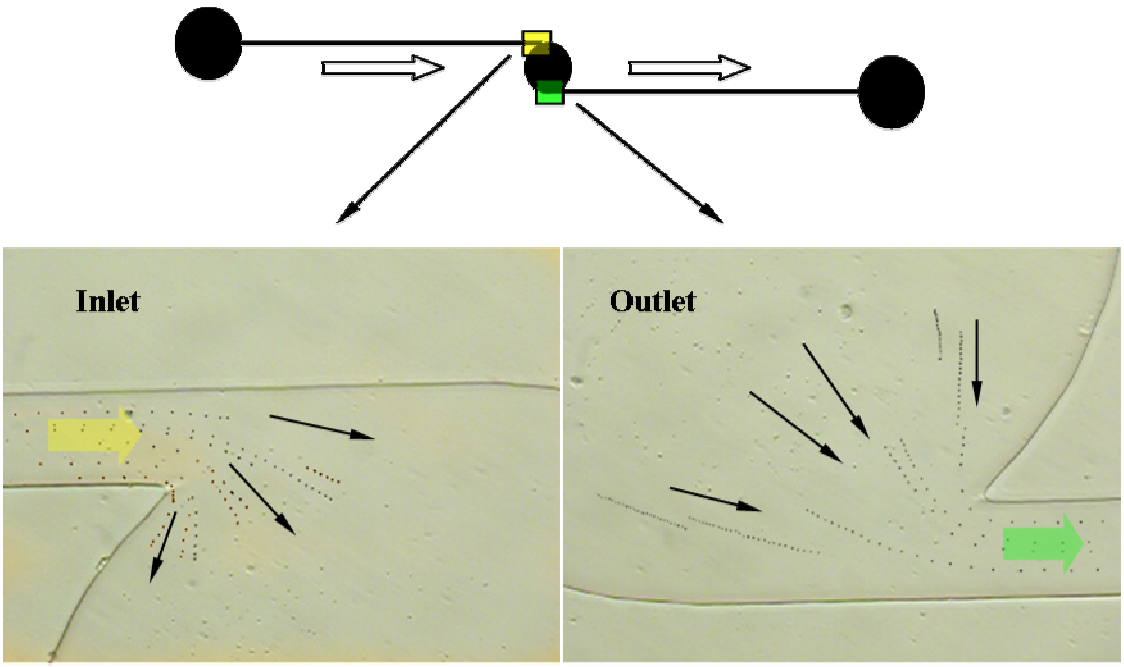

(a) (b)

Figure 5.2. An example of edited Photo Shop images in (a) the inlet and (b) the outlet of circular shape of microfluidic system. The flow in both (a) and (b) pictures show almost laminar flow

The experiment for measuring maximum flow velocities in the main channel of the SMC-TRMS (Figure 3.5) was performed. The dimensions of the SMC-TRMS used in the experiment are shown in Table 5.1. The height Δh_2 is fixed to find the relationship between Δh_1 and maximum flow velocities ($\boldsymbol{u}_{m\_max}$) in the main channel. First, the same amount of pure water (density: 997.05 Kg/m^3) is injected in reservoir 1, reservoir 2, and reservoir 3 to adjust heights in the reservoirs to near equal levels. Then same amount of pure water is added to reservoir 1 and reservoir 2 to generate the hydrostatic pressure. The maximum flow velocities are measured by increasing about 10μl (about 0.57mm height) of pure water in reservoir 1 each time. The experiments were performed three

times for Δh_2=2.29*mm* and Δh_2=3.43*mm* respectively. Figure 5.3 shows the experimental results indicating the averaged maximum flow velocities. Even though experiment results of the maximum flow velocities are not close to theoretical predictions, these follow similar slope with theoretical predictions. The profile of the fluid flow in the Six-JCs'-TRMS is also shown in Figure 5.5. The flows in the above two main channels, ***ch2*** and ***ch4***, are opposite to the bottom two channels, ***ch6*** and ***ch8***, when enough hydrostatic pressures are applied.

Table 5. 1. Dimensions of the single main channel TRMS.

channel	*channel A* (driven)	*channel B* (main)	*channel C* (outlet)
Length (l_n)	*23 mm*	*8 mm*	*5.5 mm*
Width (a_n)	*100 μm*	*50 μm*	*50 μm*

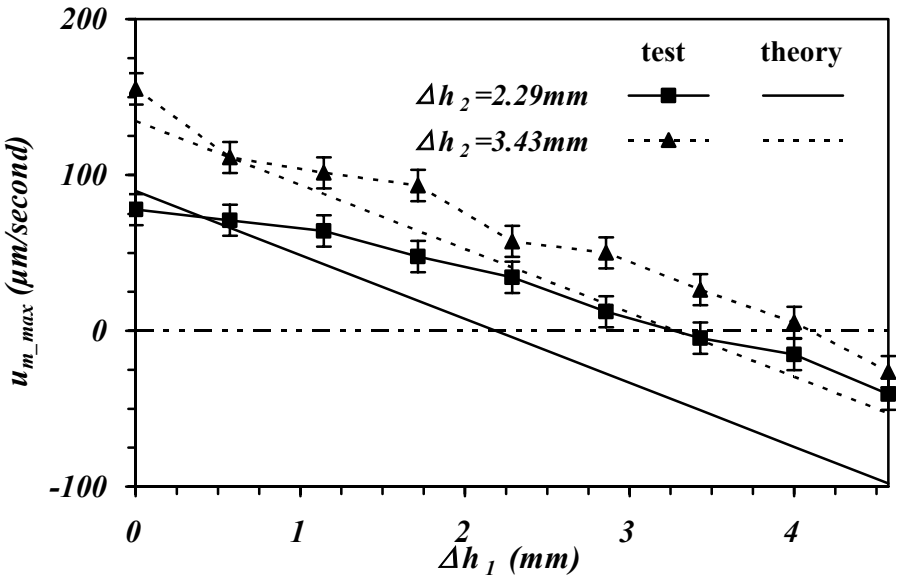

Figure 5.3. Experimental result for measuring maximum flow velocities

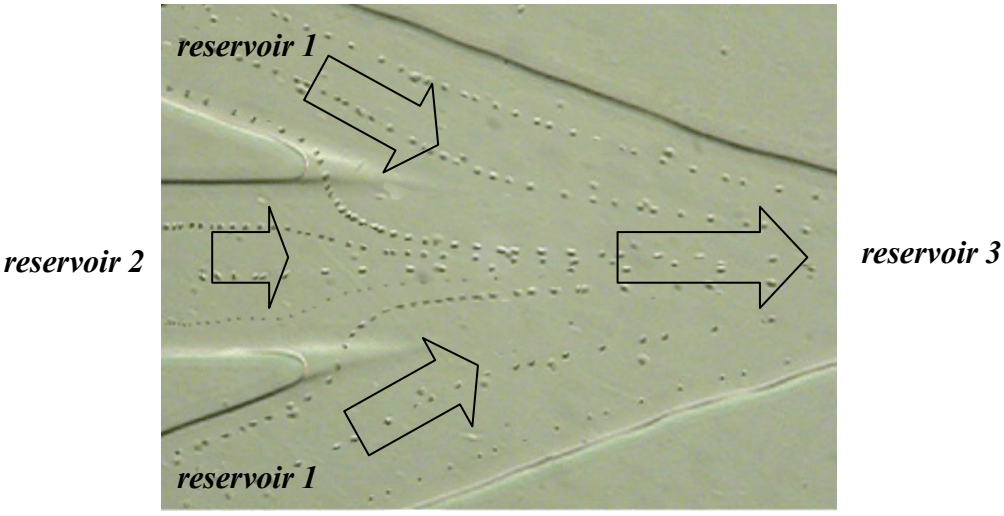

(a)

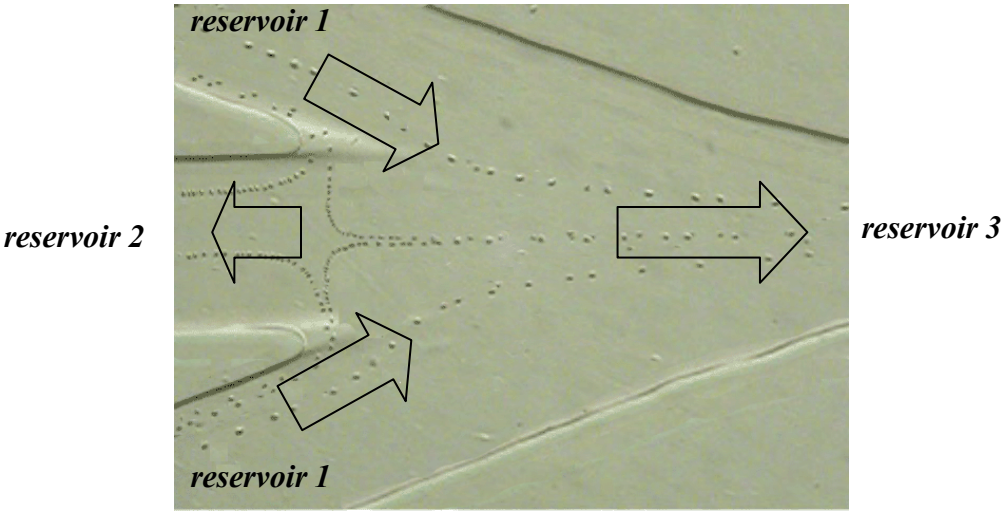

(b)

Figure 5.4. The profile of fluid flow at the junction of single main channel TRMS when $\Delta h_2 = 3.43\ mm$: (a) $\Delta h_1 = 3.43\ mm$ and (b) $\Delta h_1 = 4.57\ mm$

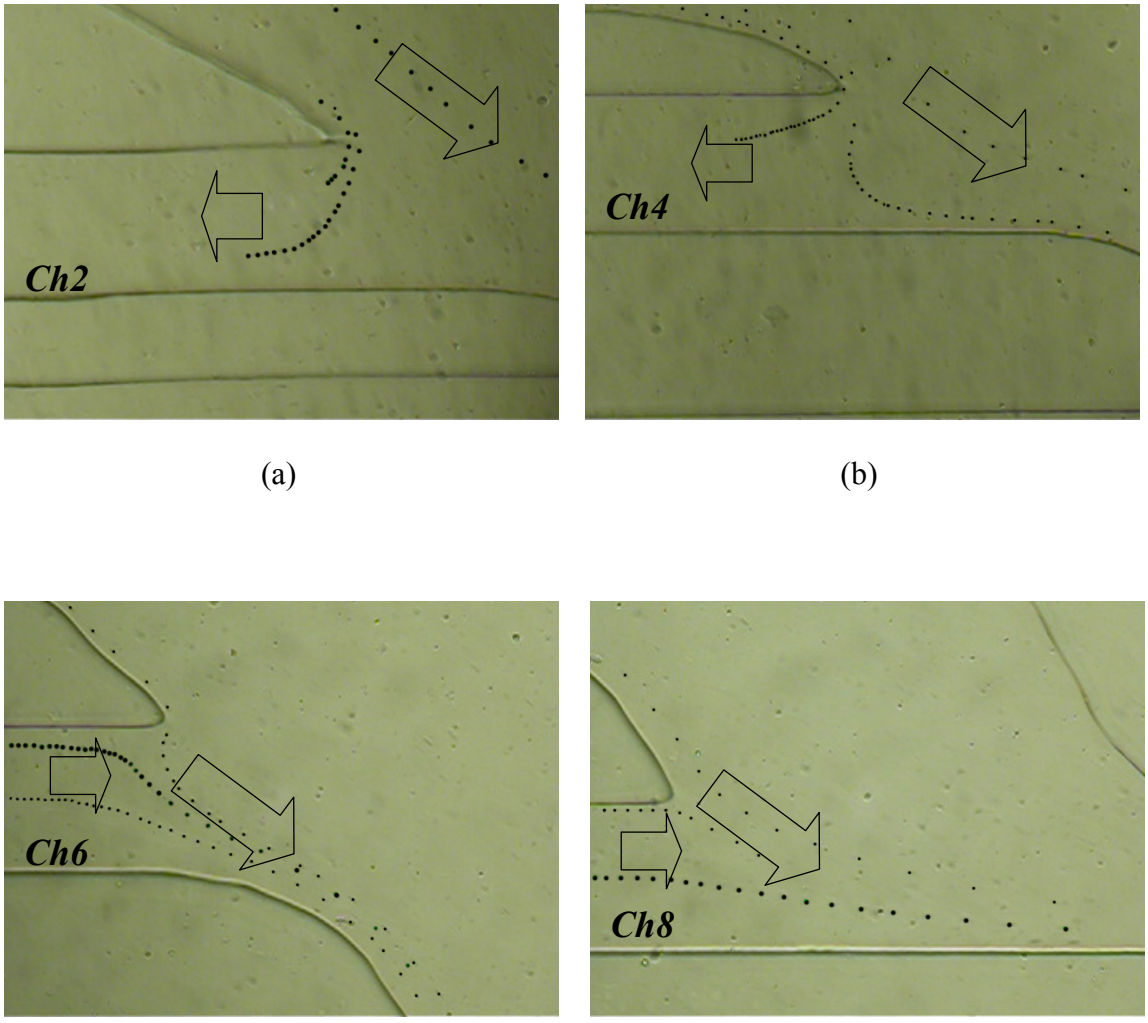

Figure 5.5. The profile of fluid flow at the junctions of Six-JCs'-TRMS (a) ***Ch2*** junction, (b) ***Ch4*** junction, (c) ***Ch6*** junction, and (d) ***Ch8*** junction.

5.3 Motile sperm Sorting Microfluidic System (MSMS)

The development of the MSMS is based on two well-known observations: (1) motile sperm orient themselves against the flow and (2) motile sperm can swim against the flow with specific flow velocity ranges. To quantify these observations, a microchannel with a cross section of 30 μm by 25 μm was fabricated. Human sperm were introduced into the inlet reservoir (Figure 5.6). A hydrostatic pressure, about $\Delta h=4.5\ mm$ ($45\ N/m^2$ pressure), was applied to the inlet reservoir. The movement of the solution and sperm from inlet to outlet takes place. The results show that over *80 %* of the motile sperm have a tendency to swim and orient their heads against the flow direction as shown in Figure 5.7.

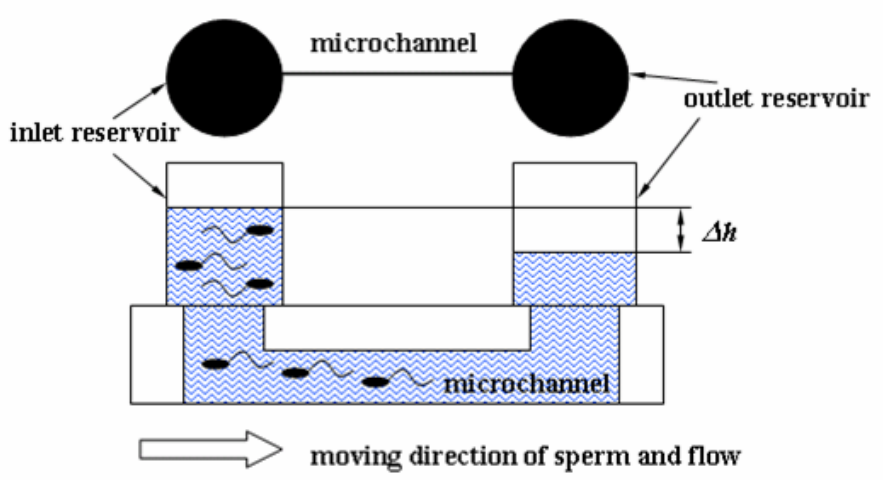

Figure 5.6. Orientation of motile cells in a channel with flow driven by hydrostatic pressure.

Based on the above observations, the MSMS (SMC-TRMS) was fabricated. It consists of four channels and three reservoirs as shown in Figure 5.8. The flow is driven by hydrostatic pressure created by the height of liquid columns at the reservoirs. These four channels meet at one point called a 'junction'. Reservoir 2 contains the sperm to be sorted and reservoir 3 collects sorted sperm. The liquid in channel C (outlet channel) flows from the junction to reservoir 3. By controlling the hydrostatic pressure carefully, the liquid in channel B (main channel) flows from the junction to reservoir 2. By swimming against the flow in channel B (main channel), motile sperm in reservoir 2 can reach the junction. At the junction, motile sperm is transported to reservoir 3 by a much faster flow in channel C (Figure 5.9).

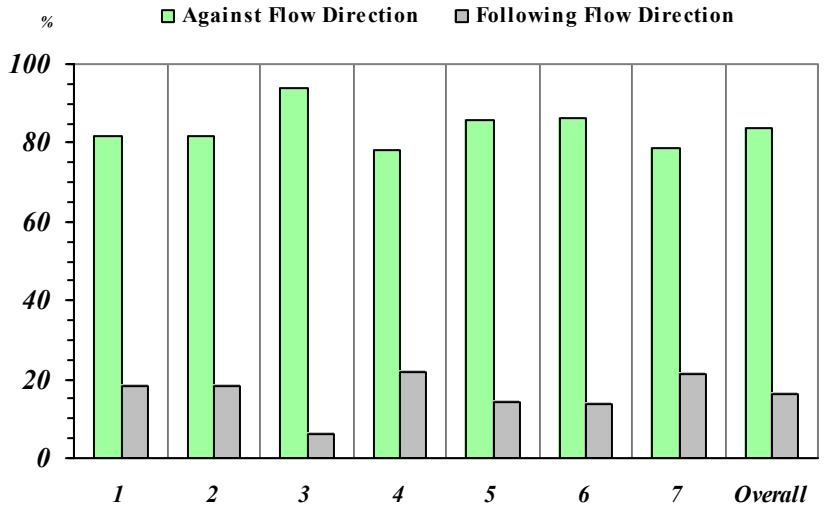

Figure 5.7. Orientation of human motile sperm head in flow. Data collected using a single microchannel with cross section of *30 μm* by *25 μm*. The pressure driving the flow is approximately *45 N/m*^{2}.

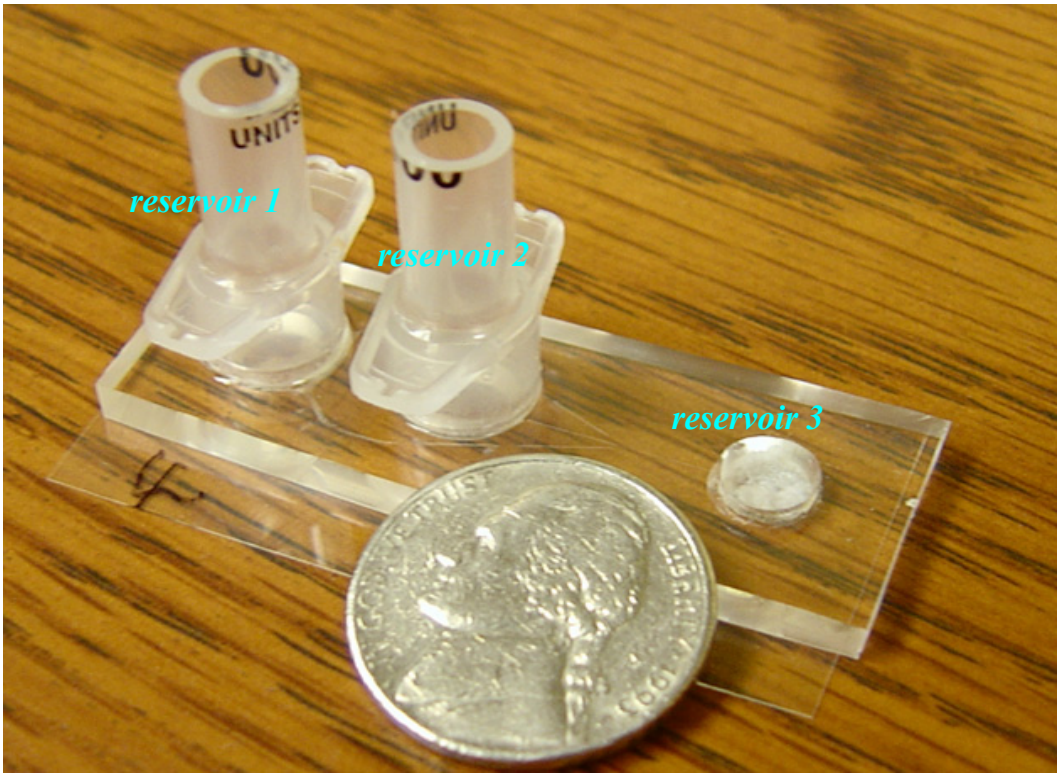

Figure 5.8. The Motile sperm Sorting Microfluidic System (MSMS)

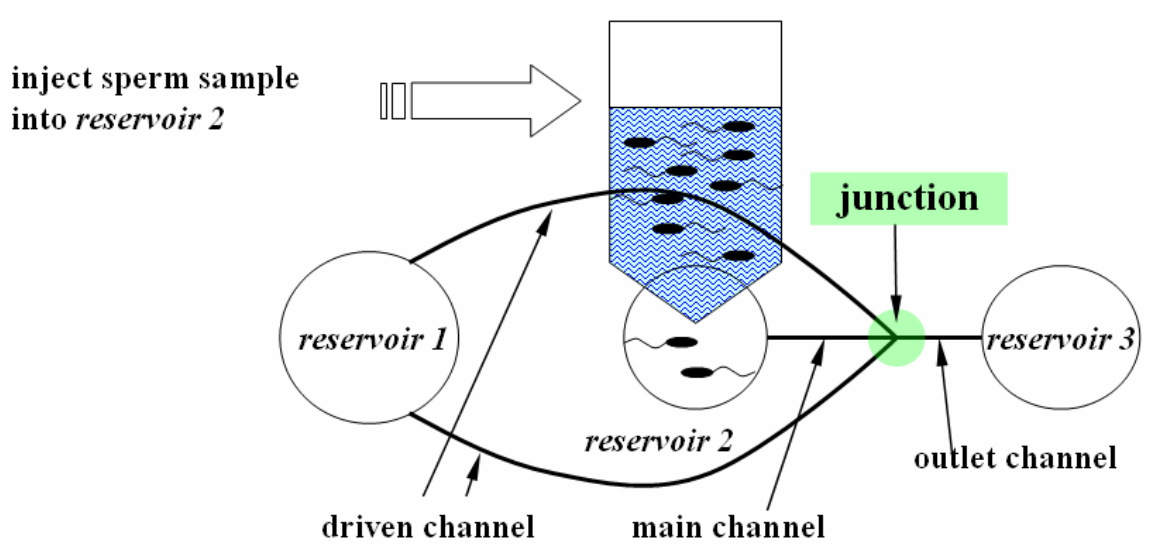

(a)

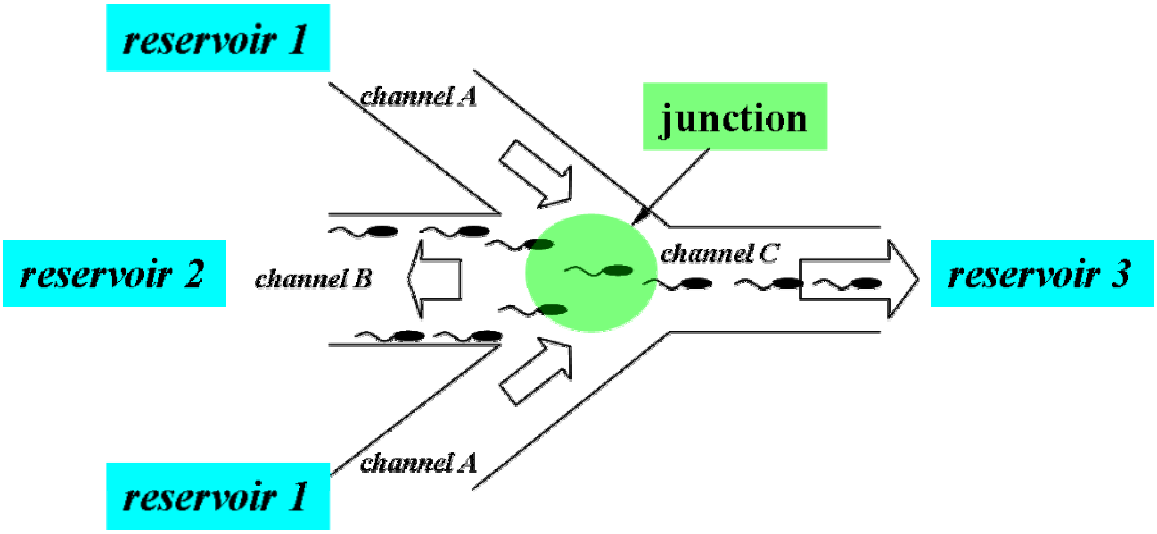

(b)

Figure 5.9. Motile sperm sorting mechanism at the junction of MSMS.

The design of the MSMS is obtained based on the following two considerations: (1) to allow easy control of flow direction and velocity using hydrostatic pressure, and (2) to allow enough space for the sperm to swim against the flow direction without "clogging" the channel. Geometric parameters such as height, width, and length all affect the flow velocity and direction in channels. Among these parameters, the channel widths ($2a_n$) and lengths (l_n) are defined by the patterns on the optical mask. The channel height is defined by the thickness of the SU-8 coating on the wafer which is used as the mold for the PDMS channel. Large channel width is desired to maximize the throughput of the sorting device. However since the microchannels are made of polymeric material, the channels could close-up under external pressure if they are too wide.

To have fastest unidirectional flow velocity in channel C (outlet channel), the length and width of channel C must be smaller than the other two channels. We set the lengths of each channel as l_1=*23.46 mm*, l_2=*8 mm*, and l_3= *5.5 mm*. The widths were also set as $2a_1$=*200~210 μm*, $2a_2$=*95~105 μm*, and $2a_3$=*95~105 μm*. The width of channel A (driven channel) was selected as a middle value between entrance and exit width. The channel height is determined based on two considerations. First of all, we found that cells clog easily in very narrow channels. Clogging is most likely to occur at the channel entrance as shown in Figure 5.10

Figure 5.10. Clogging of sperm cells at the entrance of channel B with 7μm height

Channels with *25 μm* height were proven to be convenient in terms of ease of the flow velocity control using hydrostatic pressure. Without precision flow pumps, we can adjust the hydrostatic pressure by adjusting the height of the liquid columns. We can manipulate a *10 mm* height liquid column with ease. Using liquid columns about *10 mm* in height, the maximum velocities in the channel vary significantly. Since the human motile sperm's self-propulsion velocity is estimated to be approximately *70 μm/sec*, the channel with a *25 μm* height allows us to easily vary the maximum flow velocity between *-100* and *+100 μm/sec* when the height of the liquid columns varies within *10 mm*.

5.4 Sorting experiments

Sorting experiments were performed using the MSMS. The MSMS were completely filled with solution (0.1 micron filtered Dulbecco's Phosphate-Buffered Saline, GIBCO) to control flow easily using hydrostatic pressure before conducting each experiment. The pressure at reservoirs 1 and 2 were initially set to be almost equal (*8~10 mm* height liquid). Reservoir 3 was set at a lower pressure (less than 1*mm* height) than the others. *20 μl* of sperm sample was loaded into reservoir 2. The pressure at reservoir 1 was increased by adding *20~40 μl* solution (about *1.14~2.28 mm* height) each time, to observe sperm movement in the channel. The sperm swims from left to right, when the flow in channel B moves from right to left. At the junction, motile sperm is swept into channel C which is at a much faster flow velocity, and thus the sperm is gathered in reservoir 3 (Figure 5.11).

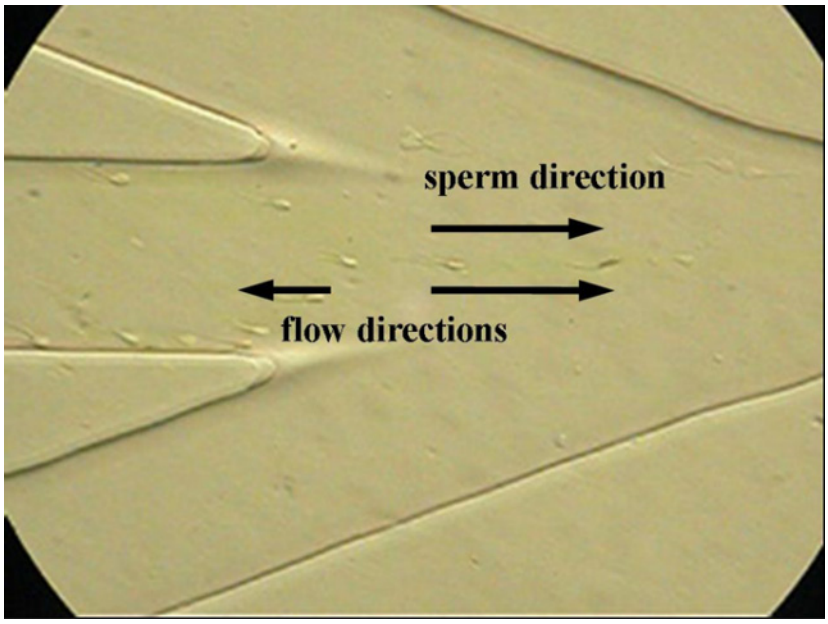

Figure 5.11. The movement of bull motile sperm at the channel junction. Sperm is pushed to the right as it passes the junction by a much faster flow in channel C.

The MSMS was designed to maintain the desired flow direction for at least 1 hour. However, in our most recent experiments, we collected sorting data after 20 *minutes* of inserting sample. To study the variability among different species, we applied the MSMS to the sorting of bull, mouse, and human sperm. Each experiment was performed for only one species sperm. In spite of respective differences in characteristics of sperm, the experimental results show that they all have similar characteristics in terms of aligning their heads opposite to direction of the flow as well as swimming against the flow (Figure 5.12 and Figure 5.13).

From Figure 5.14 to Figure 5.16, we plot the velocities of the motile cell and the debris for three species (bull, mouse, and human) at different pressure (Δh_1) when Δh_2 is fixed. The pressure is indicated using the height difference of the liquid columns in reservoir 1 and reservoir 2. Due to slight differences in the height of the PDMS channels resulting from the variation of the SU-8 coating thickness, the height difference of the liquid columns (Δh_1) varies from one device to the other. Despite the large variability, we clearly observe that the flow and the sperm move in opposite directions.

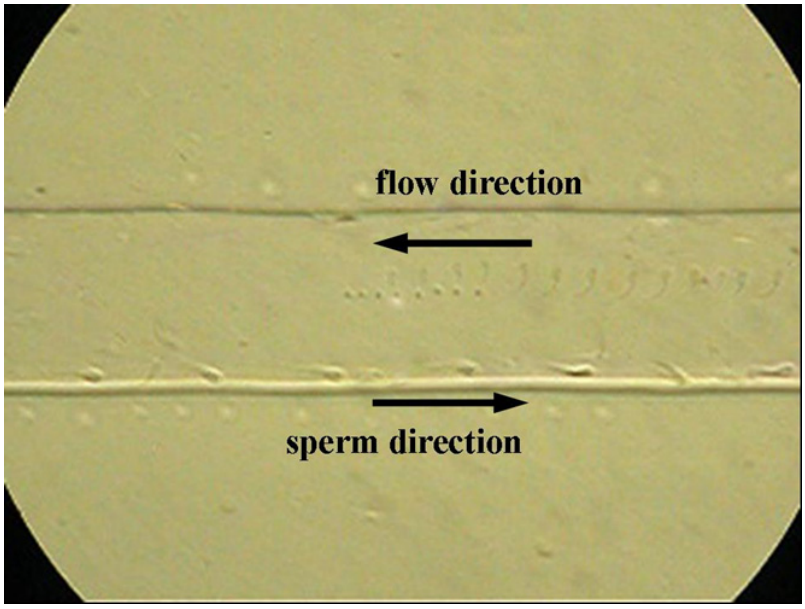

Figure 5.12. The tendency of bull sperm to swim against the flow in the main channel of MSMS (The tendency of human sperm is similar to bull sperm)

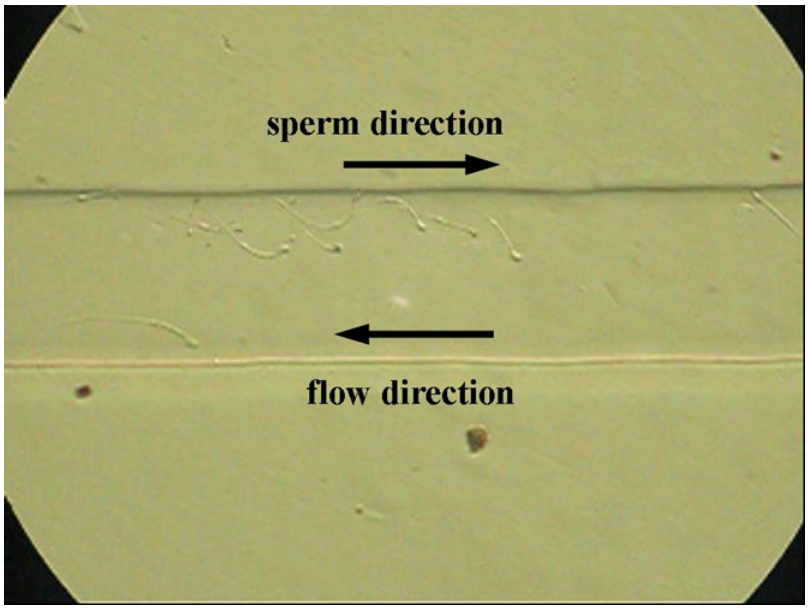

(b)

Figure 5.13. The tendency of mouse sperm to swim against the flow in the main channel of MSMS.

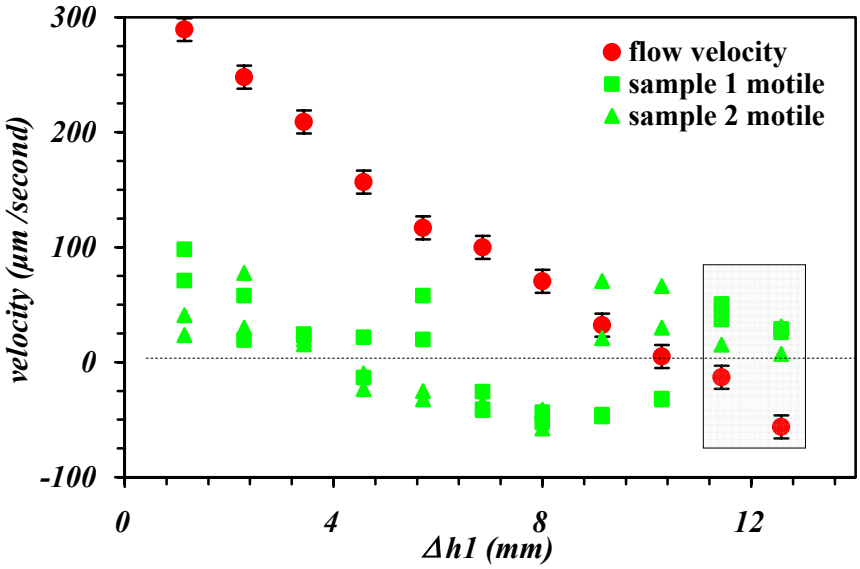

Figure 5.14. Velocity of motile bull sperm and non-motile sperm (or debris) in MSMS main channel depending on change of hydrostatic pressure Δh_1 Positive velocity indicates flow from reservoir 2 to junction direction. When the flow velocity is small, opposite directions of motion are observed as highlighted area.

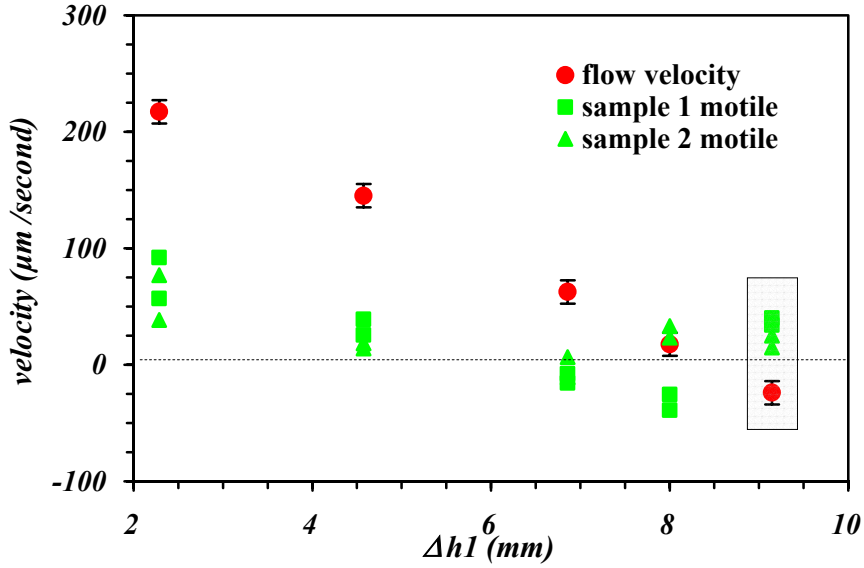

Figure 5.15. Velocity of motile mouse sperm and non-motile sperm (or debris) in MSMS main channel depending on change of hydrostatic pressure Δh_1.

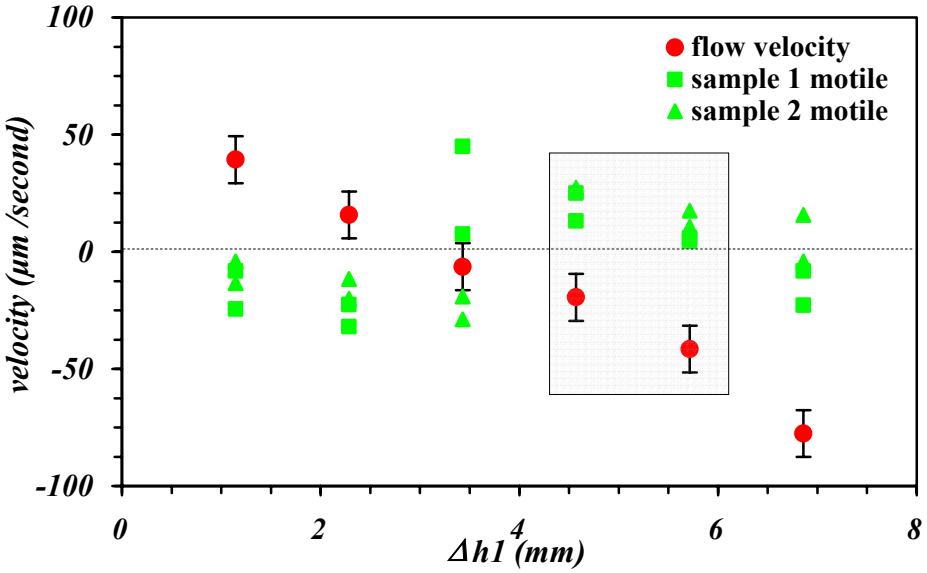

Figure 5.16. Velocity of motile human sperm and non-motile sperm (or debris) in MSMS main channel depending on change of hydrostatic pressure Δh_1.

Table 5.2 shows the results of the experiments with bull sperm sorting efficiencies using the MSMS. As shown in Figure 5.17, the motile bull sperm were sorted using the MSMS. Approximately *20 %* initial sperm motility in reservoir 2 increased to *80 %* after 20 *minutes* of sorting time.

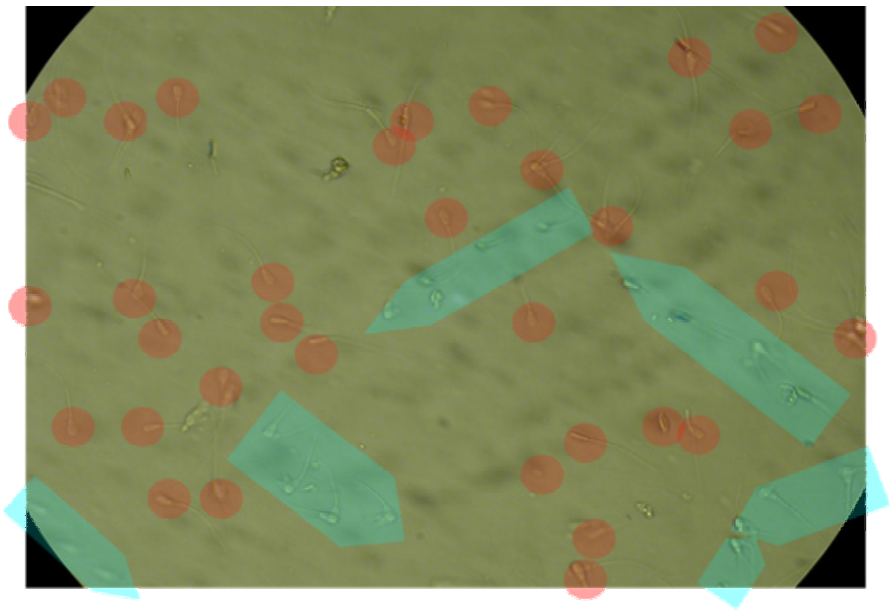

(a)

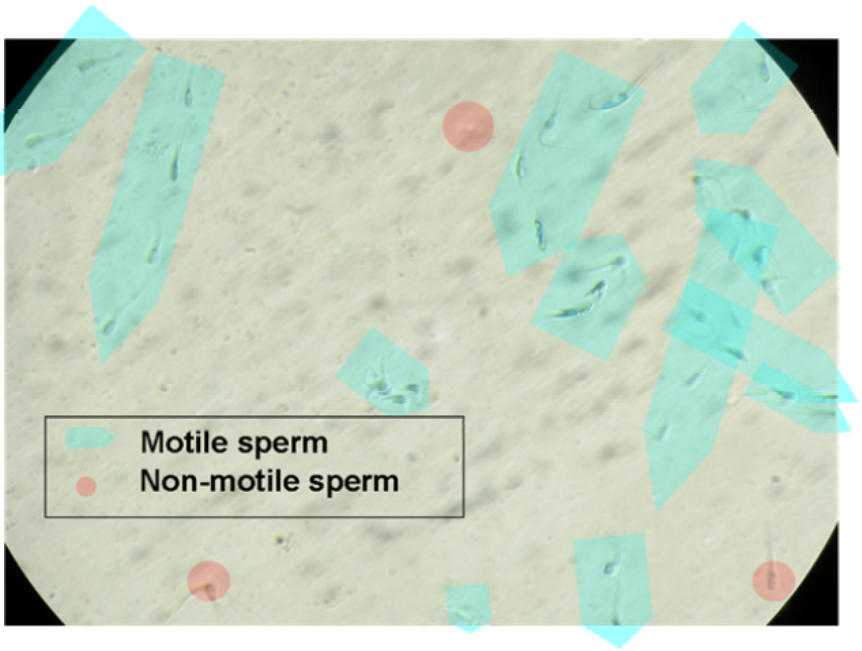

(b)

Figure 5.17. Motile and non-motile bull sperm (a) before (reservoir 2) and (b) after sorting (reservoir 3)

Table 5.2. Sorting rate of bull sperm using the MSMS

Sample No.	Approx. inlet sperm No.	Approx. inlet motile rate	Approx. outlet motile rate	Avg. sorting rate (ea/min)
1	2.68×10^5	*23.4% (33/141)*	*93.8% (15/16)*	*11*
2	4.20×10^5	*16.2% (60/370)*	*81% (30/37)*	*13.5*
3	4.90×10^5	*19.4% (21/108)*	*75.3% (70/93)*	*8*
Overall		*18.4% (114/619)*	*78.8% (115/146)*	*10.8*

(The inlet and outlet motile rates and average sorting rate was counted based on digital pictures and movie)

5.5 Conclusions and discussion

The flow in the microchannels is affected by applied hydrostatic pressures. Therefore, the flow velocities and the directions can be controlled using pressure differences in the reservoirs of TRMS. Based on these results, a motile sperm sorting microfluidic system (MSMS) manipulated by hydrostatic pressures was developed using an inexpensive fabrication method. The MSMS can be applied to sort bull, mouse, and human motile sperm by controlling maximum flow velocities in the main channel since the sorting is completed using self-movement of sperm cell swimming against the flow.

Even though the current design has a relatively low throughput, it provides proof that this approach works well. In addition, the current system has the advantage of orienting and aligning the sperm. The modification of the MSMS design to increase the

throughput is straightforward by adding multiple channels. Moreover, the system can be applied to other integrated microfluidic devices, for example, a micro Coulter-counter or other cell sensing devices.

Chapter 6

DISCUSSION AND FUTURE WORK

We have discussed the fabrication processes for the polymeric microfluidic devices, theoretical flow analyses of the microchannels depending on parameters, experimental fluid flow in the microchannels, and application of microfluidic devices for motile sperm sorting.

To complete the PDMS microchannels without defects which may occur during processes, above all, the wafer must be cleaned to remove dust. In addition, the dimensions of channels, width and height, are considered. Following the defect-free fabrication processes, not only the PDMS microchannels can be completed without a cleanroom facility but also the fabrication cost can be reduced. Therefore, the fabrication method which we have discussed in Chapter 2 can be applied to complete the PDMS microchannels for laboratory purpose.

Before the microchannels are filled with liquid, the fluid flow hardly occurs in the microschannels because the surface tension dominantly affects the flow in the microchannels. After the microchannels are completely filled with liquid, the flow in the microchannels is affected by the applied pressures. Therefore, it is possible to control flow velocities and directions using the hydrostatic pressures except in very low velocity ranges. Furthermore, our theoretical results show good agreement with experimental results which can also be a proof that the pressures can be a main factor in controlling the flow.

The fluid flow in the microchannels can be visually traced by microbeads, observed using a microscope, and recorded by a digital camera. By tracking the movement of microbeads, the maximum flow velocities can be measured. In addition, the directions of the flow can be observed. By editing recorded digital movie files which contain the movement of microbeads, the streamlines can be also visualized at the junction. The results of fluid flow in the microchannels are useful to design and to optimize the motile sperm microfluidic devices.

Based on inexpensive PDMS microchannels fabrication methods and the fluid flow results, we have developed the motile sperm sorting microfluidic system (MSMS). The MSMS can be applied not only to sort motile sperm but also to align and to orient the motile sperm at the walls of microchannels.

Ideally, the motile sperm sorting rate of the MSMS is 100%. In addition, we can sort relatively strong motile sperm because the MSMS use the self movement of motile sperm. Our results indicate about an 80% sorting rate for bull sperm. The difference appears due to relatively long sorting time (about 20 *minutes*) which may cause loss of sperm motility. In addition, the sensitivity of controlling flow in the microchannels can cause the low throughput. Therefore, it is a challenge to increase motile sperm sorting rate and throughput. If the MSMS can complete the sorting processes in a short time, the sorting rate should be increased. Adding more main channels may solve this problem. In addition, the throughput should be increased. Therefore, the MSMS must be upgraded to improve its performance.

Our next goal is to apply the MSMS in a microdissection device. By applying the laser cutter into the MSMS, the tail of sorted motile sperm can be cut automatically to

assist IVF and ICSI. Therefore, further research is needed to increase sorting rate and to integrate multi functions to complete the microdissection systems. With additional research we may ultimately develop inexpensive and convenient microfluidic systems for commercial, industrial, and biological applications.

REFERENCES

[1] R. P. Feynman, “There is plenty of room at the bottom”, The American Physical Society Meeting in Pasadena, CA , 1959.

[2] K. Kempf, “Electronic computers within the ordnance corps, Chapter II-ENIAC”, 1961. (http://ftp.arl.mil/~mike/comphist/61ordnance/chap2.html)

[3] H. L. Santos, “Introduction to microelectromechanical (MEM) microwave systems”, Artech House, Boston.London, 1999.

[4] N. Maluf, “An introduction to microelectromechanical system engineering”, Artech House, Boston.London, 1999.

[5] An Industry in Transition: 2006 MEMS Forecast (http://www.instat.com/ catalog/ Scatalogue.asp?id=47)

[6] E. Abbaspour-Sani, R. Huang, and C. Y. Kwok, “Novel electromagnetic accelerometer”, IEEE Electron Device Letters. v5, n8, pp 272-273, 1994.

[7] M. K. Lim, H. Du, C. Su, and W. L. Jin, “Micromachined piezoresistive accelerometer with high sensitivity: Design and modeling”, Microelectronic Engineering, v49, n3-4, pp 263-272, 1999.

[8] S. J. Lee and D. W. Cho, “Development of a micro-opto-mechanical accelerometer based on intensity modulation”, Microsystem Technologies, v10, n2, pp 147-154, 2004.

[9] M. Khoo and C. Liu, “A Novel Micromachined magnetic membrane microfluid pump”, Annual International Conference of the IEEE Engineering in Medicine and Biology – Proceedings, v3, pp 2394-2397, 2000.

[10] A. V. Lemoff and A. P. Lee, “AC magnetohydrodynamic micropump”, Sensors & Actuators B-Chemical, v63, n3, pp 178-185, 2000.

[11] A. Hatch, A. E. Kamholz, G. Holman, P. Yager, and K. F. Bohringer, “A ferrofluidic magnetic micropump”, Journal of Microelectromechanical Systems, v10, n2, pp 215-221, 2001.

[12] M. Knight and J. House, “Design, fabrication, and test of a peristaltic micropump”, Microsystem Technologies, v10, n5, pp 426-431, 2004.

[13] L. Lin and W. Yun, “Design, optimization and fabrication of surface micromachined pressure sensors”, Mechatronics, v8, n5, pp 505-519, 1998.

[14] S. Chang, C. Dai, J. Chiou, and P. Chang, “Capacitive micro pressure sensors with underneath readout circuit using a standard CMOS process”, Proceedings of SPIE - The International Society for Optical Engineering, v4334, pp 336-344, 2001.

[15] J. C. Mcdonald, D. C. Duffy, J. R. Anderson, D. T. Chiu, H. Wu, Olivier, J. A. Scheueller and G. M. Whitesides, “Fabrication of microfluidic systems in poly(dimethylsiloxane)”, Electrophoresis. v21. pp 27- 40, 2000.

[16] K. Takahashi, A. Hattori, I. Suzuki, T. Ichiki, and K. Yasuda, “Non-destructive on-chip cell sorting system with real-time microscopic image processing”, Journal of Nanobiotechnology, v2, pp 8- ,2004. 8p

[17] T. Goettsche, J. Kohnle, M. Willmann, H. Ernst, S. Spieth, R. Tischler, S. Messner, R. Zengerle, and H. Sandmaier, “Novel approaches to particle tolerant valves for use in drug delivery systems”, Sensors & Actuators A-Physical, v118, n1, pp 70-77, 2005.

[18] B. S. Cho, T. G. Schuster, X. Zhu, D. Chang, G. D. Smith, and S. Takayama, “Passively driven integrated microfluidic system for separation of motile sperm”, Analytical Chemistry, v75, pp1671-1675, 2003.

[19] T. G. Schuster, B. Cho, L. M. Keller, S. Takayama, and G. D. Smith, “Isolation of motile spermatozoa from semen samples using microfluidics”, Reproductive BioMedicine Online, v7, pp 71-81, 2003.

[20] K. M. Horsman, S. L. R. Baker, J. P. Ferrance, K. A. Forrest, K. A. Koen and J. P. Landers, “Separation of sperm and epithelial cells in a microfabricated device: Potential application to forensic analysis of sexual assault evidence”, Analytical Chemistry, v77, pp 742-749 ,2005.

[21] C. Ainsworth, B. Nixon, and R. J. Aitken, “Development of a novel electrophorestic system for the isolation of human spermatozoa”, Human Reproduction, v20, pp 2261-2270, 2005.

[22] D. Beebe, M. Wheeler, H. Zeringue, E. Walters, and S. Raty, “Microfluidic technology for assisted reproduction”, Theriogenology, v57, pp 125-135, 2002.

[23] Wu, J. M.; Chung, Y. Belford, K. J. Smith, G. D. Takayama, and S. J. Lahann, "A surface-modified sperm sorting device with long-term stability", Biomedical Microdevices.v8, pp 99l-107, 2006.

[24] R. S. Suh, X. Zhu, N. Phadke, D. A. Ohl, and S. Takayama, "IVF within microfluidic channels requires lower total numbers and lower concentrations of sperm", Human Reproduction, v21, pp 477-483, 2006.

[25] S. G. Clark, K. Haubert, D. J. Beebe, C. E. Ferguson, and M. B. Wheeler, "Reduction of polyspermic penetration using biomimetic microfluidic technology during in vitro fertilization", Lab on a chip, v5, pp 1229-1232, 2005.

[26] J. Yang, Y. Huang, X. Wang, F. F. Becker, and P. R. Gascoyne, "Cell separation on microfabricated electrodes using dielectrophoretic/gravitational field-flow fractionation", Analytical Chemistry, v71, pp 911-918, 1999.

[27] J. Krüger, K. Signgh, A O'Neill, C. Jackson, A. Morrison, and P. O,Brien, "Development of A Microfluidic Device for Fluorescence Activated Cell Sorting", Journal of Micromechanics and Microengineering ,v12. pp 486-494, 2002.

[28] D. Huh, H. Wei, O. D. Kripfgans, J. B. Fowlkes, J. B. Grotberg, and S. Takayama, "Gravity-driven microhydrodynamics-based cell sorter (microHYCS) for rapid, inexpensive, and efficient cell separation and size-profiling", 2002 2nd Annual International IEEE-EMBS Special Topic Conference on Microtechnologies in Medicine & Biology. pp 466-469, 2002.

[29] D. Sobek, S. D. Senturia, and M. L. Gray, "Microfabricated fused silica flow chambers for flow cytometry", Proceedings of the Solid-State Sensor and Actuator Workshop, pp 260-263, 1994.

[30] D. J. Harrison, Z. Fan, K. Seiler, and K. Flurri, "Miniaturized chemical analysis systems based on electrophoretic separations and electroosmotic pumping", Proceedings of Transducers' 93, the 7th International Conference on Solid-State Sensors and Actuators. Yokohama, Japan, (Institute of Electrical Engineerings, Japan), pp 403-406, 1993.

[31] S. C. Jacobson, R. Hergenröder, A. W. Moore, and J. M. Ramsey, "Electrically driven separations on a microchip", Proceedings of the 1994 Solid-State Sensor and Actuator Workshop, pp 65-68, 1994.

[32] A. Manz, C. S. Effenhauser, N. Burggraf, D. J. Harrison, and K. Flurri, "Electroosmotic pumping and electrophoretic separations for miniaturized chemical analysis systems", Journal of Micromechanics and Microengineering, v4, pp 257-265, 1994.

[33] A. T. Woolley and R. A. Mathies, "Ultra-high-speed DNA fragment separations using microfabricated capillar array electrophoresis chips", Proceedings of the National Academy of Science, v91, pp 11348-11352, 1994.

[34] R. W. Tjerkstra, M. de Boer, E. Berenschot, J. G. Gardeniers, A. van den Berg, and M. Elwenspoek, "Etching technology for microchannels", Proceedings of the 10th Annual Workshop of Micro Electro Mechanical Systems (Nagoya, Japan), pp 147-151, 1997.

[35] L. Lin, A. P. Pisano, and R. S. Muller, "Silicon processed microneddles", Proceedings of Transducers' 93, the 7th International Conference on Solid-State Sensors and Actuators (Yokohama, Japan), pp 237-240, 1993.

[36] P. F. Man, D. K. Jones, and C. H. Mastrangelo, "Microfluidic plastic capillaries on silicon substrates: A new inexpensive technology for bioanalysis chip", Proceedings of the 10th Annual Workshop of Micro Electro Mechanical Systems (Nagoya, Japan), pp 311-316, 1997.

[37] D. C. Duffy, J. C. Mcdonald, J. A. Scheueller, and G. M. Whitesides, "Rapid prototyping of microfluidic system in poly(dimethylsiloxane)", Analytical Chemistry. v70. pp 4974-4984, 1998.

[38] J. H. Chan, A. T. Timperman, D. Qin, and R. Aebersold, "Microfabricated polymer devices for automated sample delivery of peptides for analysis by electrospray ionization tandem mass spectrometry", Analytical Chemistry. v71, pp 4437-4444, 1999.

[39] D. SEO, "A study of microfluidic in PDMS microchannels", Dissertation for MS, University of Missouri- Columbia, 2002.

[40] A. Collins, "Rapid exchange of extra-cellular solution using a microfluidic device", Dissertation for M.S, University of Missouri-Columbia, 2003.

[41] S. Lai, Y. Hudiono, L. Lee, S. Daunert, and J. Madou, "A novel bonding method for polymer-based microfluidic platforms", SPIE- Micromaching and Microfabrcation Process Technology VII, v4557**,** pp280- 287, 2001.

[42] R. C. Anderson, G. J. Bogdan, Z. Barniv, T. D. Dawes, J. Winkler, and K. Roy, " Microfluidic biochemical analysis system", Proceeding of Transducers' 97, The 1997 International Conference on Solid-State Sensors and Actuators, v1, pp 531-534, 1997.

[43] G. T. Kovacs, "Micromachined transducers sourcebook", McGraw-Hill, 1998.

[44] D. R. Reyes, D. Iossifidis, P. Auroux, and A. Manz, "Micro total analysis systems, 1. Introduction, theoty, and technology", Analytical Chemistry, v74, pp 2623-2636, 2002.

[45] P. Auroux, D. Iossifidis, D. R. Reyes, and A. Manz, "Micro total analysis systems, 2. Analytical standard operations and applications", Analytical Chemistry, v74, pp 2637-2652, 2002.

[46] D. Li, **"**Electrokinetics in microfluidics", Elsevier Academic Press, 2004.

[47] W. Wang and S. A. Soper, "Bio-MEMS : Technologies and applications" CRC Press (Taylor & Francis), 2007.

[48] S. C. Jacobson, T. E. McKnight, and J. M. Ramsey, "Microfluidic devices for electrokinetically driven parallel and serial mixing", Analytical Chemistry., v71, pp 4455-4459, 1999.

[49] M. Deshpande et al., "Numerical framework for the modeling of electrokinetic flows", in Proc. SPIE Conf. Microfluidic Devices Syst., pp 217-227, 1998.

[50] S. V. Ermakov, S. C. Jacobson, and J. M. Ramsey, "Computer simulations of electrokinetic mass transport in microfabricated fluidic devices", in Proc. Conf. Modeling Simulation Microsystem., pp 534-537, 1999.

[51] L. Hu, J. D. Harrison, and J. H. Masliyah, "Numerical model of electrokinetic flow for capillary electrophoresis", Journal of Colloid Interface Science., v215 pp 300-312, 1999.

[52] J. Knight "Microfluidics; Honey, I shrunk the lab", Nature (news feature), v418, pp 474-475, 2002.

[53] M. Khoo and C. Liu, "A Novel Micromachined Magnetic Membrane Microfluid Pump", [Conference Paper] Annual International Conference of the IEEE Engineering in Medicine and Biology - Proceedings. v3 pp 2394-2397, 2000.

[54] A. Manz, C. S. Effenhauser, N. Burggraf, D. J. Harrison, and K. Flurri, “Electroosmotic Pumping and Electrophoretic Separations for Miniaturized Chemical Analysis Systems”, Journal of Micromechanics and Microengineering, v4. pp 257-265, 1994.

[55] S. Buettgenbach and C. Robohm, **“**Microflow devices for miniaturized chemical analysis systems”, Proceedings of SPIE - The International Society for Optical Engineering. v 3539, pp 51-61, 1998.

[56] R. B. Darlin, T. Chen, A. A. Scheidemann, P. Yager, and K. N. Bhat, **“**Microfabricated components for miniaturized chemical analysis systems”, Proceedings of SPIE - The International Society for Optical Engineering. v5062, n 2, pp 863-872, 2002.

[57] A. P. Sudarsan, J. Wang, and V. M. Ugaz, **“**Thermoplastic elastomer gels: An advanced substrate for microfluidic chemical analysis systems”, Analytical Chemistry. v77, n 16, pp 5167-5173, 2005.

[58] M. A. Burns, B. N. Johnson, S. N. Brahmasandra, K. Handique, J. R. Webster, M. Krishnan, T. S. Sammarco, P. M. Man, D. Jones, D. Heldsinger, C. H. Mastrangelo, and D. T. Burke, “An Integrated Nanoliter DNA Analysis Device”, Science, v282, pp 484-487, 1998.

[59] C. Pozrikidis, “ Introduction to Theoretical and Computational Fluid Dynamics”, Oxford University Press 1997.

[60] G. A. Karniadakis, A. Beskok, and N. Aluru, “Microflows and nanoflows: Fundamentals and simulation”, Springer, 2005.

[61] P. Yager, “ Basic microfludic concepts”, (http://faculty.washington.edu/uagerp/ microfluidicstutorial)

[62] W. W. Liou and Y. Fang, **“**Microfluid mechanics: Principles and modeling”, McGraw-Hill, 2006.

[63] S. Shoji and M. Masayoshi, “Microflow devices and systems”, Journal of Micromechanics and Microengineering, v4, pp 157-171, 1994.

[64] N. Vandelli, D. Wroblewski, M. Velonis, and T. Bifano, “Development of a MEMS microvalve array for fluid flow control”, Journal of Microelectromechanical Systems, v7, n4, pp 395-403, 1998.

[65] C. D. Meinhart and H. Zhang, "The flow structure inside a microfabricated inkjet printhead", Journal of Microelectromechanical systems, v9, n1, pp 67-75, 2000.

[66] M . L. Adams, M. Loncar, A. Scherer, and Y. Qiu, "Microfluidic integration of porous photonic crystal nanolaser for chemical sensing", IEEE Journal on Selected Areas in Communications, v23, n7, pp 1348-1354, 2005.

[67] P. Hao, F. He, and K. Zhu, "Flow characteristics in a trapezoidal silicon microchannel", Journal of Micromechanics and Microengineering, v15, pp 1362-1368, 2005.

[68] N. Ichikawa, K. Hosokawa, and R. Maeda, "Interface motion of capillary-driven flow in rectangular microchannel", Journal of Colloid and Interface Science, v280, pp 154-164, 2004.

[69] N. Fujisawa, Y. Nakamura, F. Matsuura, T. Sato, "Pressure field evaluation in microchannel junction flows through μPIV measurement", Microfluidics and Nanofluidics, v2, pp 447-453, 2006.

[70] D. C. Tretheway and C. D. Meinhart, "Apparentt fluid slip at hydrophobic microchannel walls", Physics of Fluids, v14, n3, pp L9-L12, 2002.

[71] J. Hahm, A. Balasubramanian, and A. Beskok, "Flow and species transport control in grooved microchannels using local electrokinetic forces", Physics of Fluids. v19, n1, 2007.

[72] M.Esashi, "Integrated microflow control systems", Sensors and Actuators, v21, pp161-167, 1990.

[73] J. M. Chen, T. Horng, and W. Y. Tan, "Analysis and measurement of mixing in pressure-driven microchannel flow", Microfluidics and Nanofluidics, v2, pp 455-469, 2006.

[74] R. J. Adrian, "Particle-imaging techniques for experimental fluid mechanics", Annual Review of Fluid Mechanics, v23, pp 261–304, 1991.

[75] A. M. Lanzillotto, T. S. Leu, M. Amavile, R. Samtaney, and R. Wildes, "A study of structure and motion in fluidic Microsystems", AIAA Paper 97-1790, 28th Fluid Dynamics Conference. 1997.

[76] M. G. Olsen and A. J. Adrian, "Out-of-focus effects on particle image visibility and correlation in microscopic particle image velocimetry", Experiments in Fluids v29, pp S166–S174, 2000.

[77] D. Sinton, "Microscale flow visualization" Microfluidics and Nanofluidics, v1, pp 2–21, 2004.

[78] C. Wang, Y. Gao, N. Nguyen, T. N. Wong, C. Yang, and K. Ooi, "Interface control of pressure-driven two-fluid flow in microchannels using electroosmosis", Journal of Micromechanics and Microengineering, v15, pp 2289–2297, 2005.

[79] N. Fujisawa, Y. Nakamura, F. Matsuura, and Y. Sato, "Pressure field evaluation in microchannel junction flows through μPIV measurement", Microfluidics and Nanofluidics. v2, n5, pp 447-453, 2006.

[80] J. G. Santiago, S. T. Wereley, C. D. Meinhart, D. J. Beebe, and R. J. Adrian, "A particle image velocimetry system for microfluidics", Experiments in Fluids, v25, pp 316–319, 1998.

APPENDIX

1. MATLAB code for 3-D flow in single channel

```
clear all

% basic properties of water

mu=0.000891;

ro=0.00099705; % g/mm^3

L=4; % mm

a=0.05; % mm

b=0.0125; % mm

g=9810; %


% given pressures by heights difference

dh=5;

P0=ro*g*dh;

G=ro*g*dh/L;

A=G/(2*mu);

iter=40;

C(1)=0;

iter1=20;

for n3=1:iter+1;

        for n4=1:30+1;
```

```
        y(n3,n4)=2*a/(iter)*n3-a-2*a/(iter);


            z(n3,n4)=2*b/(30)*n4-b-2*b/(30);
            for n5=1:iter1;
                    A11=(-1)^n5*cosh(an(n5)*y(n3,n4)/b)*cos(an(n5)*z(n3,n4)/b);
                       an(n5)=pi*(2*n5-1)/2;
                            C(n5+1)=C(n5)+A11 /(an(n5)^3*cosh(an(n5)*a/b));


          end
        V(n3,n4)=A*(b^2-z(n3,n4)^2+4*b^2*C(iter1+1));
end
end


figure(1)
mesh(V,y,z)
```

2. MATLAB code for the flow in DMC-TRMS

```
clear all


% basic properties of water
mu=0.000891;
ro=997.05; %kg/m^3
G=9.810; % m/sec^2


% Pressures
h2=2; % (reservoir 2)
P(2)=ro*G*h2/1000;
h3=1; % (reservoir 3)
P(4)=ro*G*h3/1000;
h1=h2+(h2-h3)*6; % (reservoir1)
P(1)=ro*G*h1/1000;
dh1(m,1)=h1-h2;
dh2(m,1)=h2-h3;


%    width A(9) matrix
a1=205/2; % (micrometer)
a2=50; % (micrometer)
a3=50; % (micrometer)
```

```
A=1/1000000*[a1 a2 a3];
% Thickness
b=0.000025/2;

% Length
for m=1:21;
   L1(m,1)=15+0.5*m-0.5;
   L=1/1000*[L1(m) 4 2];

% B Matrix
for n=1:3;
      B(n)=4*A(n)*b^3*(1-(6*b*0.10504/A(n)))/(3*mu*L(n));
end

%   Main Matrix
M=[B(1)+B(2)+B(3)];
C=[B(1)*P(1)+B(2)*P(2)+B(3)*P(4)];
P2=inv(M)*C;
P22(m)=P2;
P1=P2';
P=[P(1) P(2) P1 P(4)];
P01(m,1)=P2(1);
```

```
% Max velocity (u_m_max)
U(m,1)=b^2*(P(1)-P(3))/(2*mu*L(1));
U(m,2)=b^2*(P(2)-P(3))/(2*mu*L(2));
U(m,3)=b^2*(P(3)-P(4))/(2*mu*L(3));

U1=1000000*U;
end
plot(L1,U1(:,2))
hold on
```

3. MATLAB code for the flow in Six-JCs-TRMS depending on Δh_1

```
clear all

P=[0 0 0 0 0 0 0];

% basic properties of water
mu=0.000891;
ro=997.05; %kg/m^3
G=9.810; % m/sec^2

% Pressures
for m=1:17;
h3=0; % mm
P3=ro*G*h3/1000;
h2=1.5; % mm
P2=ro*G*h2/1000;
h1=0.5*m+h2-0.5; % mm
P1=ro*G*h1/1000;
dh1(m,1)=h1-h2;

% width of driven and junction channels
a1=300;
```

```
% width of main channels
a2=100;

% width of outlet channels
a3=100;

% width matrix A(9)
A=1/2000000*[a1 a2 a1 a2 a1 a2 a1 a2 a3];
A1=0.5*[a1 a2 a1 a2 a1 a2 a1 a2 a3];

% Length of channels
L=(1/1000)*[20 4 0.5 3 0.5 2 0.5 1 3];

% Thickness
b=0.000025/2;

% B Matrix
for n=1:9;
      B(n)=4*A(n)*b^3*(1-(6*b*0.10504/A(n)))/(3*mu*L(n));
end

% Main Matrix
```

```
M=[B(1)+B(2)+B(3) -B(3) 0 0;-B(3) B(3)+B(4)+B(5) -B(5) 0;0 -B(5) B(5)+B(6)+B(7) -
B(7);0 0 -B(7) B(7)+B(8)+B(9)];
C=[B(1)*P1+B(2)*P2;B(4)*P2;B(6)*P2;B(8)*P2+B(9)*P3];
P22=inv(M)*C;
P11=P22';
P=[P1 P2 P11 P3];
PP(m,:)=P;

% Max velocities
U(m,1)=b^2*(P(1)-P(3))/(2*mu*L(1));
U(m,2)=b^2*(P(2)-P(3))/(2*mu*L(2));
U2(m,1)=U(m,2)*1000000;
U(m,3)=b^2*(P(3)-P(4))/(2*mu*L(3));
U(m,4)=b^2*(P(2)-P(4))/(2*mu*L(4));
U2(m,2)=U(m,4)*1000000;
U(m,5)=b^2*(P(4)-P(5))/(2*mu*L(5));
U(m,6)=b^2*(P(2)-P(5))/(2*mu*L(6));
U2(m,3)=U(m,6)*1000000;
U(m,7)=b^2*(P(5)-P(6))/(2*mu*L(7));
U(m,8)=b^2*(P(2)-P(6))/(2*mu*L(8));
U2(m,4)=U(m,8)*1000000;
U(m,9)=b^2*(P(6)-P(7))/(2*mu*L(9));
```

```
end
U1=U'*1000000;
figure(1)
plot(dh1,U2);
```

VITA

DUCKBONG SEO was born on May 27, 1971 (however, the official birth day is June 7, 1971) at the Baek-Ryung Island in Korea. He graduated from Whi-Moon high school in 1990. He studied at the Hong-Ik University in Seoul, Korea and received his B.S. degree at the same University. After graduating, he served in Korea Army as an artillery officer for 28 months. He has worked for Samsung Commercial Vehicle from July, 1997 to July 1999. He started is M.S degree in the Department of Mechanical and Aerospace Engineering at the University of Missouri-Columbia in 2000, and received his M.S. degree in 2002. One year after M.S. degree, he started his Ph.D. program at the University of Missouri-Columbia and received a Ph.D. on August 2007.